DESIGN AND ANALYSIS OF MULTIBAND CIRCULARLY POLARIZED ANTENNA FOR MODERN WIRELESS APPLICATIONS

MOHAMMED ABDULRAZZAQ AZEEZ AL-MIHRAB

JANUARY 2021

DESIGN AND ANALYSIS OF MULTI-BAND CIRCULARLY POLARIZED ANTENNA FOR MODERN WIRELESS APPLICATIONS

A THESIS SUBMITTED TO
THE GRADUATE SCHOOL OF NATURAL AND APPLIED SCIENCES OF
ÇANKAYA UNIVERSITY

BY
MOHAMMED ABDULRAZZAQ AZEEZ AL-MIHRAB

IN PARTIAL FULFILMENT OF THE REQUIREMENTS THE DEGREE OF DOCTOR OF PHILOSOPHY
IN
THE DEPARTMENT OF
ELECTRONIC AND COMMUNICATION ENGINEERING

JANUARY 2021

ABSTRACT

DESIGN AND ANALYSIS OF MULTIBAND CIRCULARLY POLARIZED ANTENNA FOR MODERN WIRELESS APPLICATIONS

AL-MIHRAB, Mohammed Abdulrazzaq Azeez

Ph.D., Department of Electronic and Communication Engineering

Supervisor: Prof. Dr. Yusuf Z. UMUL

Co-Supervisor: Prof. Dr. Jawad K. ALI

January 2021, 115 Pages

In this dissertation, new five compact multiband printed antennas have been designed, and analyzed. The first two antennas have a dual-sense circular polarization while the others are single-sense circular polarization. The first one has been designed based on an open-loop hexagonal monopole radiator with two stair-shaped slits in a partial ground plane. Five operating bands with different polarization are obtained. Three bands out of these five are circularly polarized (CP) while the other are linearly polarized (LP). The -10 dB impedance bandwidths (IBWs) are (1.55-1.72 GHz), (2.51-2.64 GHz), (3.1-3.31 GHz), (4.08-5.83 GHz), and (6.14-6.7 GHz), while the 3 dB axial ratio bandwidths (ARBWs) are (1.6-1.75 GHz), (4.54-4.9 GHz), and (6.21-6.49 GHz). Also, this antenna shows a triple sense (right hand, left hand, right hand) CP, bidirectional radiation patterns. The measured gains are 1.75 dBi, 3.72 dBi, 3.2 dBi, 5.87dBi, and 7.61 dBi at frequencies 1.65 GHz, 2.55 GHz, 3.20 GHz, 4.75 GHz, and 6.35 GHz respectively. Overall dimensions are 65 mm × 45 mm × 1.6 mm. Another two stair-shaped slits in the partial ground plane have been added with a pair of rectangular strips. The IBWs are (1.478-1.714 GHz), (2.54-2.72 GHz), and (4.29-4.89 GHz), respectively. The measured 3-dB axial ratio bandwidths (ARBWs) are (1.510-1.606 GHz) and (4.035-5.07 GHz) for the lower and the upper band respectively. The measured gains are 2.5 dBi, 3.6 dBi, and 5 dBi at frequencies 1.575 GHz, 2.55 GHz,

and 4.5 GHz respectively. The side length of this antenna has been increased to be 70 mm.

The last three proposed antennas are fed by CPW with dimensions 40 mm ×40 mm ×1 mm. One of these three antennas is a slotted square ring with two rectangular strips, which are located at the opposite corner, and three bands are obtained. The IBWs are: (3.59-5.01 GHz), (7.64 to 8.43 GHz), and (10.81 to 11.28 GHz) whereas ARBWs at 3-dB are: (3.15-4.69 GHz), (7.77-8.17 GHz), and (10.84-11.25 GHz) GHz. The simulated gains are 3.75 dBi, 3.2 dBi, and 4.62 dBi at center frequencies 4.5 GHz, 8 GHz, and 11 GHz respectively.

In the first updated antenna, the CP characteristic in the first band has been boosted by adding an inverted L-strip to the ground plane on the far corner of the radiator after it was not strong in the previous antenna. The IBWs for three bands are: (3.2-5.39 GHz), (7.55 to 8.21 GHz), and (10.79 to 11.31 GHz) whereas ARBW are: (3.32-4.58 GHz) and (10.79-11.13 GHz). The simulated gains are 2.65 dBi, 3.9 dBi, and 5.3 dBi at center frequencies 3.6 GHz, 8 GHz, and 11 GHz respectively.

The second modified antenna demonstrated a new band around 5.8 GHz. The IBWs for four bands are: (3.72-4.88 GHz), (5.62-5.89 GHz), (7.68-8.27 GHz), and (10.83-11.33 GHz) whereas ARBWs are: (3.17-3.64 GHz), (5.62-5.89 GHz), and (10.64-11.1 GHz). Concerning simulated gains are 2.6 dBi, 2.1 dBi, 3.6 dBi, and 4.4 dBi at frequencies 3.6 GHz, 5.8 GHz, 8 GHz, and 11 GHz respectively. Finally, all the proposed antennas in this work have been designed using an FR4 substrate with relative permittivity of 4.4. The simulation results have been evaluated by using an HFSS simulator from Anasys.

Keywords: Circular polarization antennas, Compact multiband antennas, Axial ratio, Coplanar waveguide (CPW).

ÖZ

MODERN KABLOSUZ UYGULAMALAR İÇİN ÇOK BANTLI DAİRESEL POLARİZE ANTENİN TASARIMI VE ANALİZİ

AL-MIHRAB, Mohammed Abdulrazzaq Azeez

Doktora, Elektronik ve Haberleşme Mühendisliği Anabilim Dalı

Tez Yöneticisi: Prof. Dr. Yusuf Ziya UMUL

Eş Tez Yôneticisi: Jawad K. ALI

Ocak 2021, 115 Sayfa

Bu tezde, yeni beş kompakt çok bantlı baskılı anten tasarlanmış ve analiz edilmiştir. İlk iki anten çok yönlü dairesel polarizasyona sahipken diğerleri tek yönlü dairesel polarizasyondur. İlki, kısmi bir zemin düzleminde iki basamak şeklinde yarığı olan açık döngülü altıgen tek kutuplu bir radyatör temel alınarak tasarlanmıştır. Farklı polarizasyona sahip beş çalışma bandı elde edilir. Bu beş banttan üç tanesi dairesel olarak polarize edilirken (CP) diğeri doğrusal olarak polarize edilmiştir. -10 dB empedans bant genişlikleri (IBW'ler) (1.55-1.72 GHz), (2.51-2.64 GHz), (3.1-3.31 GHz), (4.08-5.83 GHz) ve (6.14-6.7 GHz) iken 3 dB Eksenel oran bant genişlikleri (ARBW'ler) (1.6-1.75 GHz), (4.54-4.9 GHz) ve (6.21-6.49 GHz) şeklindedir. Ayrıca, bu anten üçlü bir duyu olan (sağ el, sol el, sağ el) CP, çift yönlü radyasyon modellerini gösterir. Ölçülen kazançlar sırasıyla 1.65 GHz, 2.55 GHz, 3.20 GHz, 4.75 GHz ve 6.35 GHz frekanslarında 1.75 dBi, 3.72 dBi, 3.2 dBi, 5.87dBi ve 7.61 dBi'dir. Genel boyutlar 65 mm × 45 mm × 1,6 mm'dir. Kısmi zemin düzlemine bir çift dikdörtgen şeritle başka iki merdiven şeklindeki yarık eklenmiştir. IBW'ler (empedans bant genişlikleri) sırasıyla (1.478-1.714 GHz), (2.54-2.72 GHz) ve (4.29-4.89 GHz)

şeklindedir. Ölçülen 3-dB eksenel oran bant genişlikleri (ARBW'ler), alt ve üst bant için sırasıyla (1.510-1.606 GHz) ve (4.035-5.07 GHz) 'dir. Ölçülen kazançlar sırasıyla 1.575 GHz, 2.55 GHz ve 4.5 GHz frekanslarında 2.5 dBi, 3.6 dBi ve 5 dBi'dir. Bu antenin yan uzunluğu 70 mm'ye çıkarıldı.

Önerilen son üç anten, 40 mm × 40 mm × 1 mm boyutlarında CPW ile beslenir. Bu üç antenden biri, karşılıklı köşede bulunan iki dikdörtgen şeritli yarıklı kare bir halkadır ve üç bant elde edilir. IBW'ler şunlardır: (3.59-5.01 GHz), (7.64 - 8.43 GHz) ve (10.81 - 11.28 GHz) 3-dB'deki ARBW'ler: (3.15-4.69 GHz), (7.77-8.17 GHz) ve (10.84 - 11.25 GHz) GHz. Simüle edilen kazançlar, sırasıyla 4.5 GHz, 8 GHz ve 11 GHz merkez frekanslarında 3.75 dBi, 3.2 dBi ve 4.62 dBi'dir.

İlk güncellenen antende, önceki antende güçlü olmadığından radyatörün uzak köşesindeki zemin düzlemine ters çevrilmiş bir L-şeridi eklenerek, ilk banttaki CP özelliği artırıldı. Üç bant için IBW'ler: (3.2-5.39 GHz), (7.55 - 8.21 GHz) ve (10.79 - 11.31 GHz) iken ARBW: (3.32-4.58 GHz) ve (10.79-11.13 GHz)'dir. Simüle edilen kazançlar sırasıyla 3.6 GHz, 8 GHz ve 11 GHz merkez frekanslarında 2.65 dBi, 3.9 dBi ve 5.3 dBi'dir. İkinci değiştirilmiş anten 5,8 GHz civarında yeni bir bant gösterdi. Dört bant için IBW'ler şunlardır: (3.72-4.88 GHz), (5.62-5.89 GHz), (7.68-8.27 GHz) ve (10.83-11.33 GHz) ARBW'ler ise: (3.17-3.64 GHz), (5.62-5.89 GHz) ve (10.64-11.1 GHz). Simüle edilmiş kazançlarla ilgili olarak sırasıyla 3.6 GHz, 5.8 GHz, 8 GHz ve 11 GHz frekanslarında 2.6 dBi, 2.1 dBi, 3.6 dBi ve 4.4 dBi vardır. Son olarak, bu çalışmada önerilen tüm antenler, 4.4 nispi geçirgenliğe sahip bir FR4 substratı kullanılarak tasarlanmıştır. Simülasyon sonuçları, Anasys'in HFSS simülatörü kullanılarak değerlendirilmiştir.

Anahtar Kelimeler: Dairesel polarizasyon antenleri, Kompakt çok bantlı antenler, Eksenel oran, Eşdüzlemli dalga kılavuzu.

ACKNOWLEDGEMENTS

In the first place, my greatest gratitude goes to the Most Merciful Allah. Who granted me the opportunity to complete a Ph.D. study in Turkey and made me choose the brilliant supervisors: Prof. Dr. Yusuf Z. UMUL and Prof. Dr. Jawad K. ALI, they gave me limitless support.

Special thanks to Asst. Prof. Dr. Ali J. SALIM from the University of Technology - Baghdad for his objective guidance and firm support.

Also, I must not forget to thank Çankaya University, and especially the Department of Electronic and Communication Engineering for their precious encouragement and facilities.

Finally, special words of thanks to my loving family, thanks to my father my mother, my brothers, my sisters, and my wife Eng. Sura Samir (Um Jana), whom without their unlimited patience this work might never see the light.

TABLE OF CONTENTS

LIST OF TABLES

LIST OF FIGURES

LIST OF ABBREVIATIONS

2-D	Two Dimensional
3-D	Three Dimensional
5G	Fifth Generation
AR	Axial Ratio
ARBW	Axial Ratio Bandwidth
CP	Circular Polarization
CPSSA	Circularly Polarized Square Slot Antenna
CST	Computer Simulation Technology
DBS	Direct Broadcasting Service
DRA	Dielectric Resonator Antenna
FD	Frequency Domain
FDTD	Finite Difference Time Domain
FNBW	First-Null Beamwidth
FSS	Frequency Selective Surface
GNSS	Global Navigation Satellite Systems
GPS	Global Positioning System
HFSS	High-Frequency Structure Simulator
HPBW	Half-Power Beamwidth
IBW	Impedance Bandwidth
IE	Integral Equations
LHCP	Left Hand Circular Polarization
LP	Linear Polarization
LTE	Long-Term Evolution
MIC	Microwave Integrated Circuit
MIMO	Multi Input Multi Output
MMIC	Microwave Monolithic Integrated Circuit
MoM	Method of Moments

NEC	Numerical Electromagnetics Code
PCB	Printed Circuit Board
PQHA	Printed Quadrifilar Helix Antenna
QHA	Quadrifilar Helix Antenna
RFID	Radio Frequency Identification
RHCP	Right Hand Circular Polarization
SRRs	Split Ring Resonators
TD	Time Domain
TEM	Transverse Electromagnetic Wave
VSWR	Voltage Standing Wave Ratio
WiMAX	Worldwide interoperability for Microwave Access
WLAN	Wireless Local Area Network
WPAN	Wireless Personal Area Network

LIST OF SYMBOLS

$Z_\circ$	Characteristic Impedance
f_o	Resonant Frequency
ε_r	Relative Permittivity
λ_g	Guided Wavelength
R_{in}	Input resistance
V^-	Reflected wave voltage
V^+	Incident wave voltage
X_{in}	Input reactance
Z_L	Load impedance
Z_{in}	Input impedance of the patch antenna
ε_{eff}	Effective Dielectric Constant
$\eta_\circ$	Overall Efficiency
η_c	Conduction Efficiency
η_d	Dielectric Efficiency
η_r	Efficiency of wave reflection to power source
$\lambda_\circ$	Free Space Wavelength
μ_r	Relative Permeability
c	Free Space Velocity of Light ($\approx 3 \times 10^8 m/s$)
dB	Decibel
h	High of Dielectric Between Conductor and Substrate
T	Thickness of Conductor
Ω	Ohm
f	Frequency
Γ	Reflection Coefficient
α	Pitch angle
δ	Loss angle
θ	Evaluation Angle

λ	Wavelength
ω	Angular Frequency
ϕ	Azimuth Angle

CHAPTER 1

INTRODUCTION

1.1 Background

In the wireless communication world, everyone knows that there is one important part plays an important role to work a wireless device efficiently this part is called antenna. Antennas consider the backbone of wireless communications, for this reason, the scientists and researchers go to research on it. One type of antenna remaining active research till now is called circular polarization (CP) antennas. CP antennas consist of two orthogonal modes are excited with a 90° time-phase difference between them [1]. They exist in many shapes and sizes according to the application of wireless devices. They are used in many wireless systems including satellite communications, mobile communications, global navigation satellite systems (GNSS), wireless sensors, radio frequency identification (RFID), wireless power transmission, wireless local area network (WLAN), wireless personal area network (WPAN), Worldwide Interoperability for Microwave Access (WiMAX) and Direct Broadcasting Service (DBS) television reception systems [2].

1.2 Microwave

Microwave consider part of electromagnetic spectrum that frequency extend from 300 MHz to 300 GHz or in respect to a wavelength (λ) between 1m to 1mm. Generally, most of current excited researches and wireless communication systems are lid these frequencies range. Several aspects such as radiation, coupling electromagnetic issues and scattering that have to be taken into mind when employing these frequencies [3]. Usually, microwave issues for high frequencies (short wavelengths) cannot be solved by standard circuit theory. Also, the physical dimensions of microwave devices play a significant role in the changing phase and current because they rely on the microwave length. While at low frequencies, the wavelength is large and there are not major alterations in the phase across the component [4].

1.3 Modern circular polarization applications

Indeed, the radiated wave with circularly polarized (CP) characteristic has many privileges and able to be overcome many wireless known issues such as multipath interfaces [4,5], fading, and minimize Faraday rotation effect due to ionosphere [6,7] as well as the flexibility to orientation between transmitting and receiving antennas [4]. These features gave justification to many wireless applications to employ an antenna that radiates a circular polarization wave. The following systems consider good examples for using a CP antenna:

1. Satellite communications
2. Mobile communications
3. Global navigation satellite systems (GNSS)
4. Radio frequency identification (RFID)
5. Wireless local area network (WLAN)
6. Wireless personal area network (WPAN)
7. Worldwide interoperability for microwave access (WiMAX)
8. Wireless sensors
9. Wireless power transmission
10. Direct broadcasting service (DBS) television reception systems.
11. Space probes and ballistic missiles

For instance, mobile satellite communications are benefit from no rigorous property where it is not easy to maintain a fixed antenna orientation. Also, the CP antennas are widely employed for telemetry applications of a satellite, ballistic missiles and space probes exploiting a minimize Faraday effect merit [4].

The CP antennas can be used in Ka-band mobile communication systems, which provide high data-rate wideband links. They can be placed on the airplane's board to provide the Internet in the sky or in high-speed trains. GNSS (American GPS, Russian Glonass, European Galileo and Chinese BeiDou-2) need particular antenna designs [9-11] since the system calculates the distance between the satellite and the based receiver on the earth, depend on the time it takes for a radio signal to travel this distance. However, if the signal is reflected, the time it takes to reach a receiver will be longer and a positioning error appears. The employ of CP permits the repression of some of the reflected signals, as right-hand circular polarization (RHCP) signals reflected from

a uniform surface becomes left-hand circular polarization (LHCP) and vice-versa. By utilizing an antenna with good AR, this signal can be funneled and hence enhance positioning accuracy.

1.4 Literature Survey

In 2008, X. Bao, and M. J. Ammann [12], had designed dual-band dual sense CP antenna. As seen in Figure 1, the antenna constructed from the single-layer substrate (FR4) and annular slot with four unequal longitudinal slots that are responsible for generating CP waves. On the other side, a microstrip feed line. The -10 dB reflection coefficient IBWs for the lower (1.5 GHz) and upper (2.6 GHz) bands are 26.7% and 11.3%, respectively whereas the 3 dB ARBWs are 6.1% and 6.0%. The overall size of the antenna is 80×80×1.52 mm^3.

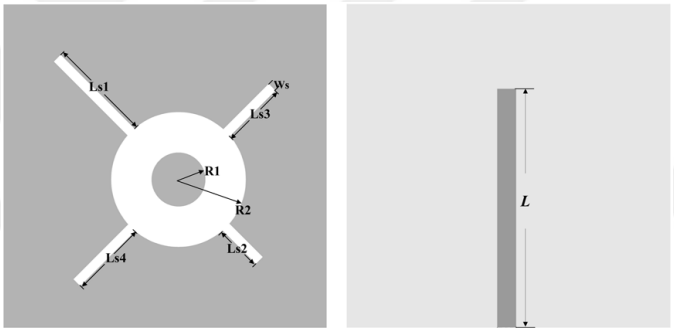

(a) (b)

Figure 1 The geometry of dual band CP slot antenna (a) Slot, (b) Microstrip line

In 2009, C. Chen and E. K. N. Yung [13], had designed a square slot antenna excited by CPW. As noted in Figure 2, the two loaded spiral slots in the ground plane etched so as to get different senses of CP. The dual-band operation is obtained by employing the T-shape strip. The radiator and ground plane printed on one side of FR4, which has a thickness of 1.6 mm. The practical result 10-dB reflection coefficient IBWs are 8.7% and 23% for the lower and the upper band respectively whereas 3-dB ARBWs are 8.4% and 19.24%, with respect to 1.6 GHz and 2.2 GHz, respectively.

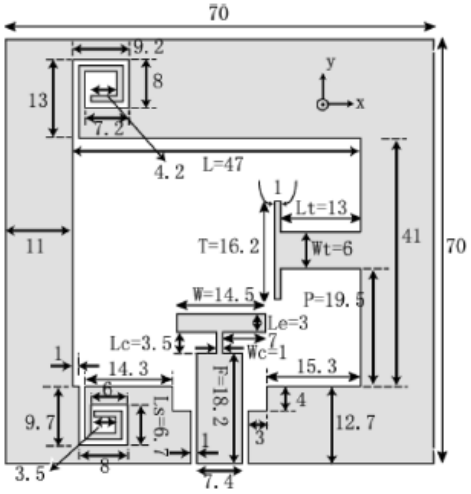

Figure 2 The geometry of dual band dual sense square slot antenna

In 2011, S. A. Rezaeieh and M. Kartal [14], had designed a square slot antenna for achieving CP radiation. As noted in Figure 3, the antenna is a single layer and consists of two equal-sized crooked T-shaped and F-shaped strips placed on the patch. The overall size is 40×40×0.8 mm^3. The total IBWs of 8.04 GHz and offering a (4.6-6.1 GHz) 3-dB ARBW.

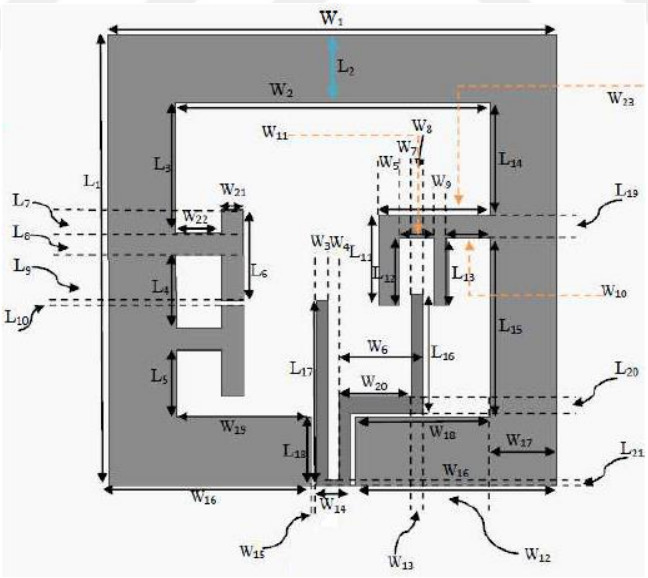

Figure 3 The structure of square slot antenna with multi-polarization

In 2012, L. Wang, et al [15], had proposed a single feed triple-band slot antenna for CP operation employing two annular slots excited by an inverted h-shape microstrip line presented as shown in Figure 4. A triple CP antenna operates at 1.58, 2.42, and 3.0 GHz and 3-dB ARBWs for these bands are about 65, 85, and 30 MHz, respectively.

The frequency ratio can be changed by setting the dimensions of two annular slots. The antenna was constructed on a RO4003 substrate with thickness h = 0.813mm, relative permittivity ε_r=3.38, and tangent loss tanδ= 0.0027. The overall dimensions are 100×80×0.813 mm^3.

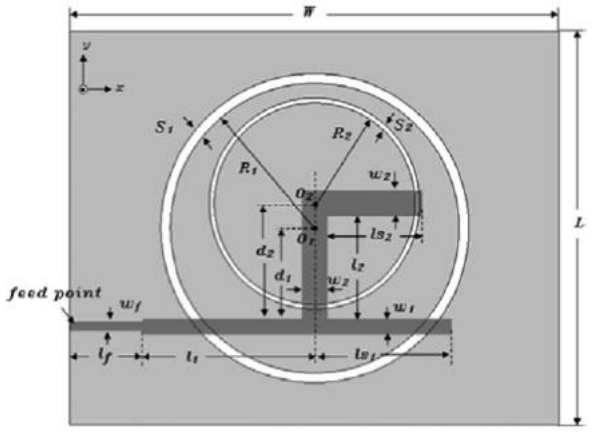

Figure 4 The geometry of proposed triple band CP antenna

In 2012, Y. Shao, and Z. Chen [16], had designed a dual-band dual sense printed monopole antenna with center frequencies at 2.4 GHz and 5.8 GHz. It consists of an annular slot and cross slot printed on side of substrate whereas on the other side is the microstrip feed line which consists of stubs and impedance transformer as noted in Figure 5. The role of unequal cross slot and pair of notches is to produce CP waves in both bands.

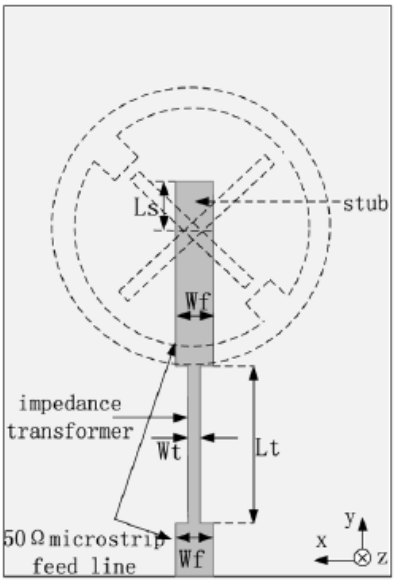

Figure 5 The geometry of dual band dual sense CP printed slot antenna

In 2013, S. M. NOGHABAEI, et al [17], introduced a dual-band CP microstrip antenna for WiMAX applications. As noted in Figure 6, the radiator is truncated square patch embedded with asymmetrical T-slot in the center of the patch and two vertical slots and slits. The radiator printed on the FR4 substrate and excited by the microstrip feed line. The antenna operates at 7.2% (2.53 GHz) and 3.6% (5.73 GHz) and 3 dB axial ratio of 2 % and 3.2 % at the lower and upper band, respectively. The overall dimensions of the antenna are 55×55×1.6 mm^3.

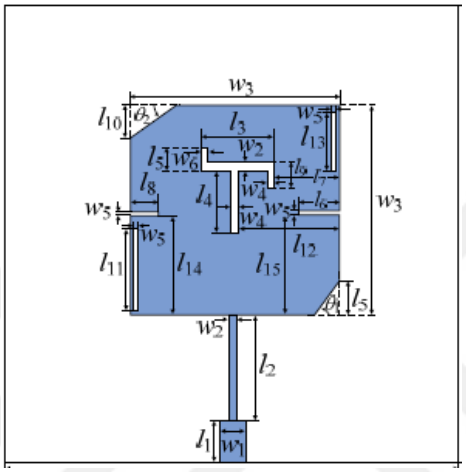

Figure 6 The geometry of dual band CP antenna

In 2014, M. Bod, and H. R. Hassani [18], had introduced a single layer triple-band CP printed slot antenna fed by microstrip line. It consists of a wide circular slot with embedded four L-shaped arms as illustrated in Figure 7. This structure is employed and printed on the FR4 substrate to produce a multiband CP antenna. The resonance frequency of each of the band can be appointment by adjusting the total length of the appropriate slot arms. The arc is integrated into the upper part of the circular slot antenna to produce the 3rd CP band. The antenna has CP radiation at center frequencies1.5 GHz, 2.4 GHz, and 3.75 GHz with 14%, 22%, 12% IBW and 9%, 7%, 11% ARBW, respectively. The dimensions of it are 58×58×1.6 mm^3.

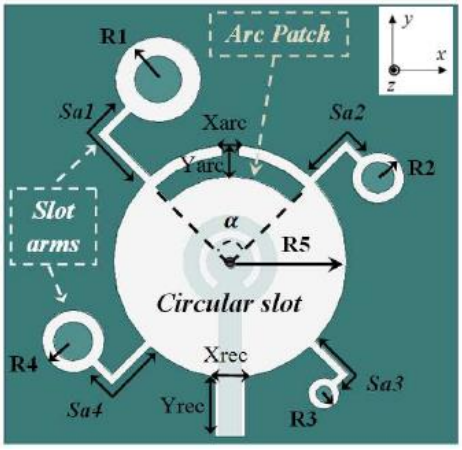

Figure 7 The geometry of multiband CP printed slot antenna.

In 2015, T. V. Hoang, et al [19], had designed a CP antenna with quad-band for WLAN and WiMAX applications. Three CP bands implemented by a patch antenna which consists of tilted inverted U-shaped radiator with additional I-shaped and L-shaped strips as shown in Figure 8 (b). The fourth CP band carried out via putting FSS (frequency selective surface) 6× 6 square metallic patches under antenna so as to converts the band at 5.8 GHz region from linear polarization to circular polarization as noted in Figure 8 (a). The configured antenna operates at (2.37–2.75 GHz) and 4.6 GHz (3.4–8 GHz) while 3-dB AR covers from (2.35−2.48 GHz), (3.45−3.75 GHz), (5.25−5.45 GHz) and (5.7−5.87 GHz). the antenna fabricated on Taconic RF-35 substrate with a thickness of 1.52 mm, $\varepsilon_r = 3.5$ and tanδ = 0.0018. The total size of the antenna with FSS is 133.2 × 133.2 mm^2.

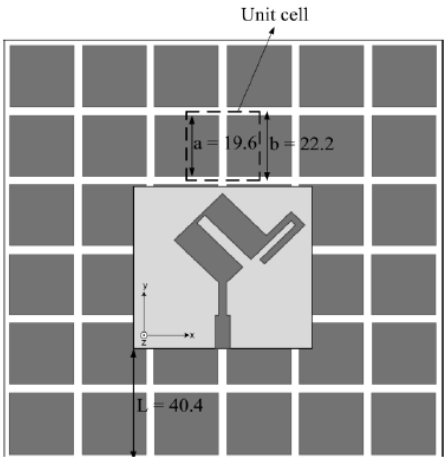

(a)

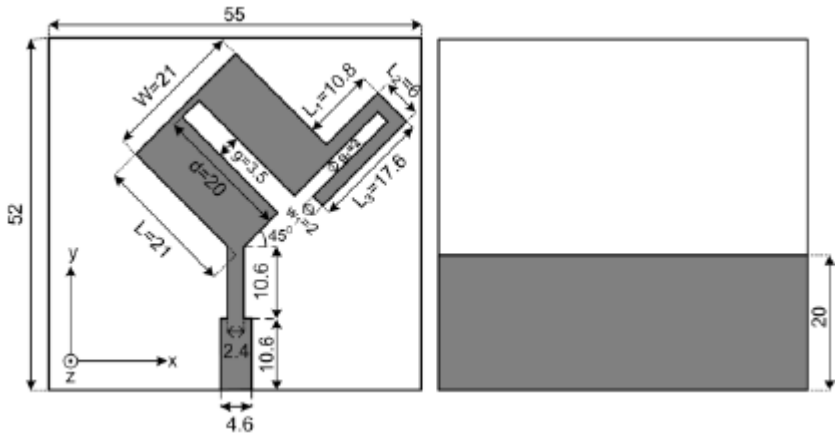

(b)

Figure 8 Configuration of the proposed quad band CP antenna. (a) Top view (b) Tri-band (without FSS)

In 2016, R. S. Brar, et al [20], had investigated a triple CP band with a dual sense for GPS, LTE, and UMTS applications by using an antenna with Y-shaped radiator which printed on FR4 substrate and on another side, the partial ground plane with slot-loading as shown in Figure 9. The triple-band operation is obtained because of the resonances of unequal monopole arms in addition to that, the L- shape slot in the partial ground plane. The antenna exhibits IBWs of 13.1, 9.7, and 7.4% at the frequencies of 1.57, 2.02, and 2.55 GHz, respectively. At these three resonances, 3-dB ARBWs of 3.7, 4.9, and 5.06% are implemented. The antenna dimensions are 45×65×1.6 mm^3.

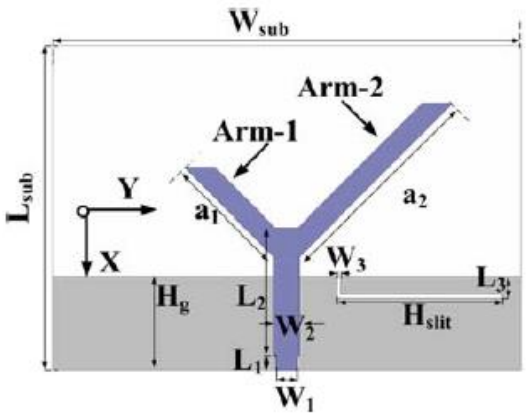

Figure 9 The geometry of the Y- shaped multiband CP antenna

In 2017, Wang, et al [21], a dual-band dual sense CP antenna implemented by a capacitively-loaded annular ring slot as seen in Figure 10. To obtain dual sense CP, two capacitances are embedded across the outer and inner annular ring slots at opposite

positions with respect to the direct feed line. The designed antenna operates at (1.527 – 1.917 GHz) and (2.598 – 3.248 GHz) whereas AR at 3-dB is (1.579 – 1.637 GHz) for the lower band and (2.670 – 2.822 GHz) for upper band. It printed on FR-4 substrate with relative permittivity ε_r = 4.4, loss tangent tanδ = 0.02. The overall dimensions are 55×66×1.6 mm^3.

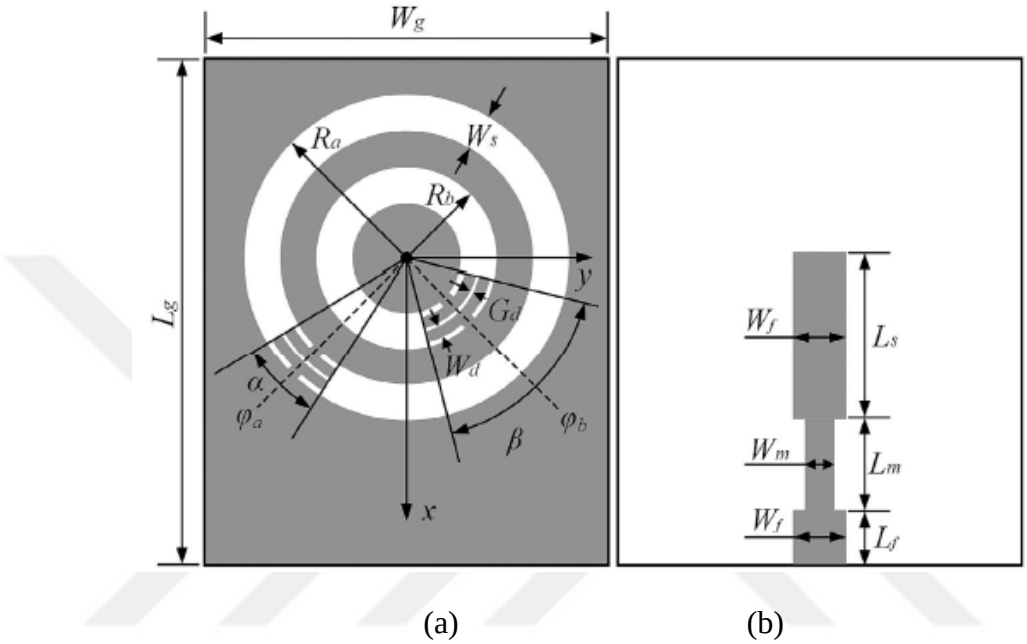

Figure 10 The geometry of capacitive load dual band dual sense CP antenna (a) Top view, (b) Bottom view

In 2017, S. Patil, et al [22], had designed a wide slot antenna for dual-band and dual sense CP. The radiator composed of a C-shaped patch and a wide square slot embedded on the ground with pair strips for generating a CP at two bands. As illustrated in Figure 11, the radiator printed on top of the substrate FR4 type whereas on the other side the square slot ring with two perturbation strips. the antenna operates at resonance frequencies 2.38 and 4.43 GHz whereas the percentage of AR at lower band and the upper band is 18.8% and 13.3% respectively. the volume of the antenna is 40×40×1mm^3.

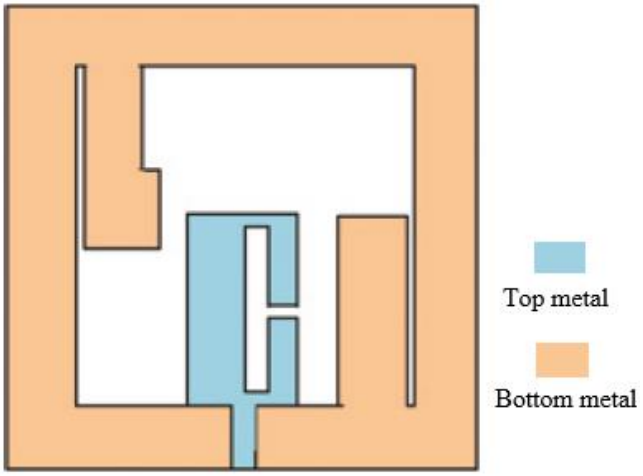

Figure 11 The geometry of C-shaped dual band dual sense wide slot antenna

In 2018, A. Altaf, and M. Seo [23], investigated a printed monopole antenna with dual-band dual sense CP. The combining of inverted C-shaped and tilted I-shaped led to construct the radiator which fed by microstrip feed line and printed on the top of Taconic TLY-5 substrate whereas on the other side is that partial ground plane as seen in Figure 12. The antenna provides IBW for -10 dB of (3.47–11.07 GHz) totally covering both CP bands with 3 dB ARBWs of (4.28–5.86 GHz) and (7.49–9.4 GHz) at lower and upper band respectively. The overall size of the antenna is 54×60×1.52 mm^3.

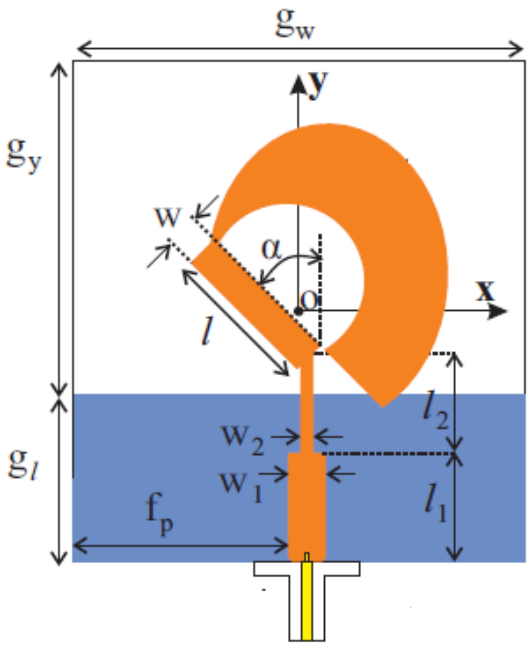

Figure 12 The geometry of tilted D-shaped dual band dual sense antenna

In 2018, R. K. Saini, and P. S. Bakariya [24], had configured the slot antenna which excited by the coplanar waveguide. The radiator consists of an F-shaped feed line and parasitic elements for dual-band and dual sense CP whereas the ground plane is asymmetric rectangular slot as shown in Figure 13. The radiator and ground plane printed on an FR4 substrate with a dielectric permittivity of 4.4 and loss tangent tanδ=0.02. The antenna had overall size 63.5×55×1.6 mm^3. The measured IBWs are (1.57GHz–2.04 GHz) and (2.87GHz–3.47GHz) for the lower and upper band respectively. The measured ARBWs under 3-dB is (1.6 GHz–2GHz) and (3.15GHz–3.5GHz) for the lower and upper band respectively.

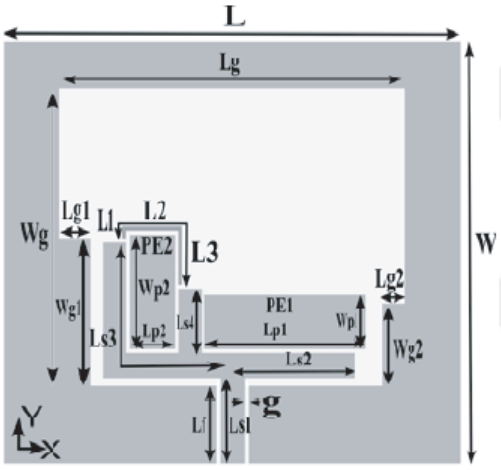

Figure 13 The geometry of wide slot dual band dual sense CP antenna with CPW-fed

In 2019, P. K. T. Rajanna, et al, [25] had proposed a square slot antenna excited by CPW fed. The slot is a hexagonal shape loaded with split ring resonators (SRRs) as seen in Figure 14. The antenna provides three CP bands. First band at 4.15 GHz which produced because of the hexagonal slot whereas the other two bands (4.77 and 5.1 GHz) obtained via loading parts (split-ring resonators). The measured results exhibit IBW of 64.54% and ARBWs of 11.76%, 1.9%, and 3.87% at first, second, and the third band, respectively.

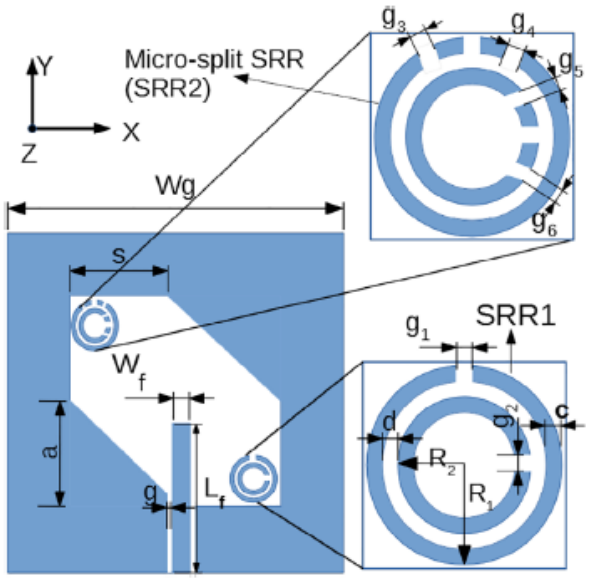

Figure 14 Configuration of hexagonal slot antenna loaded with the SSRs

1.5 The Main Goals of This Thesis

The goal of this dissertation is to design and analyze a compact multiband circular polarization printed antennas by using a single-layer substrate FR4 type. These new antennas are suitable for employ in modern wireless applications such as GPS, GNSS, WiMAX, and satellite. The proposed CP antenna designs have been modeled, simulated and evaluated using reliable HFSS (high-frequency structure simulator) V.13.

1.6 Thesis Layout

This thesis is organized as follows:

- Chapter 2 includes the basic antenna parameters, modelling techniques and feeding methods..
- Chapter 3 exhibits the fundamentals of circular polarization antenna and its types.
- Chapter 4 contains the design, analysis, and results of the first proposed antenna with CP multi-sense and its modification depends on the open-loop hexagonal ring, and microstrip feed line.
- Chapter 5 contains the design, analysis, and results of the second proposed antenna and its modifications depend on circularly polarized square slot antenna (CPSSA).
- Chapter 6 involves the conclusion and suggestions for future work.

CHAPTER 2

BASICS OF ANTENNA PARAMETERS AND MODELLING TECHNIQUES

2.1 Introduction

This chapter represents the general parameters of the antenna as well as some specific parameters that are related to circular polarization. Furthermore, it displays antenna modeling techniques which comprise two main types: analytical methods and full-wave methods. In addition, the feeding methods are introduced and explained with details. The advantages and disadvantages of each one are clarified. Moreover, the benefits of circular polarization antennas.

2.2 Antenna Parameters

An antenna can be introduced is the first device from the receiving side and last inside of the transmission. When it's operating on the receive side, the main role will gather the radio signals (electromagnetic waves) from free space then, transfers them into guided waves in transmission lines and vice versa in the transmitting side. Sometimes, an antenna performs dual-task transmitting and receiving.

Figure 15 illustrates the basic concept of the transmitter system, which consists of three main components [1]. First is that radio transmitter, the work of it is that converting (processing) the information such as (voice, image, video or data) to signals which deliver and propagate into second part transmission line, then the guided wave signals converted to electromagnetic waveform by antenna and radiated (final stage).

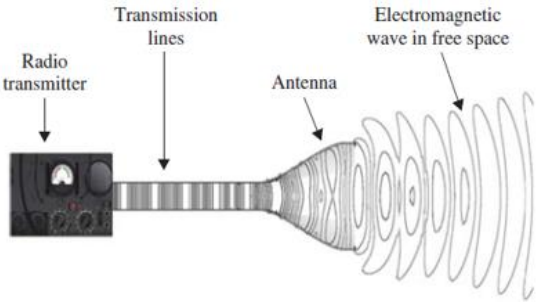

Figure 15 Components of a wireless system from the transmit side [1]

2.2.1 Input Impedance

The input impedance Z_{in} is that an impedance of the antenna at the connection point with the transmission line, or in the simplest form, it can be defined depending on Ohm's law is that the voltage to current at the connection point (feed point) with another part (transmission line) [4]. Z_{in} can be expressed a complex number and it also frequency depended the general expression is that

$$Z_{in} = R_{in} + jX_{in} \tag{2.1}$$

2.2.2 Reflection Coefficient and Return Loss

The reflection coefficient concept is related to input impedance Z_{in} from the antenna side and characteristic impedance $Z_\circ$ from the transmission side. So as to an antenna radiated efficiently, it should be matching with transmission line well, this is to inquire by making $Z_{in} = Z_\circ$, otherwise, the signals will be reflected (returned) to the signal source generator. Figure 16 describes the simple realize diagram between Z_{in} and $Z_\circ$, the Z_{in} of antenna considers a load impedance Z_L form view of the transmission

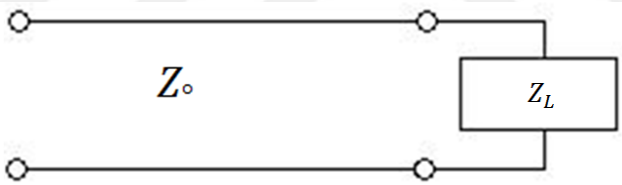

Figure 16 Realize diagram between $Z_\circ$ and ($Z_L = Z_{in}$)

Actually, the impedance of the end of the transmission line which feeds the antenna is that 50 Ω. Gamma (Γ) is known symbol of the reflection coefficient which can be defined that the ratio of reflected wave voltage (V^-) to incident wave voltage (V^+) so, it can be expressed as [4]:

$$\Gamma = \frac{V^-}{V^+} = \frac{Z_{in} - Z_\circ}{Z_{in} + Z_\circ} \tag{2.2}$$

From equation (2.2), if Z_{in} is equal to $Z_\circ$, it means that Γ equal to zero. In this case, there is no reflected wave voltage ($V^- = 0$).

Also, Γ can be presented (in dB) form is called Return Loss (RL), which can be expressed as:

$$RL = -20log|\Gamma| \quad (2.3)$$

2.2.3 Voltage Standing Wave Ratio (VSWR)

VSWR is one of the important indicators to identify antenna specifications. By invoking of it, the range of matching of the antenna from side and characteristics of transmission line and radio transmitter or receiver form another side can be known numerically by following the equation shown below [4,26]

$$VSWR = \frac{1+|\Gamma|}{1-|\Gamma|} \quad (2.4)$$

The equation (2.4), presents that it is a function of Γ, also it clarified that when the reflection coefficient equal to zero the VSWR will be one, means that no reflected power back towards power source, otherwise, it means that there is mismatch between Z_{in} and $Z_{\circ}$ leads to appears reflected voltage along the transmission line in form of peak and concave as seen in the Figure 17.

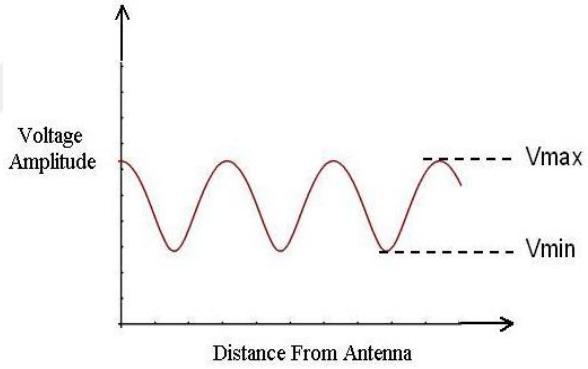

Figure 17 Voltage measured along a transmission line [27]

2.2.4 Radiation Patterns

The Radiation Patterns are an important indicator to study the radiation characteristics (power flux density, radiation intensity, field strength, directivity, phase or polarization) of the antenna in the space. Often, the radiation pattern is represented graphically in two dimensions (2-D) or three dimensions (3-D). Usually, it can be calculated and found in the far-field region and it's expressed as a function of directional coordinates. Figure 18 shows the allocation of radiated power, the most of power is concentrated along of the propagation direction (z-axis). As per Figure 18, there are four types of lobes; main, minor, side, and back lobes. The signs plus (+) and

minus (−) in the lobes presents the relative polarization of the amplitude between the various lobes, which alternates as the nulls are crossed [28]. Also, in the below figure, there are two new concepts, Half-Power Beamwidth (HPBW) and First-Null Beamwidth (FNBW). The HPBW describes as the angular width on the main lobe between two points where power is half of the maximum radiated power (i.e. -3-dB beamwidth) whereas, FNBW is angular width which is measured between first nulls or first side lobes on the antenna radiation pattern. The beamwidth of an antenna is a very significant figure of feature and often is employed as a trade-off between it and the side lobe level; that is, as the beamwidth reduces, the side lobe grows and vice versa.

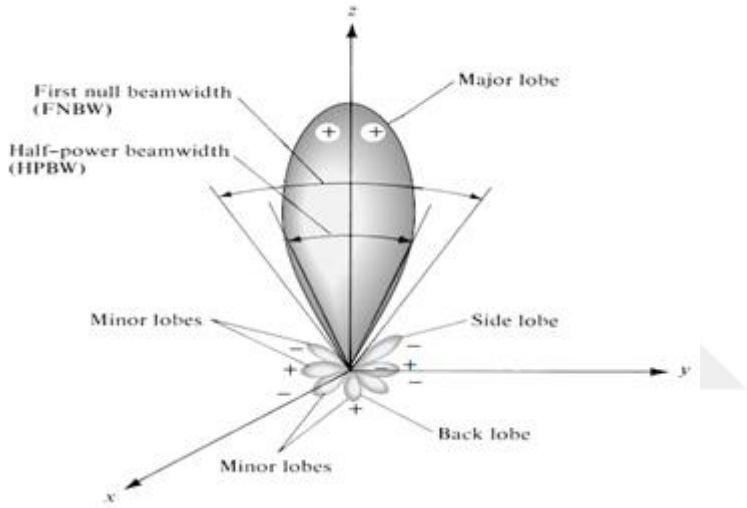

Figure 18 Radiation lobes and beamwidths of an antenna pattern [28]

Indeed, there are many types of radiation patterns, the common types in the following points:

- Isotropic: is an ideal radiator, it is possible when an antenna is lossless and it radiates in all directions with the same intensity.
- Directional pattern: it is defined when the power concentrated in direction is more than other directions. For instance, in the figure shown above, the power is centered on the evaluation angle along propagation direction.
- Omnidirectional pattern: radiation response will be distributed uniformly in one of plane such as azimuthal plane [f(ϕ),θ] as shown in Figure 19

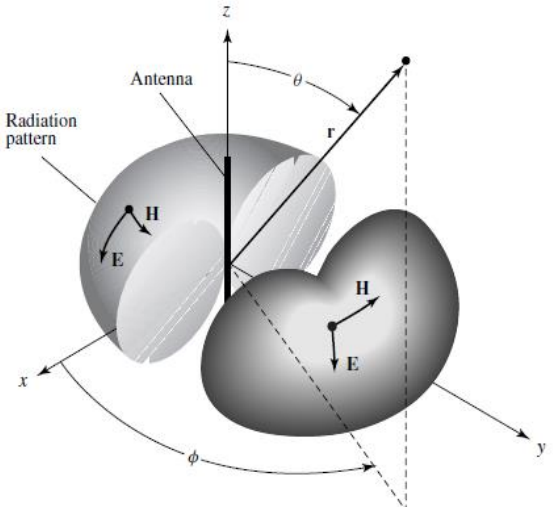

Figure 19 3-D omnidirectional antenna patterns [28]

2.2.5 Directivity

Directivity describes the ratio of radiation intensity for a directional radiation pattern as compared to intensity for all directions. The total power radiation by antenna divided by 4π is express the average radiation intensity. If the directions not specified, the direction of maximum radiation intensity is implied. [28]

In other meaning, the directivity for the directional radiation antenna is equal to its radiation intensity over than a homogenous (isotropic) source. So, depending on the definition, the directivity can be expressed by:

$$D = \frac{U}{U_\circ} = \frac{4\pi U}{P_{rad}} \tag{2.5}$$

Where U can be calculated by:

$$U = \frac{1}{2} r^2 Re[E \times H^*] \tag{2.6}$$

Substitution Eq. (2.6) in Eq. (2.5) then

$$D(\theta, \phi) = \frac{2\pi\, Re[E \times H^*]}{P_{rad}} \tag{2.7}$$

Where

D (θ, ϕ) is the directivity of an antenna as a function of the elevation angle and the azimuth angle.

U is radiation intensity (W/unit solid angle).

$U_\circ$ is the radiation intensity of isotropic source (W/unit solid angle).

P_{rad} is total radiated power (W).

E is the peak value of electric field intensity.

H^* is the peak value of magnetic field intensity conjugate.

r is the distance between the source and test point which is in the far-field region.

2.2.6 Efficiency

The efficiency of an antenna comprises to known the losses at the input terminals which can be calculated and demonstrated by invoking to gamma (Γ) and the losses at the structure of the antenna [28,29]. The losses at the input terminals can be expressed by:

$$\eta_r = 1 - |\Gamma|^2 \tag{2.8}$$

The η_r is the efficiency of wave reflection to power source.

The losses at the structure comprise conduction losses and dielectric losses. Figure 20 describes all the antenna losses

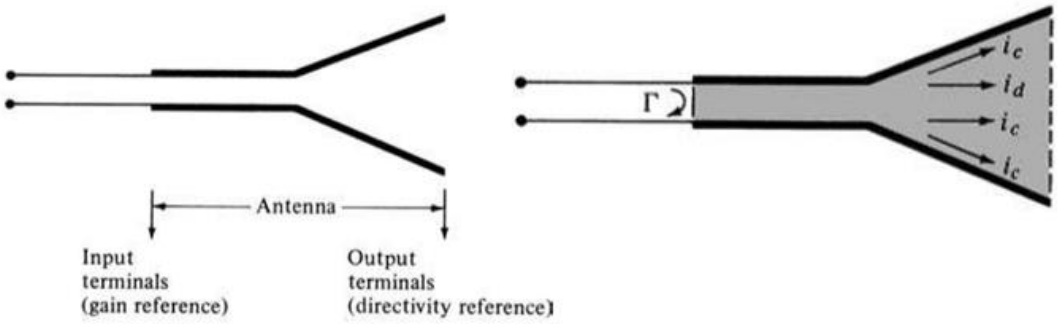

(a) (b)

Figure 20 Reference terminals and losses of an antenna: (a) Antenna reference terminals, (b) Reflection, conduction, and dielectric losses [28].

So, the overall efficiency ($\eta_\circ$) can be expressed by:

$$\eta_\circ = \eta_r \eta_c \eta_d \tag{2.9}$$

The η_c is the conduction efficiency while η_d is the dielectric efficiency these two efficiencies are not easy to compute so, they can be found experimentally. Actually, the η_c and η_d can be abbreviated in one term is that $\eta_{cd} = \eta_c \eta_d$ which is called antenna radiation efficiency and it plays an important role to determine the gain of an antenna.

2.2.7 Gain

The gain considers one of the important measurements to measure the performance of an antenna. In spite of it gets mainly depending on directivity, but the efficiency of the antenna should be found and taken into account additionally its directional abilities. Gain can be defined that the ratio of radiation intensity in a given direction to the radiation intensity that could be got if the power accepted by the antenna was radiated homogenously [28,29]. So, it can be expressed as:

$$Gain = 4\pi \frac{radiation\ intensity}{total\ input\ power} \tag{2.10}$$

Or it can be presented as:

$$G(\theta, \phi) = \eta_{cd} D(\theta, \phi) \tag{2.11}$$

2.2.8 Polarization

It is considered one of the essential characteristics of an antenna. Actually, polarization describes the orientation of the electric field along the propagation axis. Also, the polarization of the transmitted wave is introduced that the characteristic of an electromagnetic wave depicting the time changing direction and relative magnitude of the electric-field vector. Basically, it is classified into three main types [28,29]. First, is called linear polarization, when the electric field oscillates (varying with time) with respect to the single-axis along the orientation of radiation. Figure 21 presents the types of linear polarization. In the Figure 21 (a), the direction of the electric field with respect to y-axis means that the electric field varying vertically with time so is called vertical polarization whereas, in Figure 21 (b), the orientation of electric field with respect to x-axis is called horizontal polarization. The last one is the slant polarization, the electric field is tilted from x-axis in another meaning, it lies between x and y planes.

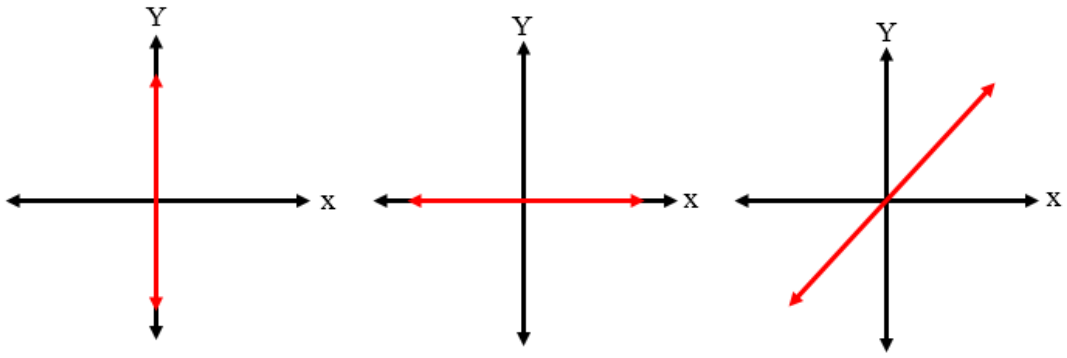

(a) (b) (c)

Figure 21 Types of linear polarization (a) Vertical, (b) Horizontal, (c) Slant.

The second one is that circular polarization, which means that the electric field rotates with respect to time and the magnitude of it along the axis will not change. For instance, consider that the propagation along the z-axis (time axis) with electric field $\overrightarrow{E}$ components in x and y directions [29]. When z=0, the time-harmonic electric field is presented as:

$$E = E_x \cos(wt) a_x + E_y \cos(wt + \delta) a_y \tag{2.12}$$

Where E_x and E_y is the maximum value of the electric field in x-plane and y-plane respectively whereas, δ is the phase angle which impels that y-directed vector is leading the x-directed counterpart. To imagine all polarization types, all of the hypotheses will be applied to the above equation.

1- When $E_x = E_y$, and $\delta = 0$, then E_x and E_y will become in-phase and the net vector tilted 45° from x-axis as shown in Figure 21(c)

2- If one of a component of an equation in above goes to zero, then the linear polarized wave is shown with respect to x-axis or y-axis.

3- If $E_x \neq E_y$, and $\delta = 0$, then the slant linear polarization will be seen and net vector tilted according to the following equation

$$\gamma = \tan^{-1}[\frac{E_y}{E_x}] \tag{2.13}$$

4- If the $E_x = E_y$, and $\delta = \pm 90$, in this case the field vector change in a circular path as can be shown in Figure 22

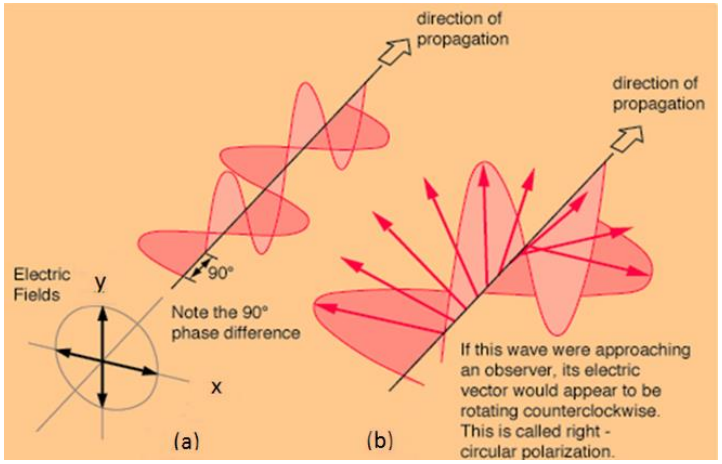

Figure 22 Circular polarization representation [30]

In the Figure 22 shown above, the field rotates with respect to time-varying in the direction of propagation. Indeed, the circular polarization (CP) can be classified into two kinds, first is that right hand circular polarization (RHCP) is called when the propagated wave rotates in a counterclockwise towards the observation point as shown in Figure 22 (b). Another type is the left-hand circular polarization (LHCP), is happens when the wave rotates clockwise towards the observer.

5- Elliptical Polarization (EP) is inquired if $E_x \neq E_y$, and $\delta \neq (0^{\circ} or\ 180^{\circ})$ or If $E_x = E_y$, and $\delta \neq 90^{\circ}$ or $(0^{\circ} or\ 180^{\circ})$ the field vector rotates in an elliptical form due to difference in vector length between field vectors or $\delta \neq 90^{\circ}$ as seen in Figure 23 the $E_x \neq E_y$. Actually, it is like to CP has two kinds right hand elliptical polarization (RHEP) and left hand elliptical polarization (LHEP).

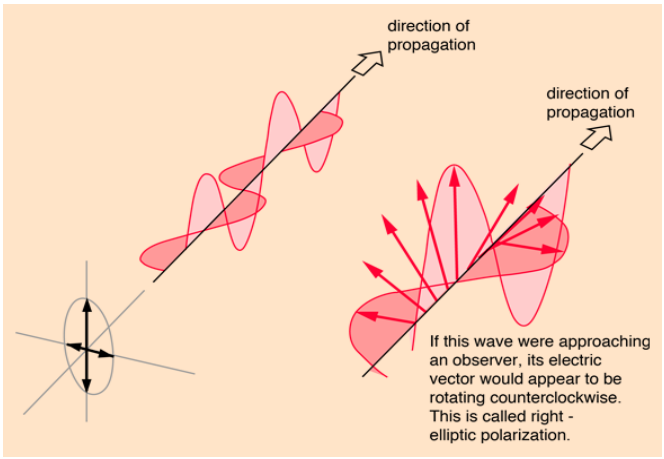

Figure 23 Right hand elliptical polarization [30]

2.2.9 Axial Ratio

Indeed, it is very hard to implement circular polarization practically. So, most of the antennas which have propagated CP wave are elliptical wave as shown in Figure 24. This elliptical wave considers CP if the Axial Ratio (AR) is less than or equal to 3dB in most of the researchers. The AR can be expressed as [31]:

$$AR = 20\log_{10}[\frac{a}{b}] \text{ (dB)} \tag{2.14}$$

Where a is the major axis of field vector whereas, b is the minor axis as seen in the Figure 24. So, the AR is a main key for identifying the circular polarization.

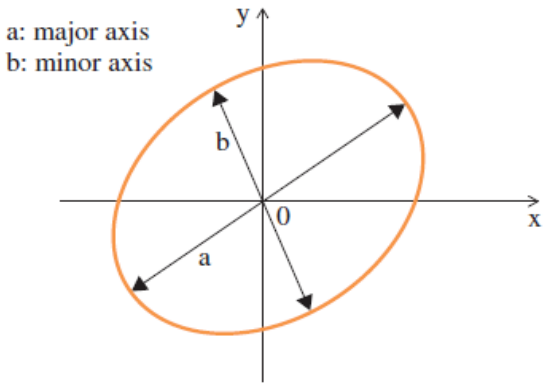

Figure 24 2-D elliptical polarization trace

2.2.10 Bandwidth and Resonant Frequency

Indeed, an antenna is engineered to work within the desired frequency range. The BW of an antenna is often obtained by the frequency range within which the main parameter of the antenna pleases a certain demand, for instance, the minimum S_{11} (Return loss) of -10 dB. At the resonant frequency of an antenna, Z_{in} is will be resistive. Usually, the resonant frequency is selected as the middle of the frequency bandwidth $f_\circ$ of an antenna. The BW of an antenna can be computed by appointing the upper f_2 and lower f_1 edges of the implemented frequency range [1,28]:

$$BW = \frac{f_2 - f_1}{f_\circ} \times 100\% \tag{2.15}$$

Notice that this introduction is for antennas with BW is less than 100%. For antenna has BW above 100%, the BW can be computed by employing the ratio between f_1 and f_2. For LP antenna Z_{in} is often resistive parameters as compared with the other

parameters such as gain, polarization. For this reason, the BW of LP antenna is usually indicated as the impedance bandwidth, but it can also be to achieve with others such as polarization, gain.

In the valuing the bandwidth of circular polarization (CP) antennas, the impedance BW and AR should be check, the impedance bandwidth in desired range frequencies must be less than or equal -10 dB and in the same time, the AR is less than or equal 3dB at these frequencies as seen in Figure 25 below [1]:

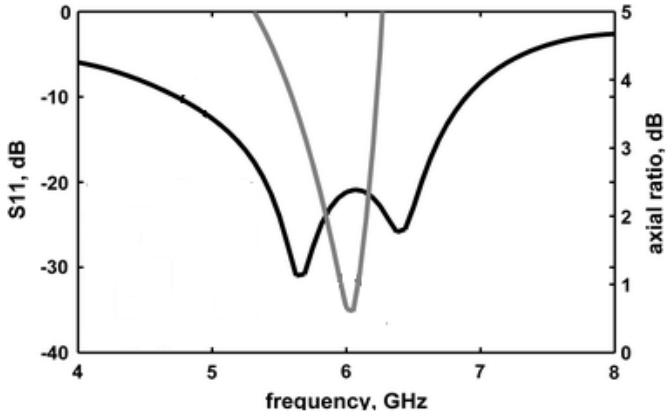

Figure 25 The |S11| and the AR of the CP antenna [1]

2.3 Scattering Parameters

Scattering Parameters depict the electrical attitude of the linear electrical network when subject to different steady-state stimuli by electrical waves. Generally, these parameters are beneficial for many branches such as communication systems particularly for microwave systems where signal power and energy regards are more readily measured than currents and voltages by VNA. The S-parameters employ the matched loads on the contrary of other parameters (Y, H, and ABCD parameters) [4]. Also, through the S-parameters, many electrical properties of networks can be presented like reflection coefficient, voltage standing, and gain.

The term scattering is more popular in optical systems than in the radiofrequency system. The scattering indicates to the route that traveling currents and voltages in the transmission line are impacted when they convene a discontinuity occurred because of the enrollment of a network in the transmission line.

Also, the scattering matrix offers a good depiction of a high-frequency network as noted in the matrix below by its N ports, in terms of the incident/reflected voltage traveling waves. For this reason, this matrix turned into a worthy tool to estimate the antenna performance. The scattering matrix for N port can be expressed:

$$\begin{bmatrix} V_1^- \\ V_2^- \\ \vdots \\ \vdots \\ \vdots \\ V_N^- \end{bmatrix} = \begin{bmatrix} S_{11} & S_{12} & \dots & \dots & S_{1N} \\ S_{21} & S_{22} & \dots & \dots & S_{2N} \\ \vdots & \vdots & & & \vdots \\ \vdots & \vdots & & & \\ \vdots & \vdots & & & \vdots \\ S_{N1} & S_{N2} & \vdots & \vdots \quad \vdots & S_{NN} \end{bmatrix} \begin{bmatrix} V_1^+ \\ V_2^+ \\ \vdots \\ \vdots \\ \vdots \\ V_N^+ \end{bmatrix} \tag{2.16}$$

An element of the matrix $[S]$ is known as:

$$S_{ij} = \left. \frac{V_i^-}{V_j^+} \right|_{V_k^+ = 0 for\ k \neq j} \tag{2.17}$$

Meaning that S_{ij} (transmission coefficient) can be found by putting through port j an incident voltage wave of amplitude V_j^+ and measuring the reflected wave amplitudeV_j^- from port i [4].

2.3.1 Scattering Matrix for Two Inputs – Two Outputs System

In two inputs and two outputs system, the scattering matrix 4×4 has been built as shown in Eq. (2.18) which means that sixteen types of S-parameters appeared start from$S_{11}$and ends with S_{44}. These parameters can describe the relationship between the reflected and incident power signals at four ports.

$$\begin{bmatrix} a_1^- \\ a_2^- \\ a_3^- \\ a_4^- \end{bmatrix} = \begin{bmatrix} S_{11} & S_{12} & S_{13} & S_{14} \\ S_{21} & S_{22} & S_{23} & S_{24} \\ S_{31} & S_{32} & S_{33} & S_{34} \\ S_{41} & S_{42} & S_{43} & S_{44} \end{bmatrix} \begin{bmatrix} a_1^+ \\ a_2^+ \\ a_3^+ \\ a_4^+ \end{bmatrix} \tag{2.18}$$

$$a_1^- = S_{11}\, a_1^+ + S_{12}\, a_2^+ + S_{13}\, a_3^+ + S_{14}\, a_4^+$$

$$a_2^- = S_{21}\, a_1^+ + S_{22}\, a_2^+ + S_{23}\, a_3^+ + S_{24}\, a_4^+$$

$$a_3^- = S_{31}\, a_1^+ + S_{32}\, a_2^+ + S_{33}\, a_3^+ + S_{34}\, a_4^+$$

$$a_4^- = S_{41}\, a_1^+ + S_{42}\, a_2^+ + S_{43}\, a_3^+ + S_{44}\, a_4^+$$

The positive sign on the letter (a) indicates the forward traveling waves while the minus sign presents the backward traveling waves. To obtain the S-parameters, for one of the ports for example port 1 as illustrated in Figure 26, a signal fed (injected) the port1 whereas other input ports put zero. This means that the ports 2, 3, and 4 are no signal injected are match terminated so no reflection happens (a_2^+=a_3^+=a_4^+=0). Then the equation will be:

$$a_1^- = S_{11}\, a_1^+$$

$$a_2^- = S_{21}\, a_1^+$$

$$a_3^- = S_{31}\, a_1^+$$

$$a_4^- = S_{41}\, a_1^+$$

So, when the port 1 injected also, and a_x^+=V_x^+ and a_x^-=V_x^-, where x=1,2,3,4

The S-parameters for port1 will be

$S_{11} = \frac{a_1^-}{a_1^+} = \frac{V_1^-}{V_1^+}$, $S_{21} = \frac{a_2^-}{a_1^+} = \frac{V_2^-}{V_1^+}$, $S_{31} = \frac{a_3^-}{a_1^+} = \frac{V_3^-}{V_1^+}$, and $S_{41} = \frac{a_4^-}{a_1^+} = \frac{V_4^-}{V_1^+}$

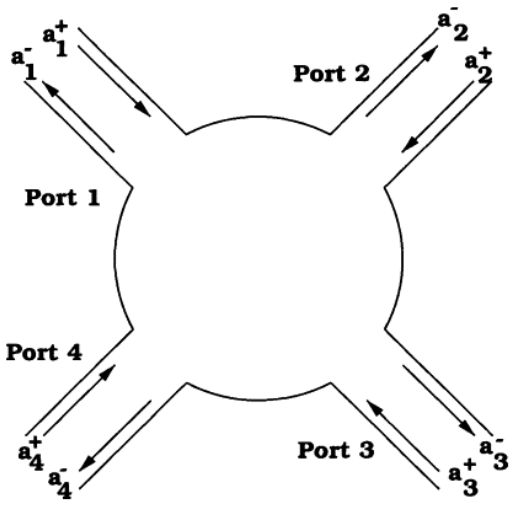

Figure 26 Two inputs –two outputs ports system [32]

The same operation can be repeated to other ports to complete all of the scattering matrix parameters. The main diagonal elements of the above scattering matrix

represent the reflection coefficients which refer to how much of the reflected signal in the transmission medium at the same port while the others express the forward signal.

2.4 Antenna Modeling Techniques

The operating principles, developing a new design, and modifying an already existing design can be realized through the analysis of the antenna. The different radiation characteristics like reflection coefficient, radiation pattern, gain, polarization, and efficiency, etc. can be indicated during this analysis.

Actually, there are two general types of analysis. First, it's called analytical methods which are used efficiently for simple structures with regular patch shapes. They offer simplicity at the expense of precision. On the other hand, full-wave methods build on numerical techniques that are highly precise but strict in the procedure. The prominent analytical and full-wave methods are shown in Figure 27.

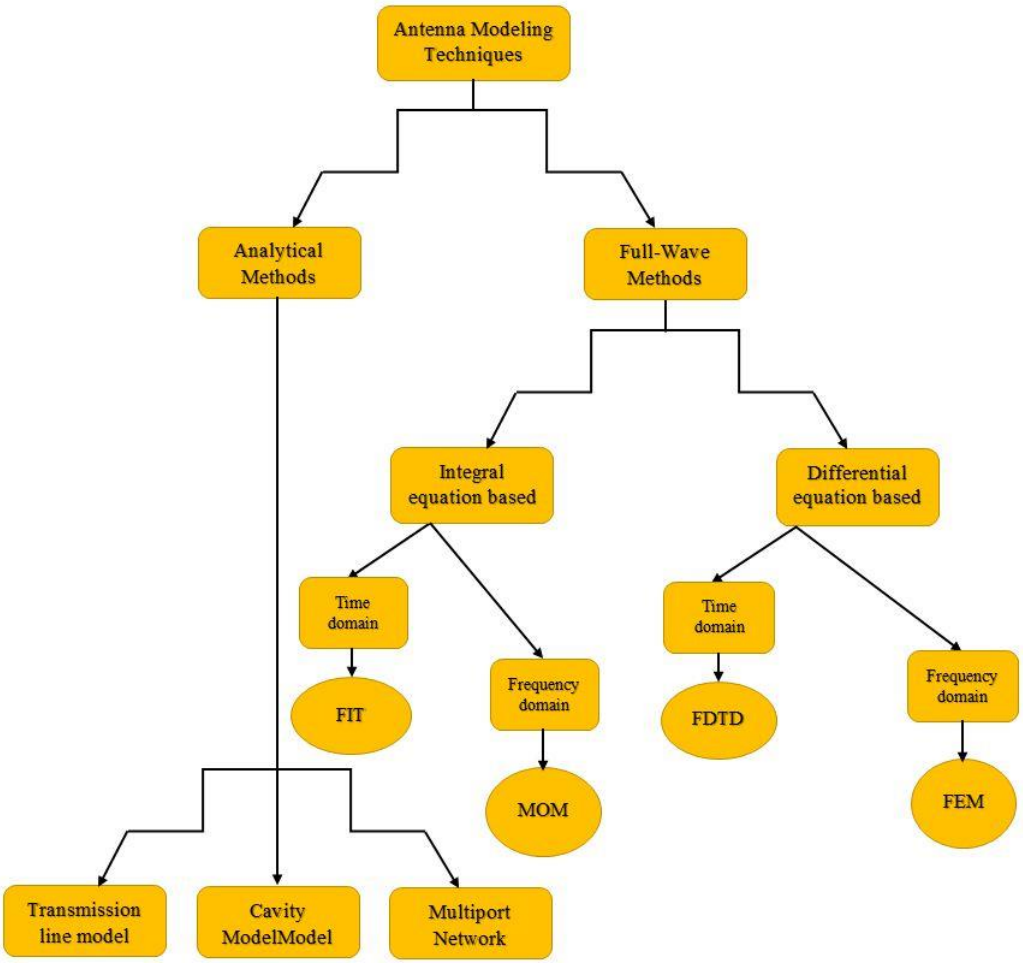

Figure 27 Diagram of antenna modeling techniques

2.4.1 Analytical Methods

Actually, the CP antenna has been passed to many analytical methods. The purpose of these methods is to provide a visual perception about the operation of antenna and its characteristics such as directivity, gain, efficiency and so on. Indeed, these approaches able to apply for all types of CP antenna such as microstrip, wire, helical and so on. Moreover, they are very beneficial to extend a good insight into the physical mechanism of its functionality but the defect of these models is that poor precision due to they rely on some approximate presumptions. The famous analytical methods used are [33,34]:

2.4.1.1 Transmission Line Model

This mechanism sophisticated by Munson [35] was going early to analyze a rectangular microstrip antenna. Indeed, in this model, the patch is dealt with as a transmission line resonator with no transverse fields whereas the radiation at most happens because of the fringing fields at the open-circuited ends. Also, the effective dielectric (ε_{reff}) constant is held a little less than the dielectric constant (ε_r) of the substrate so that the fields not completely get reserved to the substrate but also fringe and disperse in the air as shown in the Figure 28

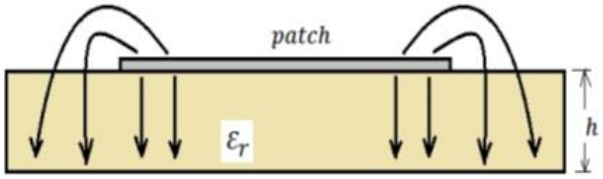

Figure 28 Transmission line model

Figure 29 presents an antenna as a transmission line diagram. The diagram contains two slots, the apace between two slots expressed by the length of the resonator represents the patch. Because this model does not take care of the difference of field in the perpendicular direction to the direction of propagation, all types of geometries cannot be analyzed using this method. However, it is easy to apply.

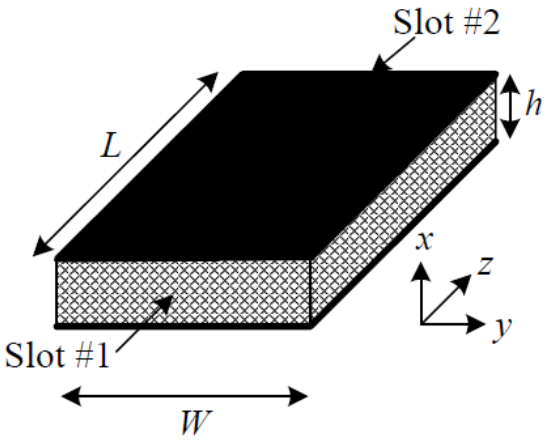

Figure 29 Transmission line and its equivalent model

2.4.1.2 Cavity Model

The cavity model is based on the supposition that the area between patch radiator and ground is a resonance cavity, which is encompassed by electric fields on the top and bottom surface and magnetic on the external surface as shown in the Figure 30

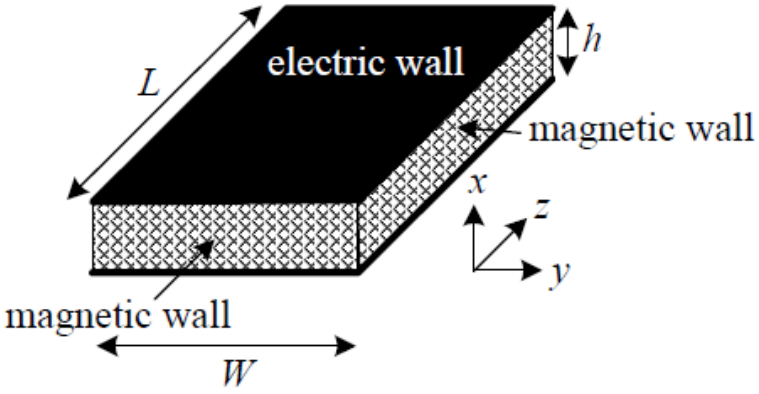

Figure 30 Cavity model diagram

The λ (wavelength) is larger than the thickness of the substrate thus the field inside the two surfaces stay uniform along the substrate but the magnetic current counts the far fields and radiation [36].

2.4.1.3 Multiport Network Model

This model is a stretch of the cavity model. The electromagnetic fields bottom the patch and those outgoing the patch are individually patterned. The patch is fashioned

as a 2-D (two dimensions) planer network, with a large number of ports coordinated around the ends. The outer fields are expressed by equivalent networks attached to these ports [37]. The total impedance matrix is estimated by the division (segmentation) approach. By invoking voltage allocation around the outer edge, the radiation field can be evaluated.

2.4.2 Full-Wave Methods

The underrating of electromagnetic theory considers the main key to build an antenna properly. Indeed, there are many ways to implement an antenna. First, it can be performed by using a closed-form analytical solutions which are applicable for a few simple and uniform shapes under perfect conditions. Another approach is going to the experimental implementation of an antenna; this approach considers a lousy way since it is wasting money and time. An optimized solution for this issue is invoking a numerical technique and synchronism with a modernistic computer to investigate and simulates the performance of an antenna quickly. Numerical techniques indicate the approach of solving relevant Maxwell's equations by transferring them into matrix or chain equations, which can be fixed either by iteration or by matrix inversion. They are generally categorized depending on the kind of Maxwell's equations employed; Differential Equation methods and Integral Equation methods [29,38]. These methods are categorized further into two kinds; Time Domain (TD) and Frequency Domain (FD). An example of Frequency Domain Integral Method is the Method of Moment while an example of Time Domain Differential Equation is the Finite Difference Time Domain (FDTD) method. Each method has its own abilities and restrictions. It is more appropriate to utilize the most effective technique for a particular problem. In this chapter, four main numerical methods are indicated briefly.

2.4.2.1 The Method of Moments (MOM)

MOM is categorized as a Frequency Domain (FD) method, The MoM this an of an efficient way to the solution of Maxwell's Integral Equations (IE) by finding boundary value problems with the aid of IE. The first application of this method to solve IE came from Harrington's paper in 1967 [39]. It includes converting an integral equation into a set of linear equations in matrix style and then finding the solution by inverting the unknown matrix. This technique works effectively for wires and flat plates or planar

construction in general and resonators [40]. However, it is inappropriate for applications that contain pulse excitations. Examples of vastly employed MOM based commercial software are FEKO (The name is derived from the German abbreviation "FEldberechnung für Körper mit beliebiger Oberfläche", which can be interpreted as "field calculations involving bodies of arbitrary shape" [41], NEC (Numerical Electromagnetics Code) [42].

2.4.2.2 Finite Difference Time Domain (FDTD)

This approach can solve Maxwell's Differential Equations in time domain form. The mechanism of this approach is that dividing the shape into a grid of nodes [43,44]. After that, Maxwell's Differential Equations and boundary conditions are manipulated into a set of linear equations on the grid points [45]. Indeed, FDTD has advantages and disadvantage, one of the benefits is that it involves a wide response with a single excitation and fixing arbitrarily 3-D structures [29]. It is advised for geometries with few numbers of ports. On another hand, the disadvantage is that the structures must be dividing of special scale otherwise it may be effective to the accuracy of results, for this reason, it is not effective with thin structures. Furthermore, it takes some time. Examples of commercial software are Apsim FDTD [46] and Remcom XFDTD [47].

2.4.2.3 Finite Element Method (FEM)

FEM is located under a frequency domain method; it considers an efficient method to solve the Maxwell's Differential Equations [48]. Besides, it's qualified to analyze any non-uniform structures eligibility. The principle work of it is similar to the superposition method by dividing (discretizing) the geometry into small elements, then collect the sub-geometries' equations in a matrix form [45]. This approach is advised for geometries that have a large number of ports such as ICs. Ansoft HFSS [49] is regarded as one of the major commercial software based on FEM. It has been employed in this dissertation to simulate some multi-band CP antenna designs.

2.4.2.4 Finite Integral Technique (FIT)

The FIT was first displayed in 1977 by Prof. Thomas Weiland [50]. It considers an efficient way to solve Maxwell's Integral Equation in time domain form. FIT employs

each six vector components of electric field strength and magnetic flux density on a dual grid configuration; space and time which yield discrete grid equations [51]. Also, it's similar to the FDTD method, but it's more effective than FDTD when the structure more complicated and contains curved boundaries. The Computer Simulation Technology (CST) microwave studio [52] is deemed as the major commercial software that is based on it.

2.5 Feeding Methods

A planner antenna can be excited by different methods as illustrated in Figure 31. These methods can be divided into two types according to connectivity [33]. The first type is the contacting, which the feed line is connected directly to the radiator like microstrip line feed and coaxial probe feed. Another type is non-contacting which is not connect directly to the radiator such as proximity coupled feed and aperture coupled feed.

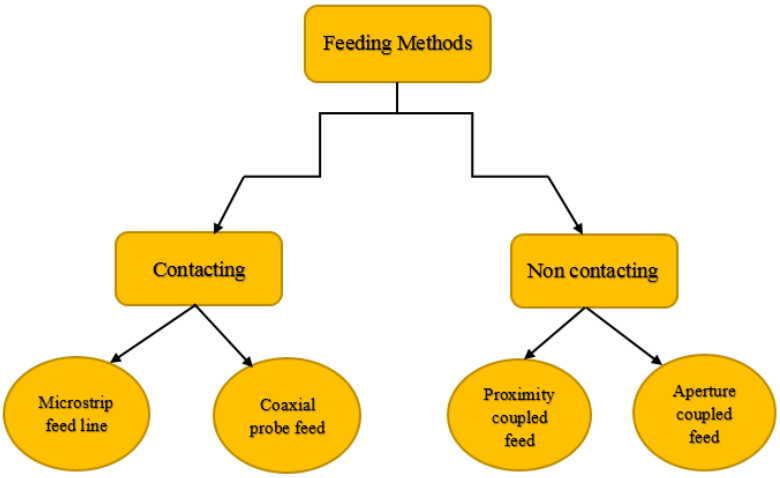

Figure 31 Diagram of feeding types

2.5.1 Microstrip Line Feed

This approach of feed considers one of the simple types, which contacts directly to the radiator part as noted in Figure 32. In addition, this approach is called edge feed because of contacting strip is linked to an edge of the feed. The defect of this type is the appearance of bogus radiations from the transitions, bends, and junctions which affect negatively cross-polarization levels and the side lobe of the antenna [53,54].

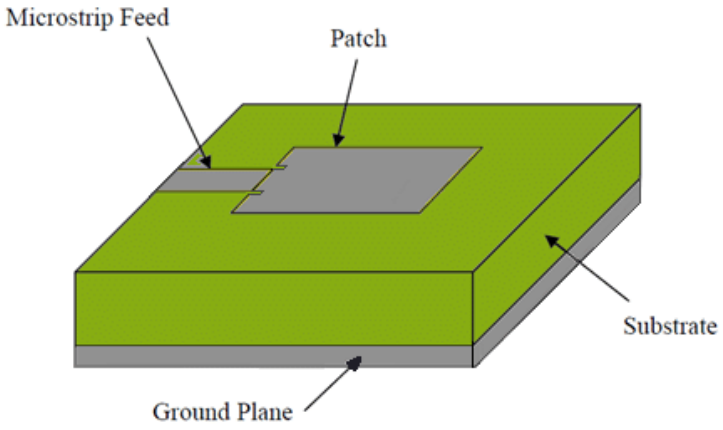

Figure 32 A planar antenna excited by a microstrip line [53]

2.5.2 Coaxial Probe Feed

This type of feed is the traditional type for microstrip antennas usually when the antenna consists of the multilayer. The conductor inserts through all layers and contact to the patch. The outer conductor is set on the bottom of the ground plane as seen in Figure 33. Employing this scheme, the feed can be appropriately put on any point on the patch that gives the best impedance matching. In CP antennas, the feed position at the radiator can define the circular polarization wave-type RHCP or LHCP [55]. The benefits of coaxial probe feed are easy to fabrication and match also, low bogus radiation whereas, the drawbacks are that the bandwidth is narrow as compared to microstrip feed line type. Also, difficult to model it especially when the substrate is thick [54].

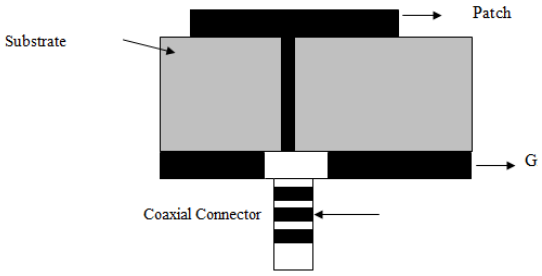

Figure 33 A planar antenna excited by a coaxial probe [53]

2.5.3 Proximity Coupled Feed

This approach is also renowned as an electromagnetically coupled feed. This type of feed can be used when the antenna contains two layers of substrate. As seen in Figure

34, the microstrip feed line is placed between the substrates with different relative permittivity. However, this causes complications in the alignment of the patch and the feedline, for this reason, the fabrication will be more difficult [56]. On the other hand, using this technique leads to suppresses spurious feed radiation and improves the bandwidth reach to 13% because the overall thickness antenna is increased.

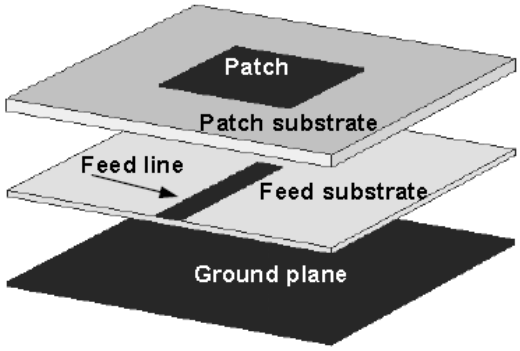

Figure 34 A planar antenna excited by proximity coupled [53]

2.5.4 Aperture Coupled Feed

This technique also stands to multilayer principle but the difference is that the ground plane is lies between the microstrip feed line and the upper substrate as noted in Figure 35. A feed line on the top of the lower substrate is electromagnetically coupled to the radiator (patch) through an aperture or slot, which etched from the ground plane. The amount of coupling from the microstrip feed line to the radiator is depended on many parameters such as the shape, size, and location of the aperture. This aperture must be aligned properly under the patch and far completely from the edge of the patch to avert backward radiations. The antenna which stands on this type of feed provides a high bandwidth of about 21% [54]. Also, the effect of spurious radiation is reduced significantly as compared to others. The disadvantage of this technique is that it is hard to fabricate because of multiple layers.

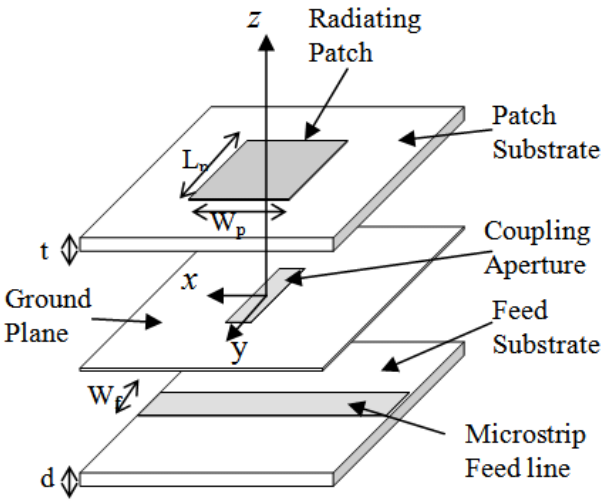

Figure 35 A planar antenna excited by aperture coupled [53]

2.6 Advantages of CP Antennas

There are many advantages of antenna, which has a circular polarization characteristic. So, it entered for many wireless applications such as satellite communication, mobile communication, global navigation satellite systems (GNSS) and so on. As it's known, when a transmitted wave that has not circular polarization characteristic collides to ground, buildings or any object losing a ratio of it and reflected causing weak in sending a wave. The wave has circular polarization merit overtakes this obstacle easily [1]. For instance, when the radiated wave with RHCP collides to any object, the ratio of reflected will be LHCP which puts out by RHCP thus the CP considers one of the solutions for struggling the multi-path phenomenon.

When an antenna radiates linearly polarized wave, it is affected to Faraday rotation in the ionosphere layer which causes a signal loss is not less than 3-dB. This issue can solve by changing the type of polarization from linear to the circular which weakens the Faraday rotation in the ionosphere layer [7, 8]. For this reason, an antenna with CP characteristic is wildly employed for space probes and ballistic missiles and so on. Another feature of employing an antenna with CP is that no need for the strict orientation between sending and receiving antennas. In contrast, the LP antenna required strict orientation to avoid mismatch losses.

CHAPTER 3

FUNDAMENTALS OF CIRCULAR POLARIZATION ANTENNA

3.1 Introduction

This chapter considers the actual entrance to the circular polarization antennas. In the first, the basic concepts about the generation of CP have been exhibit in a simple way. Moreover, the common types of it have been explained briefly. Then, the special techniques that are related to generation multi-band CP have been presented whereas, the last part described the major challenges that facing the researchers in CP antennas design.

3.2 Generation of CP Waves

The circular polarization wave comes from two linear polarization waves. Each of LP wave is perpendicular to other further the phase time shift between them is π/4. Besides, the amplitude of these two vector fields should be equal. Relying on this introduction, the CP manufacturing may demand dual feeding which leads to an increase in physical size and intricacy. For instance, a CP can be generated by using a square patch with feeding two edges [1, 56, 57] as shown in Figure 36. As an alternative, a patch of antenna excited with single feed with a hybrid π/4 is operates as a phase shifter, to the two branches feed to a circular patch at two orthogonal points as seen in Figure 37 [58].

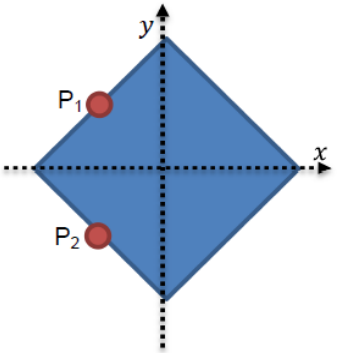

Figure 36 Dual feed CP square patch antenna [57].

In [59], there are four feeding port employed with phase difference one to other by π/4, for getting a wideband CP radiation purpose. Another usage of dual feed with hybrid is that is used as an alternative of field rotation.

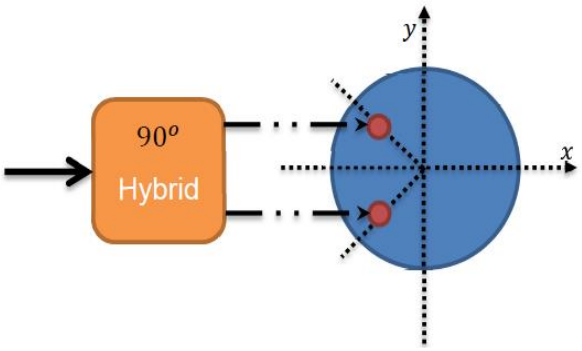

Figure 37 Single feed CP circular patch antenna with a 90º hybrid [57]

For example, the circular patch with dual-feed with a hybrid is presented in Figure 38. The dual arms can be used to generate the RHCP and LHCP [4,5]

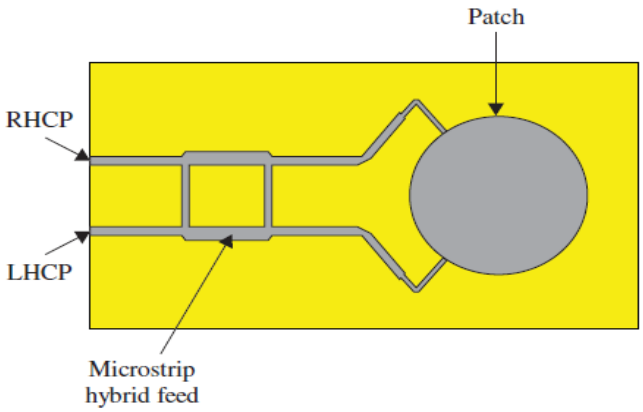

Figure 38 A circular patch integrated with a hybrid coupler [1]

The parameters such as the radius of the circular patch and desired frequency can be calculated by using the following equations [28, 60]:

$$F = \frac{8791\times10^9}{f_\circ\sqrt{\varepsilon_r}} \tag{3.1a}$$

$$a \approx \frac{F}{\sqrt{1+\frac{200h}{\pi\varepsilon_r F\left[\ln\left(\frac{\beta F}{200h}\right)+1.7726\right]}}} \tag{3.1b}$$

Where a is the radius of circular patch.

$f_\circ$ is the resonant frequency of the CP antenna.

ε_r is the relative permittivity of the dielectric substrate.

h is the thickness of the substrate.

Gradually, most of the researchers went toward a single feed excitation for generating CP waves because it considered one way to reduce the size of the antenna and be low profile. This is implemented by introducing perturbation in the antenna patch. This technique can be creating a rearrangement of fields on the patch, this exploited make fields perpendicular one to other with the same amplitude. Figure 39 displays six different structures of single-feed circular polarization microstrip patch antennas [4,56]. For instance, Figure 39 (a) displays an elliptical patch which excited along a line 45° from its major axis. The patch can be considered as a circular with perturbations, which employed to two perpendicular modes with a 90° phase difference. The CP wave can be got by employing a single feed elliptical patch, the proportion between the major axis and minor axis is given by:

$$\frac{a}{b} = 1 + \frac{1.0887}{Q} \tag{3.2}$$

The Q is symbolizing a quality factor that can be calculated by invoking to cavity model [28,56]. Alternatively, it can be measured experimentally, or employ results from a full-wave electromagnetic analysis to estimate value Q.

$$Q = \frac{f_{\circ}}{\Delta f}\frac{VSWR-1}{\sqrt{VSWR}} \tag{3.3}$$

The $f_{\circ}$ is the resonant frequency of an antenna and Δf is the bandwidth of an antenna. Figure 39 (b) indicates a closely square patch as another form of single-feed CP. The feed point lies along the diagonal line of the patch. For CP generation efficiently, there is a condition should be satisfied. This condition expressed as:

$$L = W(1 + \frac{1}{Q}) \tag{3.4}$$

Where the parameters L and W are represented to length and width of rectangular patch respectively. The quality factor Q can be calculated employing the Eq. (3.3). Further, the length and width of the rectangular microstrip patch can play an important role to determine first and last edges resonant frequencies ($f_1$andf_2) which can be computed depending on the following equations:

$$f_1 = \frac{f_\circ}{\sqrt{1+\frac{1}{Q}}} \tag{3.5}$$

$$f_2 = f_\circ\sqrt{1+\frac{1}{Q}} \tag{3.6}$$

Where $f_\circ$ is the center frequency of the bandwidth.

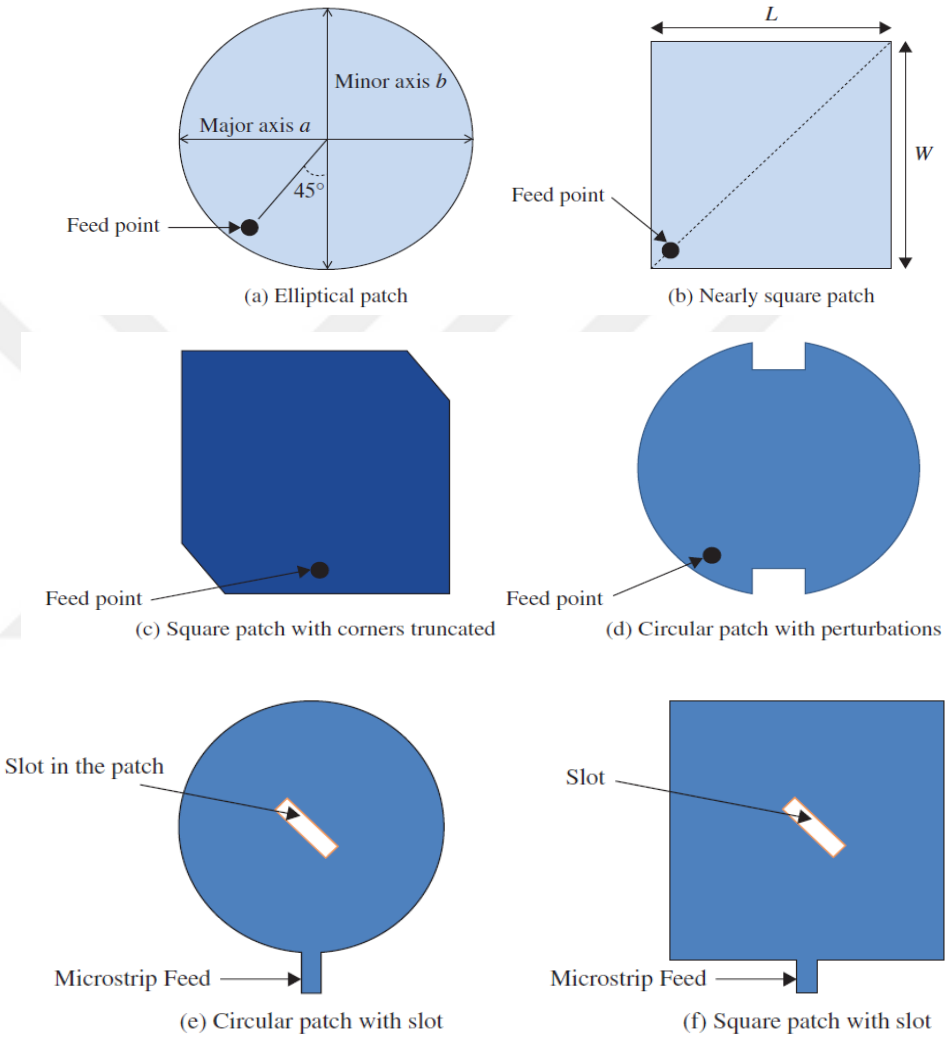

Figure 39 Single feed CP patch antenna [4]

Figure 39 (c) and (d) present a perturbation by truncation. Both patches are truncated from sides that have effected directly to field arrangement and radiation. Actually, these kinds of patch excited by probe feed. Another face of perturbation is exciting in Figure 39 (e) and (f) by etching the center of the patch and making a slanted slot. Indeed, the circular and square patches are considered basic patches and other patches can be derivative from these shapes such as pentagons and annual elliptic patches

which are used to produce CP waves [4,56]. The main defect of the single feed technique is a narrow band axial ratio achievement typically 1-2%.

3.3 Popular CP Antenna Types

3.3.1 CP Microstrip Patch Antennas

Microstrip patch antenna considers one of famous kind of antennas, since its benefits of low profile, plain fabrication, inexpensive. CP in patch antennas can be implemented employing a multi-feed technique or a single-feed technique [28,29,60-63]. Figure 40 clarifies a simple circular polarization microstrip patch antenna employing a dual-feed approach. The top and side views of the antenna are illustrated in Figure 40. To generate CP, a square microstrip patch is excited by two perpendicular microstrip feedlines as noted in Figure 40 (a). Both microstrip feed lines feed the patch antenna in TM_{01} and TM_{10} modes For this reason, it radiates both a horizontally and a vertically polarized wave together [28,29, 60-63]. A microstrip hybrid is used in Figure 40 (a) to generate a 90^0 phase difference between two perpendicularly polarized waves. Figure 40 (b) clarifies the side view of the antenna. The patch (radiator) on the top of a dielectric substrate having thickness h and relative permittivity ε_r. The dielectric substrate is backed by a metallic ground plane. To configure the antenna resonant at a frequency $f_\circ$, the length L of the patch can be estimated by employing the following equation:

$$L \approx \frac{c}{2f_\circ\sqrt{\frac{\varepsilon_r+1}{2}}} \tag{3.7}$$

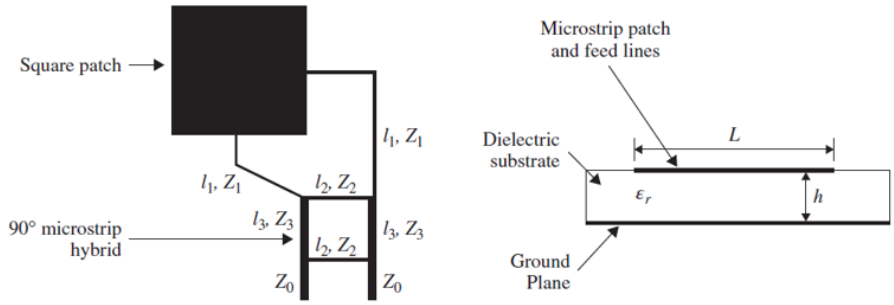

(a) (b)

Figure 40 Microstrip line feed patch antenna with a 90^0 hybrid (a) Top view, (b) Side view [1]

Where c is the velocity of light. To achieve accurate antenna designs, full-wave electromagnetic simulators can be employed to do simulations and optimizations of the dimensions of the antenna. The results from Eq. (3.7) can be used as an initial value for the antenna optimization. As illustrated in Figure 40 (a), there are two microstrip feed lines excited the square patch and two ports of the microstrip 90° hybrid. The microstrip line behaves as an impedance transformer between the input ports of the hybrid and the input of the antenna . The length (l_1) and impedance (Z_1) of the feed lines can be calculated by

$$l_1 = \frac{\lambda_g}{4} \tag{3.8}$$

$$Z_1 = \sqrt{Z_{in} Z_0} \tag{3.9}$$

Where λ_g is the guided wavelength of the microstrip line,

Z_{in} is the input impedance of the patch antenna.

Z_0 is the characteristic impedance of the microstrip line at the input of hybrid circuit.

The microstrip 90° hybrid circuit composed of four parts of microstrip lines. The following equations can be used to find the length and width of each part of microstrip lines:

$$l_2 = l_3 = \frac{\lambda_g}{4} \tag{3.10}$$

$$Z_2 = Z_0 \tag{3.11}$$

$$Z_3 = \frac{Z_0}{\sqrt{2}} \tag{3.12}$$

Where l_2 and l_3 indicate the length of microstrip lines as donated in Figure 39 (a), Z_2 and Z_3 symbolize the characteristic impedance of microstrip line parts presented in Figure 39 (a). The characteristic impedance of the microstrip line at the input of the hybrid circuit, Z_0, is usually selected to be 50 Ω. The microstrip hybrid circuit is fabricated easily and has been vastly employed in CP antennas . One obstacle of microstrip hybrid circuit is not compact.

Many approaches have been found to decrease the size of microstrip hybrid, for instance, by employing 'Π network' with one of the loading types such as stub loading or lumped element loading of transmission lines [64,65]. The hybrid circuit can be performed as well by utilizing lumped elements or left-handed transmission lines [64,65]. The circular polarization patch antenna can also employ other feeding configurations as probe feeds, slot coupled feeds, electromagnetically coupled feed and coplanar waveguide (CPW) feeds.

Figures 41 and 42 display a circular polarization patch antenna employing dual probe feeds, and a circular polarization patch with slot coupled feeds, respectively. Both the top view and side view of the antenna are noted in Figure 41. As observed, circular polarization is gotten by exciting a square patch with a 90° phase difference between two excited probes put symmetrically on the two perpendicular edges of the patch. In this status, an external phase shifter is demanded generating the 90° phase difference between two exciters. The antenna in Figure 42 uses a microstrip hybrid circuit for generating the 90° phase difference between two exciters. The microstrip hybrid is placed at the bottom of it, whereas coupled to the square patch on the top by two orthogonal slots truncated in the ground plane. The slot coupled circular polarization has been vastly employed in wireless systems during the last years, as it has many benefits compared with the same type of antennas which utilizing other feed configurations:

1. It grants the patch antenna and the feed circuits to use various dielectric substrate for this reason both the patch antenna and the feed circuits can perform optimized behavior.

2. It is able to integrate easily for performing the circuits with the feed network.

3. The parasitic radiation of the feed network is decreased because of the isolation of the ground plane. The slot coupled circular polarization patch antenna is a common selection for radiating parts in phased arrays for satellite communications.

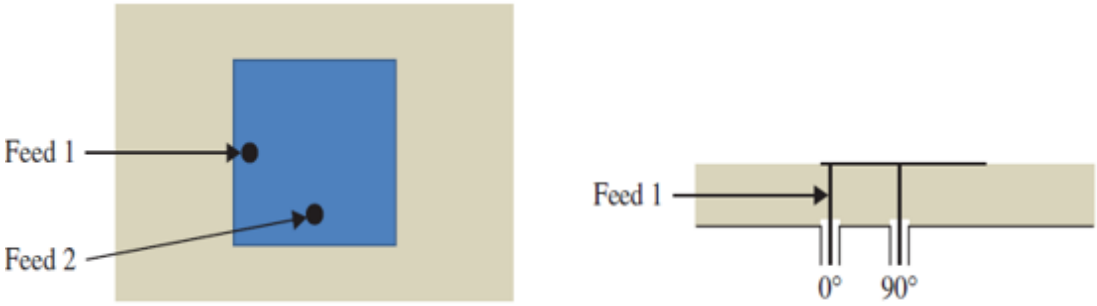

(a) (b)

Figure 41 A probe-feed patch antenna with an external 90° phase shifter (a) Top view, (b) Side view [1]

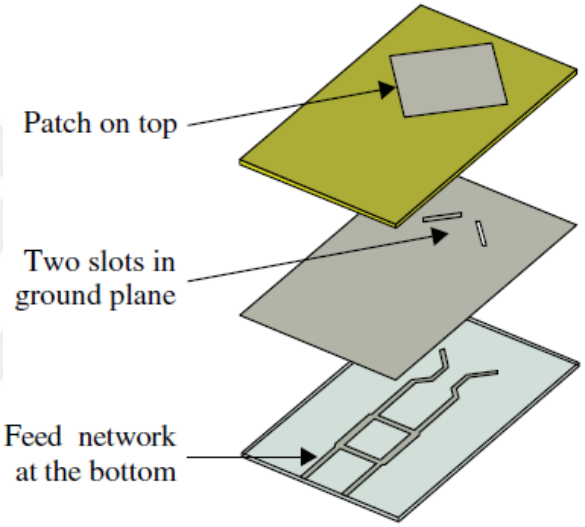

Figure 42 Slot coupled CP patch antenna (dual feed with a hybrid coupler) [1]

3.3.2 CP Wire Antennas

Crossed dipoles employing wires have been used to find CP for many years. Figure 43 clarifies a dipole antenna and a crossed dipole antenna. Figure 43 (a) shows the half wavelength ($\lambda/2$) dipole antenna which radiates vertically polarized and has an omnidirectional pattern whereas in Figure 43 (b) is the crossed dipole which consists of two dipoles are mounted perpendicular to each other and excited with a 90^0 phase difference between them. The 90^0 phase network can use one quarter wavelength of coaxial cable.

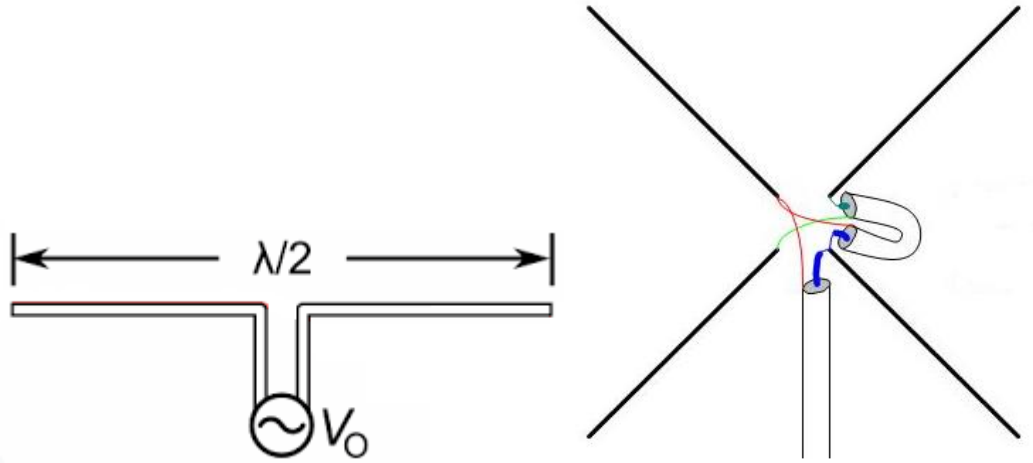

(a) (b)

Figure 43 Dipole and crossed dipole antenna (a) Dipole, (b) Crossed dipole [66,67]

3.3.3 Helix Antennas

The helix antenna is one of the most auspicious antenna kinds for circular polarization applications [50-52]. Figure 44 clarifies a helix antenna. It is essentially a conducting wire wound in the form of a screw thread. A helix antenna depends on the following parameters:

1- Diameter of one turn (D).

2- Circumference of one turn (C).

3- Vertical separation between turns (S).

4- Number of turns (N).

5- Pitch angle (α), which controls how far the helix antenna grows in the axial-direction per turn.

The helix antenna has used wide application due to its unpretentious structure and easy to configuration, broad operation bandwidth and CP. It can work at three different modes [50-52]:

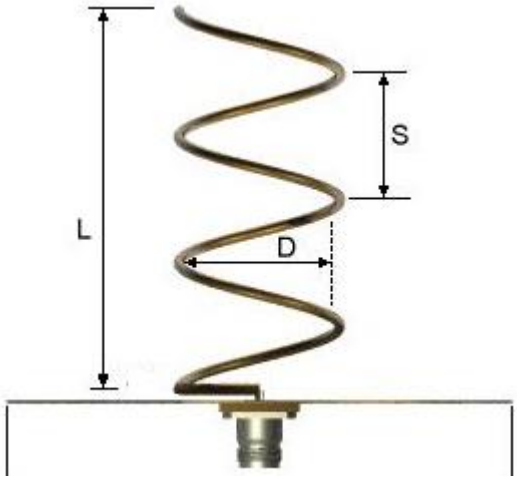

Figure 44 Helix antenna [68]

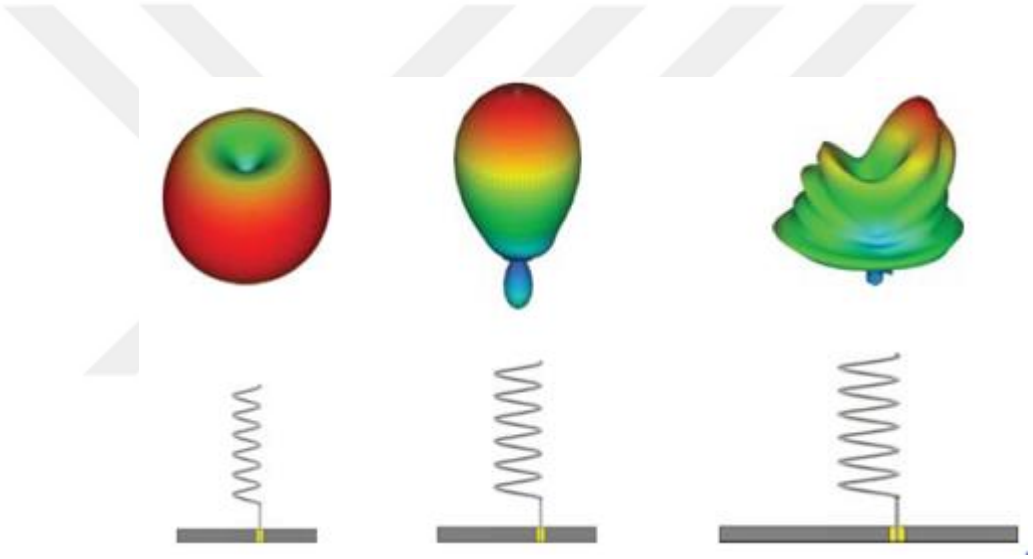

(a) (b) (c)

Figure 45 Types of helix antenna depending of radiation modes (a) Normal mode, (b) Axial mode, (c) Higher order mode [69,70]

1- Normal mode, which happens while the diameter (D) of the helix is comparatively small as compared with the wavelength (λ). Regarding the radiation pattern of this antenna in this mode, the omnidirectional pattern has been noted as presented in Figure 45 (a).

2- Axial mode, which happens while the circumference (C) of this antenna is of the order of one wavelength (λ). The extreme radiation is along the axis of this antenna viewed in Figure 45 (b).

3- Higher-order radiation mode, which happens while the dimensions of the helix override those desired for the axial mode. The main lobe is split-up as presented in Figure 45 (c).

The axial mode considers one of the attractive interests for circular polarization applications. Usually, the normal mode helix is beneficial for terminals in terrestrial cellular systems but not circular polarization applications. The equations on the below can employ to implement optimal performance in the axial mode, [60,61]:

$$\frac{3}{4}\lambda < C < \frac{4}{3}\lambda \tag{3.13}$$

$$S \approx \frac{1}{4}\lambda \tag{3.14}$$

Where α is between $12^{\circ} \leq \alpha \leq 14^{\circ}$ and λ is the free space wavelength. To realize how CP is generated via a helix antenna, the helix can be approximated by *N* small loops and *N* short dipoles then connected serially. Two perpendicularly polarized fields are generated by the loops and the dipoles, respectively.

3.3.3.1 Quadrifilar Helix Antennas and Printed Quadrifilar Helix Antennas

Quadrifilar Helix Antennas (QHA) considers one of the most employed in both satellite communications and Global Positioning Systems (GPS) applications [70–73]. The QHA can generate a radiation pattern with cardioid form as well as superb CP over a wide angular range. This type of pattern is appropriate to become more satellites visible. From Figure 46, there are two typical structures of Quadrifilar Helix Antenna. Essentially, a QHA composed of four identical helices interleaved with each other. These helices are excited with an independent phase quadrature network which supplies 0^{0}, 90°, 180°, and 270° phases to each of four helices, respectively. Regarding the end of these helices, it can be a short circuit or an open circuit as illustrated in Figure 46 (a) and (b), respectively. QHA has significant merits such as versatility and ductility, because of the many degrees of freedom; like the whole length of each part of the helices, the number of turns, the radius of a helix, pitch angle, axial length and so on. Also, the antenna can produce other kinds of the radiation pattern, gain and bandwidth performance by varying the parameters of QHA. This merit gives the QHA opportunity of a variety of applications for satellite communications and terrestrial systems. This type of antenna considers a resonant radiating configuration

when the whole length of each helical part, L_{total}, is equal to an integer number of quarter wavelengths [61].

$$L_{total} = N\frac{\lambda}{4} \dots\dots\dots\dots\dots\dots\dots (1.19)$$

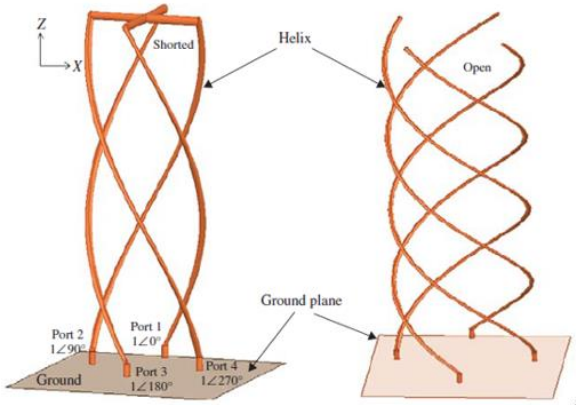

(a) (b)

Figure 46 Configurations of QHA (a) with shorted end, (b) with open end [1]

N symbolizes an integer number. In the case of N is an even number, the helices must be shorted together, as noted in Figure 46 (a); whereas N is an odd number, the helices must be open, as presented in Figure 46 (b). Figure 47 clarifies the simulated results of closed-end QHA which has helices of half-wavelength long and half turn. Figure 47 (a) presents the simulated radiation pattern of a QHA. As observed, QHA can perform a vast beam CP pattern, convenient for GPS signal reception. The simulated |S11| results are exhibited in Figure 47 (b).

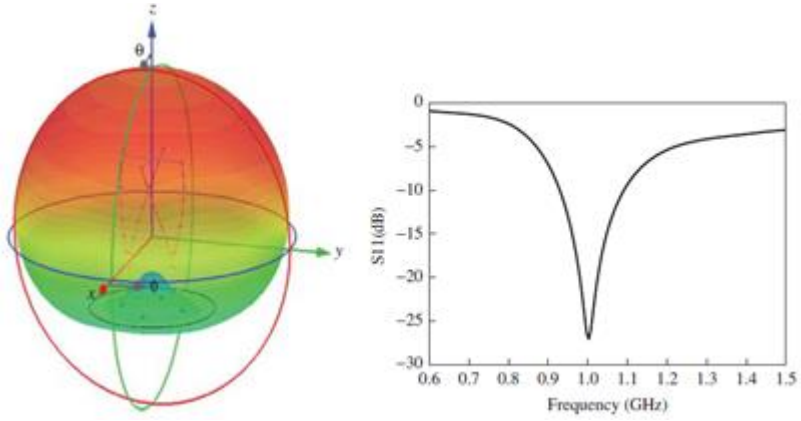

(a) (b)

Figure 47 Simulated results of an end-shorted QHA (a) Simulated radiation pattern, (b) Simulated reflection coefficient.

Figure 48 presents a PQHA, which is essentially a printed version of QHA antennas. Four printed helices are wound around a cylinder as shown in Figure 48. The four printed helices are to be excited in phase quadrature so as to generate the required hemispherical pattern. Compared with QHA antennas, PQHA is easier to industrialize in mass quantities and is inexpensive, as the antennas can be produced employing standard printed circuit board (PCB) technology. Furthermore, PQHA permits more pliability in antenna configurations. For instance, it is easy to fabricate a PQHA with meandered-line helices patterns in order to miniaturize the antenna size [20]. The same pattern will be, however, hard to achieve in wires for QHA. The employ of printed technology makes the fabrication of PQHA more accurate with fewer tolerance problems as compared to QHA. Because of using of PCB technology, it is also capable to merge PQHA with microwave diodes or devices.

Figure 48 PQHA antenna [74]

3.3.4 Spiral Antennas

This kind of antenna usually used to generate broadband or multiband frequency. Further, its parameters such as impedance, polarization, and Radiation pattern are stable and remain and unchanged over a bandwidth. Figure 49 presents one of the famous types of spiral antenna called an Archimedean spiral antenna. It involves dual conductive arms, extending from the center outwards. The antenna has a planar configuration. Each arm of the Archimedean spiral is introduced by the equation:

$$r = a\phi \tag{3.15}$$

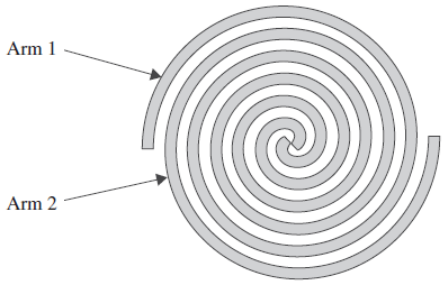

Figure 49 Spiral antenna [1].

As per of Eq. (3.15), a is radius of antenna which increases linearly with the angle ϕ. Moreover, a is a fixed which dominance the rate at which spiral flares out. Both of arms (Arm1and Arm2) are the same but first is opposite direction of rotation the second which implies the direction of antenna polarization. Further, the spiral antenna maybe containing additional arms to form a multi-spiral antenna. Typically, these types of antennas are cavity back and pattern type is unidirectional pattern due to the conductive cavity.

3.3.5 CP Dielectric Resonator Antennas

DRA is manufactured from low loss microwave dielectric materials. The resonant frequency of this antenna depends on many parameters such as size, shape and dielectric permittivity. DRA has many charming merits as compared to other antennas. For instance, it can perform radiation efficiency more than 95% and the capability to make different kinds of radiation patterns employing different modes. Moreover, it has physical merits such as low profile, flexible feed arrangement, and compact size.

Furthermore, it is not suffering from conductor losses in the patch because the radiator part is dielectric. For this reason, it is used for wireless devices that operate in millimeter-wave frequencies. The resonators can take several shapes such as rectangular, cylindrical, hemispherical, etc. In addition, several modes can be fed, exhibiting broadside or conical shaped radiation patterns for covering different areas. Antenna engineers can control over the antenna size and bandwidth.

The size and bandwidth of DRA are controlled by relative permittivity, which has a wide range extended from 6 to 100. A wideband DRA can be implemented employed low permittivity whereas miniaturization of the antenna can be implemented with high

permittivity. Figure 50 exhibits a DRA antenna for CP. A square DRA is excited by meandered line inductor feed is printed on the top of the substrate while partial ground plane is placed on bottom side [75]. A copper ground plane is at the bottom. Typically, a meandered line inductor feed is used in the case of CP microstrip antennas. The resonant frequency of rectangular DRA can be calculated via following equation:

$$f_{MNK} = \frac{1}{2\sqrt{\varepsilon\mu}}\sqrt{\left(\frac{M}{l}\right)^2 + \left(\frac{N}{w}\right)^2 + \left(\frac{K}{h}\right)^2} \tag{3.16}$$

Where ε is the permittivity while μ is the permeability.

M, N, and K are integer numbers, and l, w, and h are the length, width, and height of the rectangular DRA, respectively.

Eq. (3.16) clarifies that the DRA can resonate at different modes and the resonant frequency which is inversely proportional to the square root of the product of material parameters. When the ε material is high, the resonant frequency will shift to the lower side. DRA can be excited employing various approaches like probe feed, microstrip lines, and CPW.

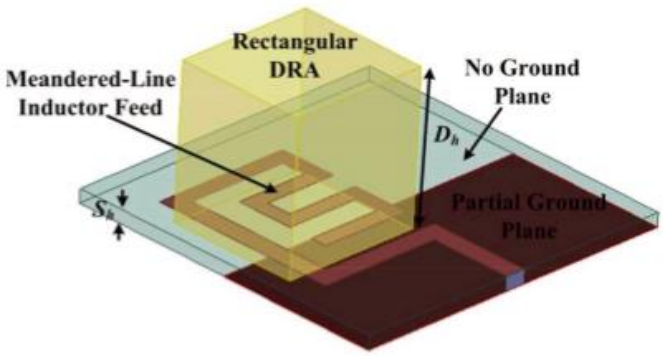

Figure 50 Dielectric resonator antenna with CP radiation [75].

3.3.6 CP Slot Antennas

The slot antenna is considered one of the traditional ways to produce a CP wave. It characterized by simplicity and low cost as compared with others. Further, a microstrip-fed slot antenna is adaptable in incorporation with other elements such as passive and active devices in a hybrid microwave integrated circuit (MIC) and microwave monolithic integrated circuit (MMIC) design [1]. Figure 51 presents a circular polarization printed slot antenna. As seen, a square slot is cut in the ground

plane, and fed by a feed network at the bottom with an appropriate dielectric substrate such as FR4 between them. The microstrip feed line has many end faces and designs, one of the famous faces of it is that the feed network employs a Wilkinson power divider in microstrip lines. The dual branches of power divider have lengths with a difference of $\lambda/4$, leading to a 90° phase difference between two perpendicular modes in the slot excited by two perpendicular feed lines. Thus, CP is created in the square slot antenna. To construct a slot antenna, the length of the slot is typically selected to be a 0.5 λ (half wavelength). There are many shapes of the slot, like an annular ring, square ring, crossed slot, circular slot and so on. Figure 51 clarifies another CP slot antenna that uses a circular slot fed via two orthogonal excited lines at the bottom. The printed slot antenna distinguished that is easy to fabricate, low profile and low cost. However, the employ of two feeds and a feed network at the base as illustrated in Figures 51 and 52 take lots of space under the ground plane. For some of the wireless devices, it is requisite to change the feed system from network feed to single simple feed as noted in Figure 53 which is basically a printed square slot antenna fed by a single microstrip line at the basis . To implement CP, a microstrip line with L-shaped is used which offers two orthogonal modes in the square ring slot. The L-shaped microstrip line has a length of a λ/4 (quarter-wavelength), so a 90° phase difference between two perpendicular modes in the slot is carried out like a circular polarization slot antenna has an unpretentious feed network and is easy to achieve. Moreover, the microstrip line feed displayed previously, slot antennas can also be fed employing other approaches like CPW or coaxial cable. One snag of these antennas radiates waves in a bi-directional form, as the slot will also propagate in the backward direction. To overcome this problem, another ground plane can be added at the bottom in this way, the antenna can implement broadside radiation only.

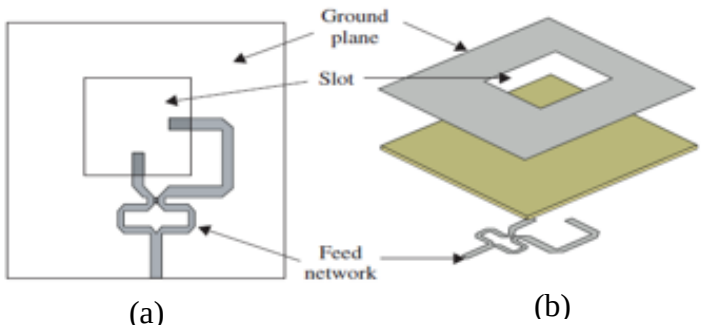

Figure 51 Square slot antenna fed by a microstrip network at the bottom (a) Top view, (b) 3-D view [1]

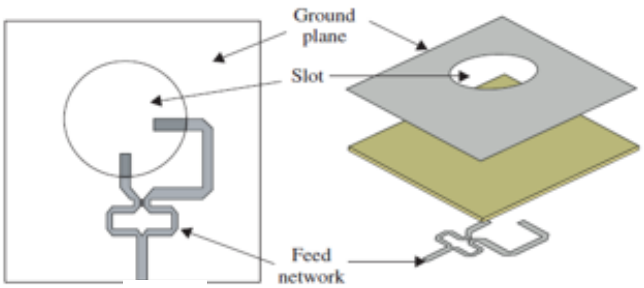

Figure 52 Circular slot antenna fed by a microstrip network (a) Top view, (b) 3-D view [1]

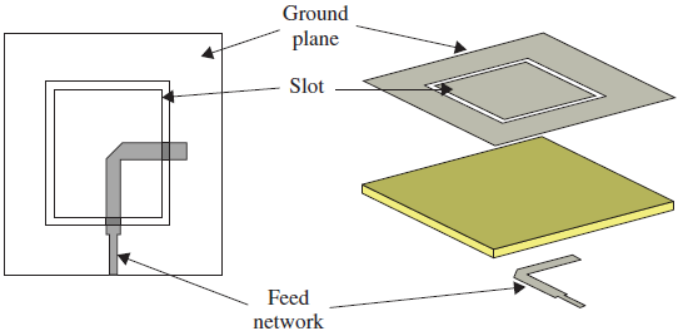

Figure 53 Circular slot antenna fed by an L-shaped fed [1]

3.3.7 CP Horn Antennas

These types of antennas belong to the aperture antenna denomination. The radiation performance is obtained via field distribution over the horn aperture [76]. The benefit of horn antennas is to supply a smooth transition between the feed waveguide and a wide aperture, which turns to centralize the main beam. Horns have used for many applications in satellite communications either as feeds for reflector antennas or earth covering antennas [28,29,61,76].

Typically, the horn antennas notified have a single feed and can radiate LP waves [76]. CP horn antennas can be achieved by employing a horn with dual perpendicular feeds and a 90° hybrid. However, the behavior of dual LP horn antennas, like the ridged horn antenna, suffers from industrialization and collecting tolerances. In addition, the employ of a 90° hybrid makes more complications and losses in antennas. Recently, many new approaches of circular polarization horn antennas have been reported in

[77,78]. Usually, CP horn antennas consist of three major elements: first, a wave launcher. Second a polarizer. Third, a beam shaper, as noted in Figure 54 [77,78]. The wave launcher in Figure 54 composed of two probes at input ports 1 and 2, which can produce RHCP and LHCP, respectively. The input probes are laid approximately one-quarter wavelength from the short-circuited end of the waveguide section 1, as seen in the figure. Waveguide 1 is a circular waveguide that permits the propagation of waves in TE11 mode [76-78].

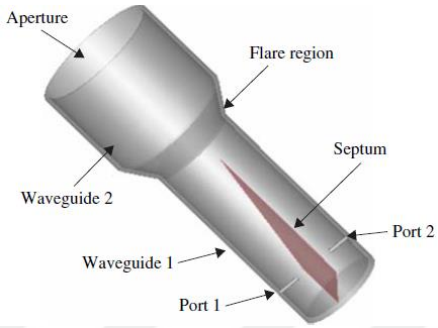

Figure 54 Schematic of a CP horn antenna.

3.3.8 CP Arrays

In the previous parts, different kinds of CP antenna elements are exhibited. An array antenna composed of a number of antenna parts whose radiation is united together to extend highly directive patterns. Circular polarization array antennas are required in some of the applications like satellite communications, transmitting antennas onboard global positioning system satellites, inter-satellite communications, and so on [62]. The array can have various geometries such as a 1-Dimension (1-D) linear array or a 2-Dimensions (2-D) planar array. Figure 55 exhibits a 2-D planar CP array with 9 identical antenna elements. As noted, Each part in this array is about a square patch excited by two probe feeds laid at two orthogonal edges of the patch with a 90° phase difference between them can radiate circular polarization wave.

Other kinds of antenna elements like a helix, DRA and so on, can also be employed to form CP arrays. Supposing identical elements are used and uniform geometries are adopted in an array, the radiation pattern of the array can be gotten from the reduplication of the radiation pattern of one element, Element(θ,φ), and the array factor AF(θ,φ) [28]:

$$E(\theta,\varphi) = E_{element}(\theta,\varphi)\, AF(\theta,\varphi) \tag{3.17}$$

The AF is depending on following

1- Array geometry.

2- Distance of inter-element.

3- Element excitement in phase and amplitude.

4- Number of elements and the frequency.

For a 1-D linear array of *N* identical elements which are regularly spaced over the *z*-axis and feed with the same amplitude and phase, the AF is:

$$AF(\theta,\varphi) = \frac{\sin(\frac{N\Psi}{2})}{\sin(\frac{\Psi}{2})} \tag{3.18}$$

Where $\Psi = kd\cos\theta + \beta$ and $= \frac{2\pi}{\lambda}$.

The spherical coordinate system is used in the Eq. (3.18). The symbols d and β express the space between elements and the phase shift between sequential elements, respectively. For constant-beam circular polarization arrays, β is set to be a constant value. The major beam of the CP array can be shifted dynamically to point in various directions by altering β electronically. This is called a phased array [28,60,62].

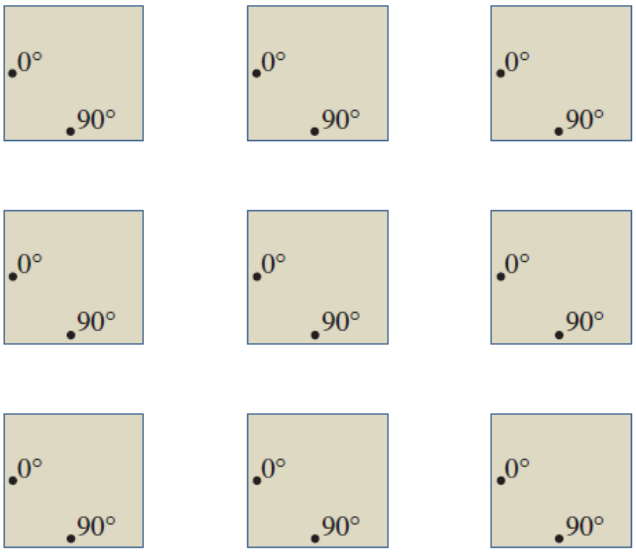

Figure 55 A nine-element CP array [1].

3.4 Some of Multiband Circular Polarization Techniques

3.4.1 Stacked Patches

The stacked patches consider one of the main techniques to generate the multiband circularly polarization antennas [80-86].It is implemented by benefiting from stacked patch configuration, in which each of the arrangement patches acts as a resonance frequency [80]. As for feeding, the probe feed technique is often used for this kind of antenna with the capability of using single or multi-feed according to the required specification. Figure 56 indicates the geometry of a single probe-fed stacked-patch antenna for performing CP operations at 1.227 GHz and 1.575 GHz. It consists of double-stacked square patches with corners truncated. The patches are printed on FR4 substrates with a thickness of 1.6 mm. Circular polarization is recognized because of the corner-truncated square patches. Also, Figure 57 presents structures of multiband CP with single feed stacked patch. It consists of three-square patches stacked on one another [82]. In [83], an antenna has been configured with two truncated stacked patches, which are excited by coaxial probe-fed to achieve dual-band CP for ISM applications. A microstrip antenna constructed by pair of truncated and semi-groove stacked patches to execute a dual-band CP has been proposed in [84]. Also, in Ref. [85], a microstrip antenna configured by a pair of substrate layers separated by an air gap, the rectangular patch printed on top of an upper substrate while the circular patch placed on the other side of it to achieve dual-band CP. Besides, the authors in [86] have presented a double layer microstrip antenna with a rectangular ring below the meandered ring to generate a dual-band resonant response. Moreover, dual pairs of inverted-L shaped strips and perturbation structures are inserted in two rings to perform CP radiation at the two bands.

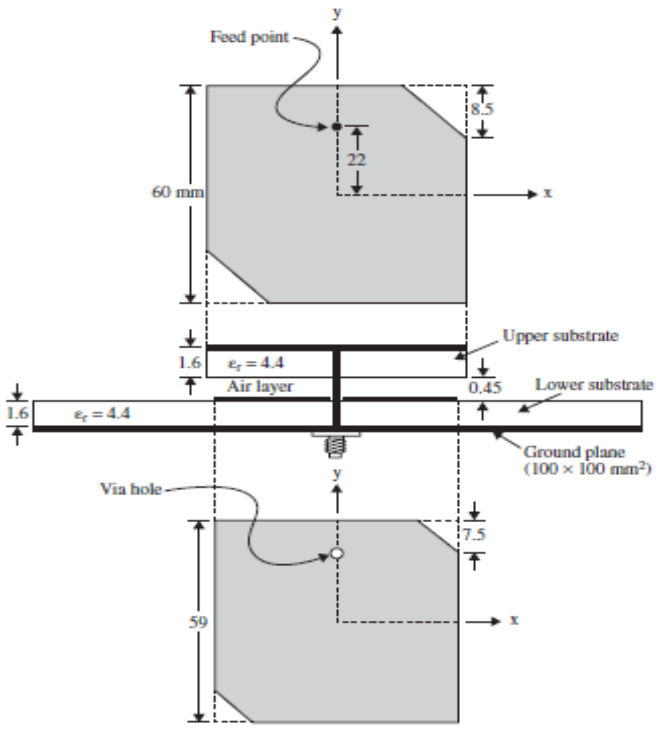

Figure 56 The geometry of a dual band CP stacked patch antenna [80]

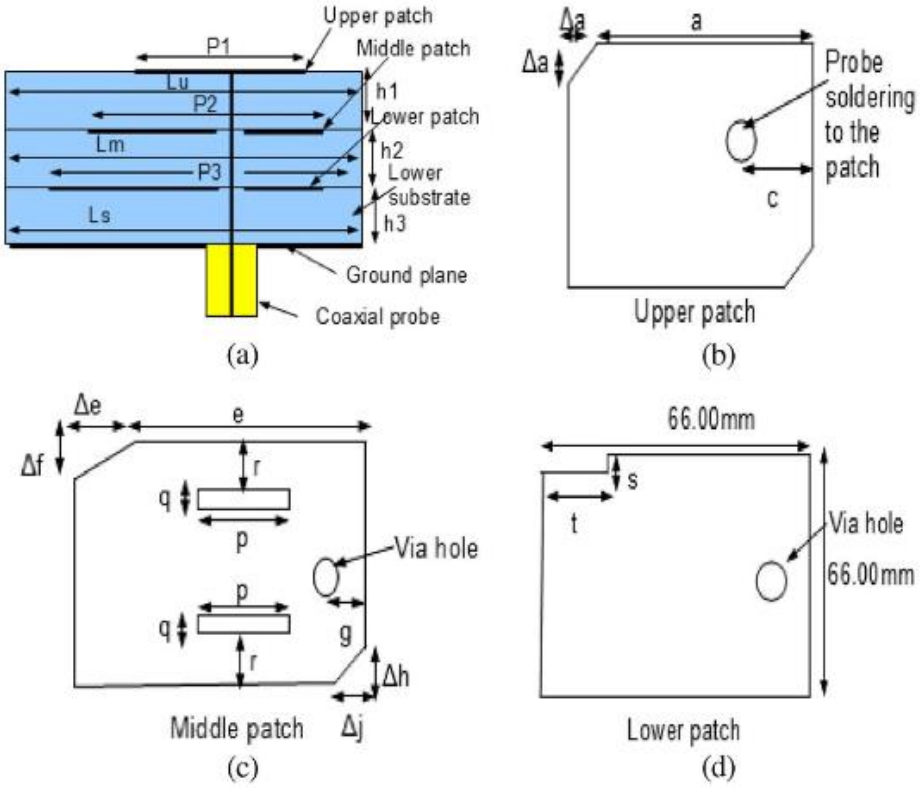

Figure 57 The geometry of the proposed stacked patch CP antenna (a) Side view, (b) Upper patch, (c) Middle patch, (d) Lower patch [82].

3.4.2 Slot Loading

The load slotting technique used for obtaining or to add an extra band [87-94]. For instance, in [87] two narrow slots etched on the rectangular patch. The slots put near the radiating edges so as to reconfigure current distribution and radiating field proper with the desired design. Based on this precept, several CP antennas with different shapes such as square, circular investigated. In Refs. [18, 90], the scene becomes clearer during the Figure 7 and Figure 58. In Figure 7, there is the ability to add second resonance by digging four slits in the square patch, while the first Figure 58 describes resonance comes from the square patch. Indeed, the CP generated for first resonance by truncating from secondary diagonal, while the second CP is found by choosing the dimensions of the inner truncated corners (s_1, s_2).

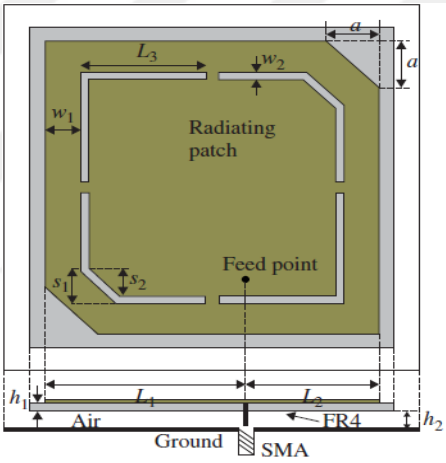

Figure 58 The geometry of the dual band CP slot loaded patch antenna [90].

3.4.3 Coplanar Parasitic Patches

This technique is used for enhancement the bandwidth. It can also be utilized to generate an extra resonance frequency [95]. Figure 59 indicates the configuration of dual-band CP with a symmetric annular ring antenna surrounding a small circular patch. According to the results, the outer ring is responsible for producing the first resonance frequency whereas the inner ring and a small patch in charge of the second resonance frequency.

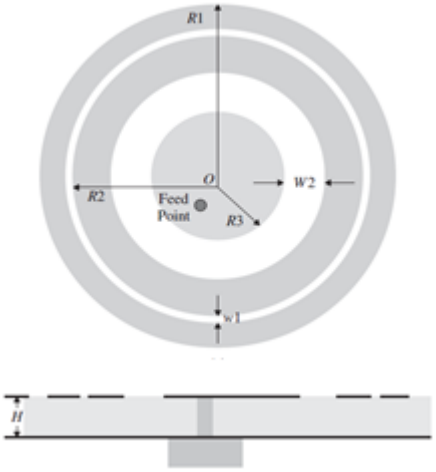

Figure 59 The geometry of the dual band CP annular ring antenna [95]

3.4.4 Multiband Quadrifilar Helix Antennas (QHAs)

QHAs are widely used antennas for UHF and microwave communications. The multi-band CP of this type can be implemented by blend two or more antennas into a single body by coaxially mounting them [1,96]. Besides, each blended antenna operates independently in terms of frequency [96]. The orders of QHAs can be categorized into three types, the first one is called “Piggyback” is defines as one antenna is on the top on the other one. The second one is called “Enclosed” which means that one antenna is inside of the other one, the last type is that, “Rotational offset” is known, as the arms of the two antennas are interleaved.

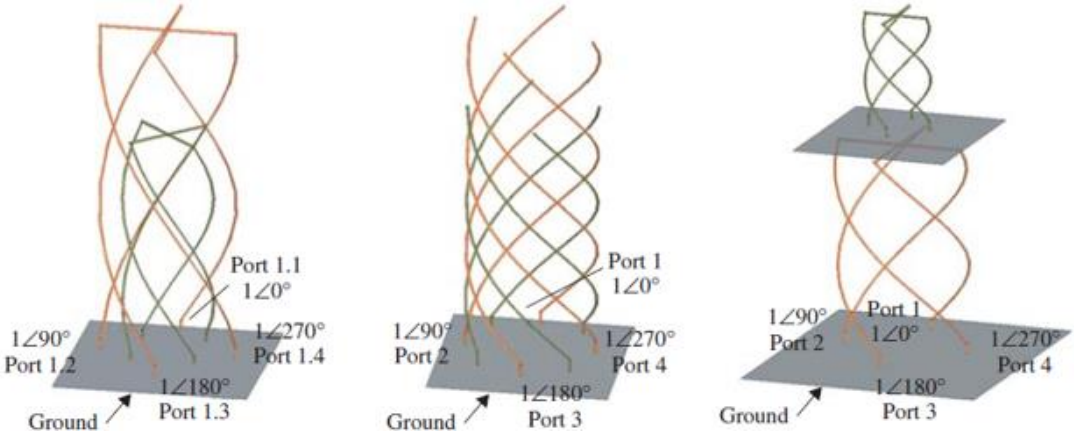

(a) (b) (c)

Figure 60 Structures of dual-band QHAs with two antennas (a) Piggyback, (b) Enclosed, (c) Rotational offset [1].

As shown in the configurations of QHA in the Figure 60, it seems to be complex for somewhat. The QHAs refabricated in a new way so as to reduce the complexity, the snails can be printed on a thin substrate sheet. The new fashion is called printed Quadrifilar Helix Antenna (PQHA). For instance, the rotational offset style in Figure 60 (c); they can be printed on a single thin substrate sheet [97] as they have the same diameter. This will facilitate the complication of the production. Figure 61 presents the unwrapped geometry and the production prototype of a dual-band PQHA [1,97].

Figure 61 The fabricated prototype of the dual band PQHA [1]

3.4.5 Multiband CP Slot Antennas

The slot type antenna is widely range used in small antenna world [1]. It's usually employed to generate a multi-band or broadband CP antennas [98-104]. Typically, when a concentric slot ring is utilized, the monopole is used as a radiator. Figure 62 (a) and (b) indicate a wide slot etched in the ground plane with appropriate monopole radiator L-shaped employed for getting triple-band CP antenna. The sense of each band is different than the other [98].

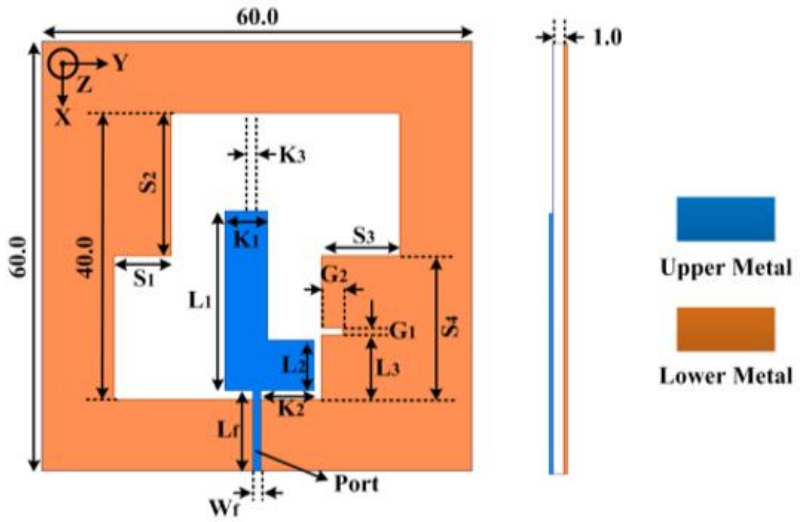

(a) (b)

Figure 62 The geometry of triple band multisense CP antenna (a) Top view, (b) Side view [98]

In addition, the slot ring can be used properly with coplanar waveguide (CPW) feed. In [99], the dual-band CP with CPW-fed is studied. The Figure 63 presents that the antenna consists of two parallel monopoles, which are responsible to produce the dual-band. The lower band is generated by longer monopole while the higher operating frequency relies on the shorter monopole.

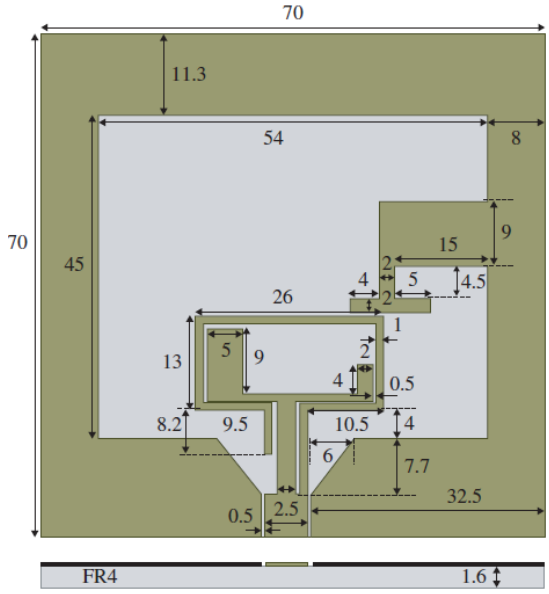

Figure 63 The geometry of the dual band dual monopole CP antenna [99]

3.4.6 Monopole Antenna without Slot Rings

The printed monopole antenna has been employed recently to generate multi-band and broadband CP [105-111]. Typically, it appears in two forms according to feed techniques. First form, it uses with a microstrip line fed another one is that coplanar waveguide (CPW) fed [109].

For instance, in Ref. [109], a triple-band CP monopole antenna with CPW-fed is presented, the radiator is that a monopole tilted asymmetrical E-shaped printed antenna and excite by a 50 Ω offset CPW feed line as shown in Figure 64. In addition, the Ref. [111] presents another example to get more than one CP band as well as more than one CP sense. Moreover, Ref. [111] contains two designs. First, it consists of the reduced ground plane with etching inverted L-stub in it whereas, the radiator is a rectangular shape with cutting a bevel shape from it as illustrated in Figure 65 (a) to enhance the BW. To improve the impedance bandwidth and axial ratio of basic shape, I- shaped sub and I-shaped slit are added as shown Figure 65 (b) in the ground plane and rectangular radiator, respectively.

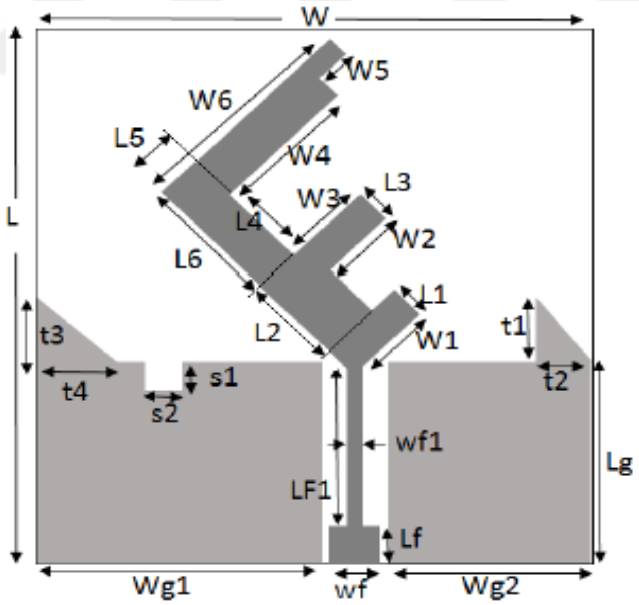

Figure 64 Configuration of the asymmetrical E-shaped tilted printed antenna [109].

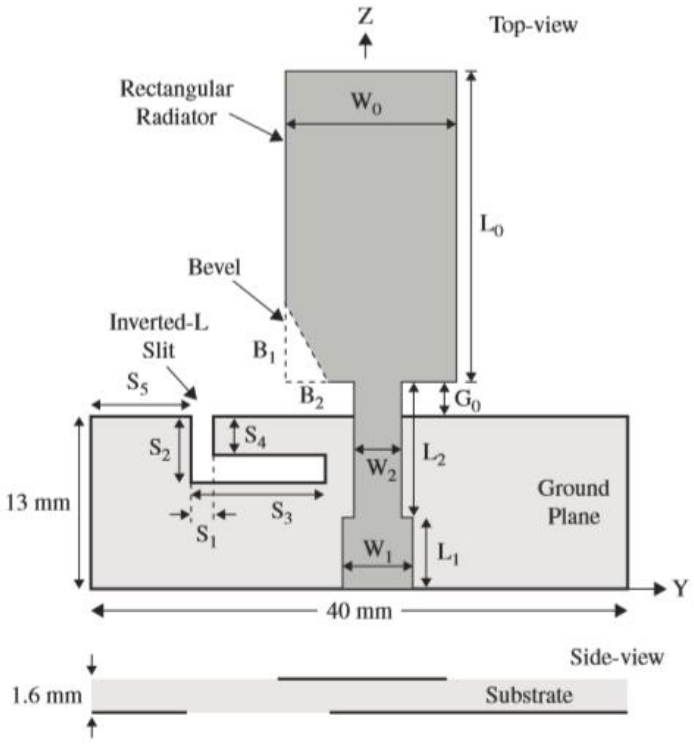

(a)

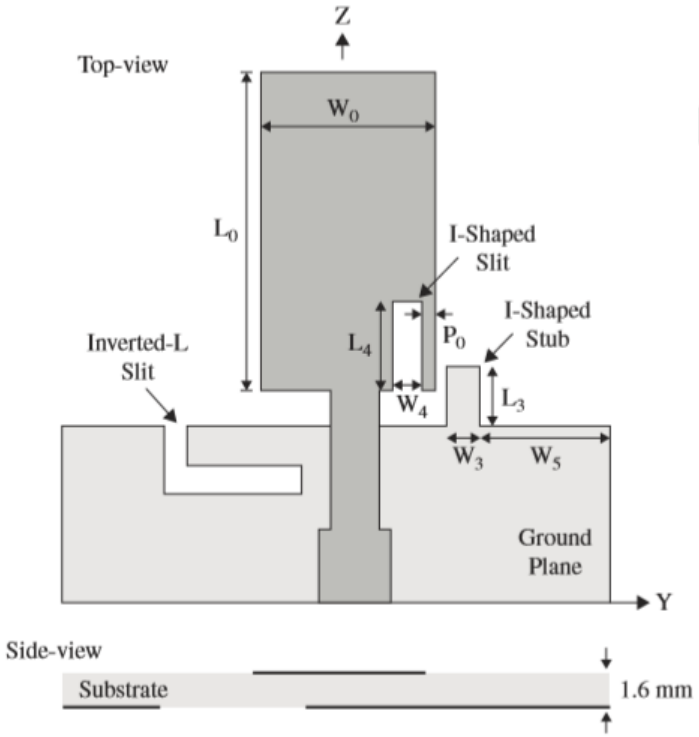

(b)

Figure 65 The geometry of dual-band dual sense CP monopole antenna (a) With an inverted-Lslit (b) With an inverted-L slit, I-shaped slit, and I-shaped strip [111]

3.4.7 Dielectric Resonator Antenna (DRA)

The DRA is different from the previous antennas because the dielectric resonator employed as a radiator [112, 113]. Typically, this kind of antenna uses at millimeter-wave applications [1]. There are many approaches used with DRA to produce multiband operation frequencies. In recent times, many searches have been investigated on DRAs with dual-frequency or wideband operation using various techniques, such as exciting two modes, or stacking two DRAs, slot coupled dielectric resonator. In Ref. [112], a dual-band CP DRA is presented, the dielectric resonator is located on the center of the ground, is made from ceramics with ε_r=20.5, whereas substrate made of Rogers with ε_r =2.55, on the top of it there is slotted ground plane, while on the bottom of it, the feed line is excited as shown in Figure 66.

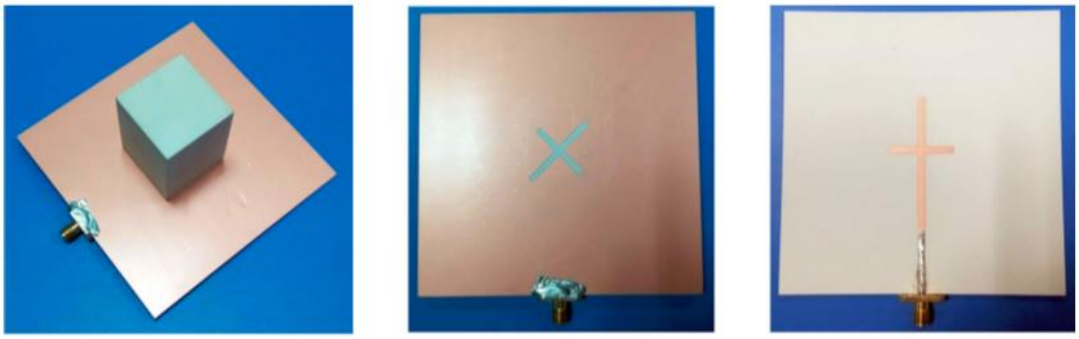

(a) (b) (c)

Figure 66 The prototype of DRA antenna (a) 3-D view of the fabricated antenna, (b) Top view of the feeding network, (c) Bottom view of the feeding network [112]

3.5 Challenging of CP Antenna

Indeed, there are many points of defy in the CP antenna is under optimization. The improvement comes to make a CP antenna harmonious with other wireless device parts. Further, to enter of enhancement to overall device performance and make it operates as a multi-device mission. The most challenging points can be summarized in the following points:

1. Miniaturization: it considers one of the common challenges of circular polarization antenna, due to make the device able to mobilize, lightweight and adaptable with wireless devices. Actually, miniaturization did successfully when it did not affect negatively other antenna characteristics like that gain, radiation pattern and so on.

2. Gain enhancement: It is required in CP antenna especially, in some applications such as radars and satellite communication systems when the alignment of transmitting and receiving antenna changes over time. For instance, in Global Positioning System (GPS) bands, a circular polarization antenna with a broad AR beamwidth of more than 120% is oftentimes required so that the wireless signal can be received efficiently at any place.

3. Axial Ratio Bandwidth (ARBW) improvement. Indeed, the enhancement of axial ratio bandwidth is depending on application kind and range of operation band. Further, the ARBW enhanced should be located at return loss is less than -10 dB.

4. Omnidirectional radiation pattern, this property is required in some of the important applications. Indeed, these applications need a CP antenna to be compact such as Radio Frequency Identification (RFID) which is valuable in security systems and remote tracking applications.

CHAPTER 4

DESIGN AND ANALYSIS OF MULTIBAND MONOPOLE PRINTED ANTENNA USING MICROSTRIP FEEDLINE

4.1 Introduction

In this chapter, a new two multiband hybrid polarization antennas have been presented for the requirements of modern wireless communication systems. These printed antennas have been configured from a single-layer substrate as well as a single feed with microstrip type contact with the open-loop hexagonal radiator. Actually, the antennas are very similar but the difference in the ground plane area. Regarding the construction, the antennas were built with a dielectric constant of 4.4 and a thickness of 1.5 mm using a FR4 substrate. These antennas differentiate from others by compact size also have unique features because they have multiband hybrid polarization and multi-sense responses that are the demands in modern wireless systems. HFSS V.13 has been used to optimize the functionality of antennas and is widely adopted in microwave research and industry. In addition, it is verified practically. The results showed that this antenna has good frequency behavior and gains too.

All CP antennas built in this chapter exist at the end of this dissertation as two publications in the list of "PUBLICATIONS RELATED TO Ph.D. THESIS"

4.2 Design and Analysis of Penta Band Antenna with Triple Sense CP

4.2.1 Antenna Structure

The configuration of the antenna is presented in Figure 67. The radiator pressed on a substrate FR-4 that has a thickness of 1.6 mm with $\varepsilon_r = 4.4$ and $\tan\delta = 0.02$. The upper surface of the substrate is imprinted by a hexagonal open loop radiator, whereas the portion of the ground level is settled on the back of the substrate with double split stairs.

The antenna excited by a 50Ω direct feed line. The radiator takes an area of 0.14λ_o ×0.08λ_o. The proposed antenna parameters described in Table 1 were optimized by intensive full wave simulation.

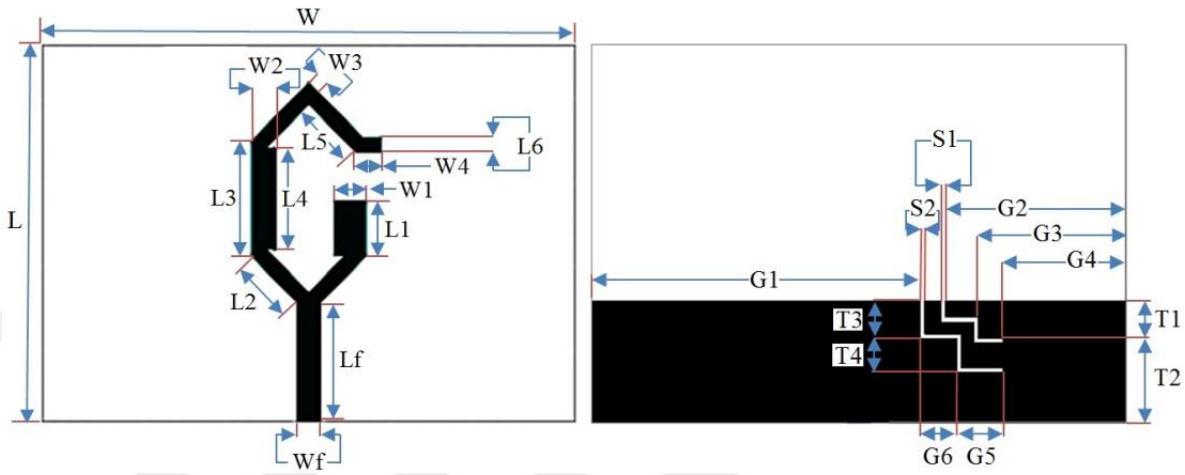

(a) (b)

Figure 67 Structure of the open ring penta band with triple sense CP antenna (a) Top view, (b) Bottom view.

4.2.2 Design Procedure

The development steps of the penta band with triple sense CP antenna are shown in Figure 68. In Ant.1, the radiator is closed ring and reduced ground plane without slits. In this case, the antenna provides two bands (2.05-2.41GHz) and (5.50-6.75 GHz) as shown in Figure 69 (a); however, as a result, it produces a wave with elliptical polarization merits at the operating frequencies as indicated in Figure 69 (b). The first operational band moved towards the L band (1.61-1.75 GHz) in Ant.2. Also, as shown in Figure 69 (a), the second band is extended across the S and C bands with a frequency range (2.95-5.45 GHz). In addition, the AR is strengthened at first operation band, which became lower than 3dB as shown in Figure 69 (b), but AR in the second band is not coupling with the |S11|. Concerning the operating frequency ranges, they expanded in the Ant.3 by incorporating radiator loading components and operating bands were (1.60-1.70 GHz), (2.93-3.42 GHz), and (4.10-6.61 GHz), but CP was proved from (1.73-1.80 GHz) that was not in line to Ant.3's first operating band. Five frequency bands are introduced in Ant. 4. On the other hand, the AR under 3dB

observed at only three bands (1.60-1.75 GHz), (4.54-4.90 GHz), and (6.21-6.49 GHz). Therefore, only these three bands are focused.

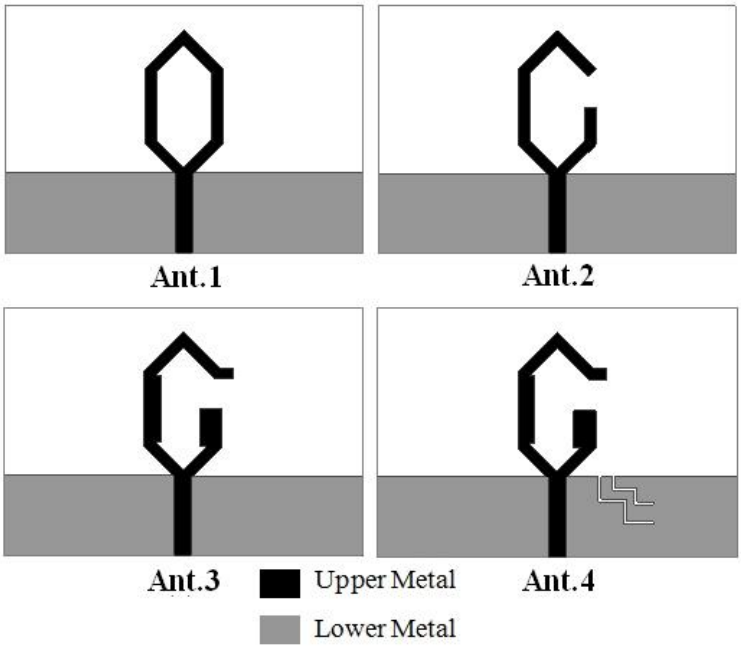

Figure 68 Steps of open loop hexagonal penta band triple sense CP antenna design

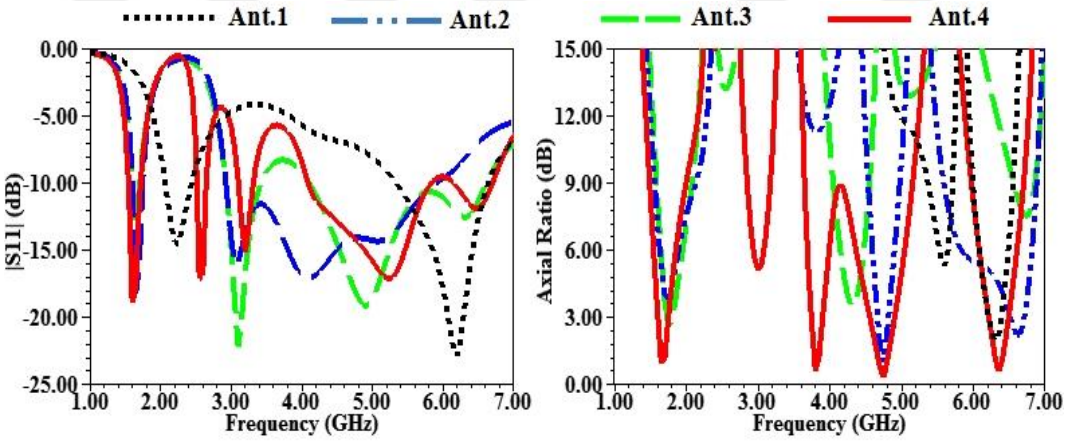

(a) (b)

Figure 69 Performance of each stage in Figure 67 (a) |S11|, (b) AR

4.2.3 Current Distributions on Surfaces

It is important to grasp the mechanism of the antenna scientifically. The current is obtained at surface of three regions:1.6 GHz, 5.25 GHz, and 6.5 GHz as observed in Figure 70 (a), (b), and (c). The current enriched on the radiator part particularly in the lower part of it as obtained in Figures 70 (a) and (b). Regarding the 3rd frequency, it

intensified in the midst and upper part. Concerning another conducting surface (ground plane), the current is heavy around the slits that participated effectively to boost the matching of the 1st band. Also, to produce the 3rd band as demonstrated in Figure 69.

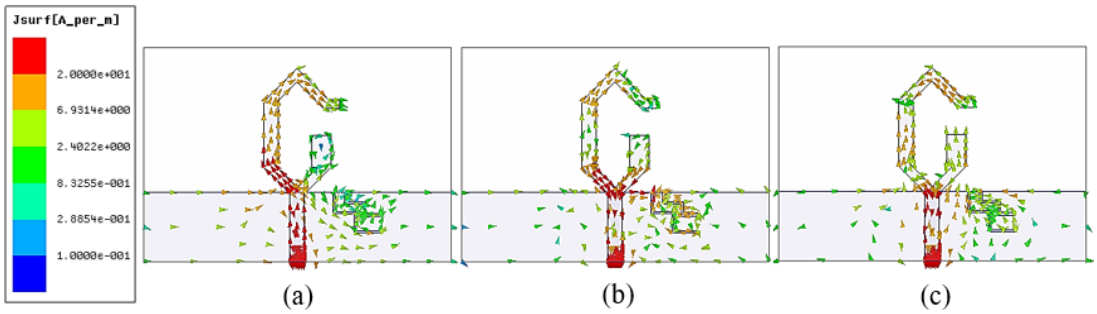

Figure 70 Allocation of currents on antenna surfaces at (a) 1.6 GHz (b) 5.25 GHz and (c) 6.5 GHz.

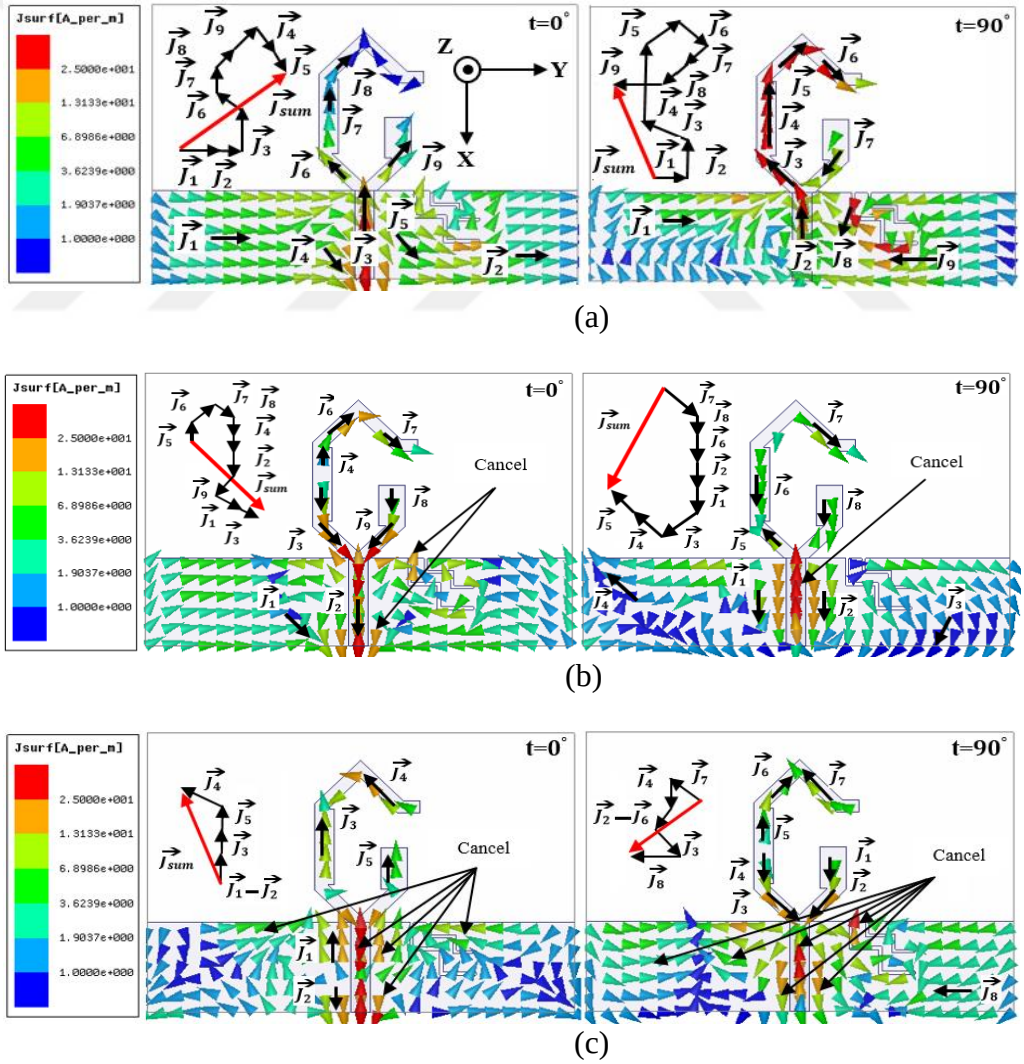

Figure 71 Allocation of currents on antenna surfaces at (a) 1.65 GHz (b) 4.75 GHz and (c) 6.35 GHz CP resonance frequencies.

Figure 71 exhibits the current allocation at three operation bands 1.65 GHz, 4.75 GHz, and 6.35 GHz with different time instants 0° and 90° so as to know the circular polarization characteristics. In Figure 71 (b) and (c), the resultant vector (red arrow) rotates anticlockwise which indicates that the wave is RHCP (right handed circular polarization) whereas, it rotates clockwise direction in Figure 71 (b) creating LHCP (left handed circular polarization). The opposite direction currents with the same magnitude are not contributed to identifying the main direction of currents rotation as demonstrated in transmission lines.

4.2.4 Parametric Study

The study of each antenna parameter will help to enhance its performance significantly by adjusting each one to reach to optimize value. For this antenna, the parameters w1, w2, w4, L1, s1, and s2 will study independently to know the weight of each one.

4.2.4.1 Impact of Parameter, w1

Figure 72 indicates the influence of w1 that represents the width of the open ended side on the magnitude of the input |S11| and axial ratio of the antenna. Also, Figure 72 exhibits the effect of rising w1 gradually towards internal which causes the presence of the 3rd frequency of CP operation from (6.14-6.70 GHz) and CP performed from (6.21-6.49 GHz) as seen in Figure 72 (b). In the meantime, on the 2nd band, the CP area moved to the left side to align more with the |S11|.

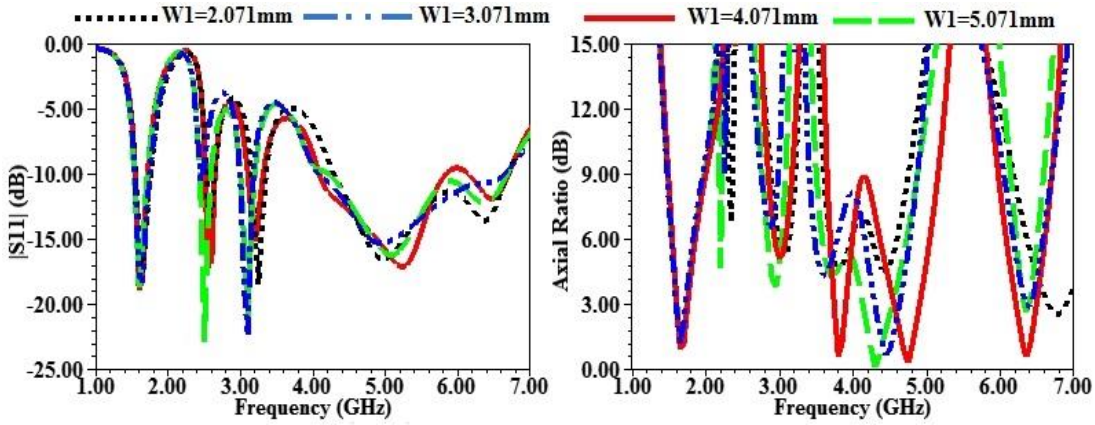

(a) (b)

Figure 72 The impact of w1on the antenna behavior (a) |S11|, (b) AR

4.2.4.2 Impact of Parameter, w2

The influence of w2 that acts the width of the long side on the radiator in reflection coefficient and axial ratio on antenna performance is demonstrated in Figure 73 (a), and (b), respectively. Figure 73, shows the power of w2 on over all bands, especially for wide part (4-7 GHz). When w2=2.071mm, the |S11| is poor in all bands. Moreover, the circular polarization displays in the 1st band only. The growth of w2 a bit leads to the occurrence of 2nd and 3rd circular polarization bands with AR less than 3-dB. Hence, the w2=3.071 mm chooses based on this survey. When the value of w2 is raised, the optimum value, it influences directly to the 3rd CP band. Furthermore, the 2nd CP band moved to undesirable area as shown in Figure 72 (b).

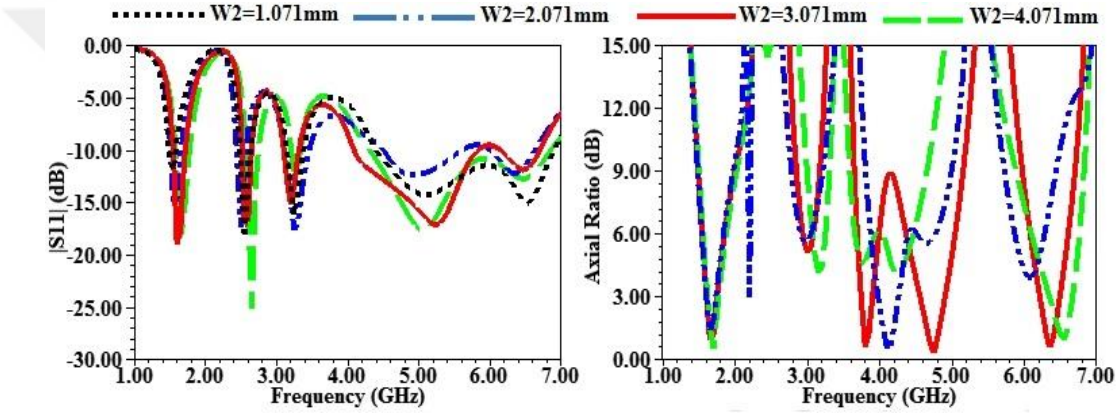

(a) (b)

Figure 73 The impact of w2 on antenna behavior (a) |S11|, (b) AR

4.2.4.3 Impact of Parameter, w4

Figure 74 describes the impact of w4 that represents a width of external loaded part linked with the ending of open direction rib to 1st band is not suitable for slightly whereas, it works a significant role. concerning the others, when w4 increased gradually, the 3rd CP band begin to emerge gradually, as depicted in Figure 74 (a), but this display must be associated with axial ratio. Also, the adjustment gives a desired result when w4= 3.343 mm, the axial ratio confirm with the reflection coefficient at (6.21-6.49) GHz as seen in Figure 74 (a), and (b).

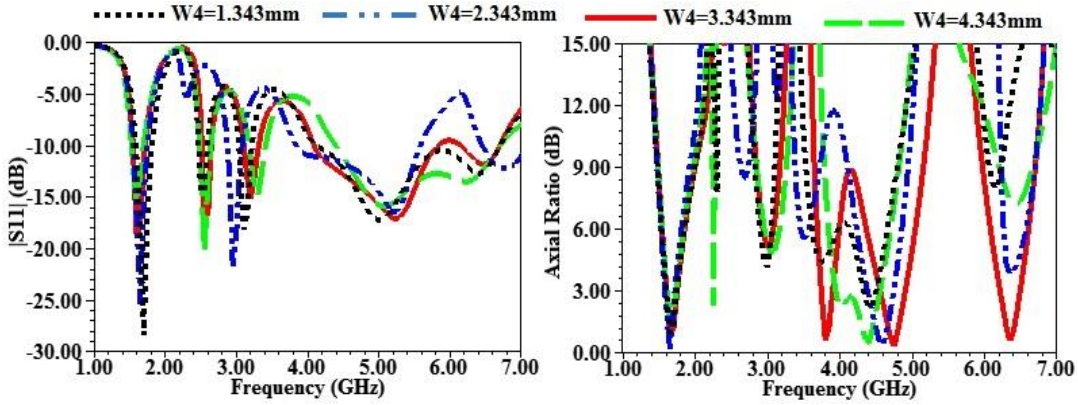

(a) (b)

Figure 74 The impact of w4 on antenna behavior (a) |S11| (b) AR

4.2.4.4 Impact of parameter, L1

The L1 represents as shown in Figure 75 (b) the open rib in the hexagonal radiator, whereas the |S11| does not overly affect the efficiency of the CP as shown in Figure 75 (a). The CP function is clearly visible in L1=6,757mm, making it 2nd and 3rd bands.

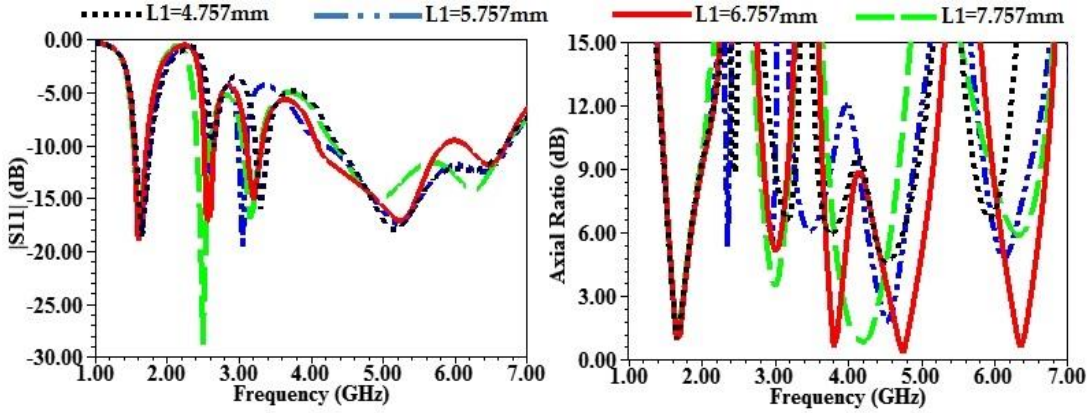

(a) (b)

Figure 75 The impact of L1 on antenna behavior (a) |S11|, (b) AR

4.2.4.5 Impact of Parameters, s1 and s2

Figure 76 clarifies the extent of effectiveness of s1and s2 on the antenna performance (reflection coefficient and axial ratio). Both the parameters act as the width of the etched slit in the ground plane. When s1 and s2 increased, the amount of harmony raised particularly at the resonant frequencies 1.65 GHz, 2.55 GHz, and 3.2 GHz. Also, the axial ratio became under the 3 dB especially at the second and third bands.

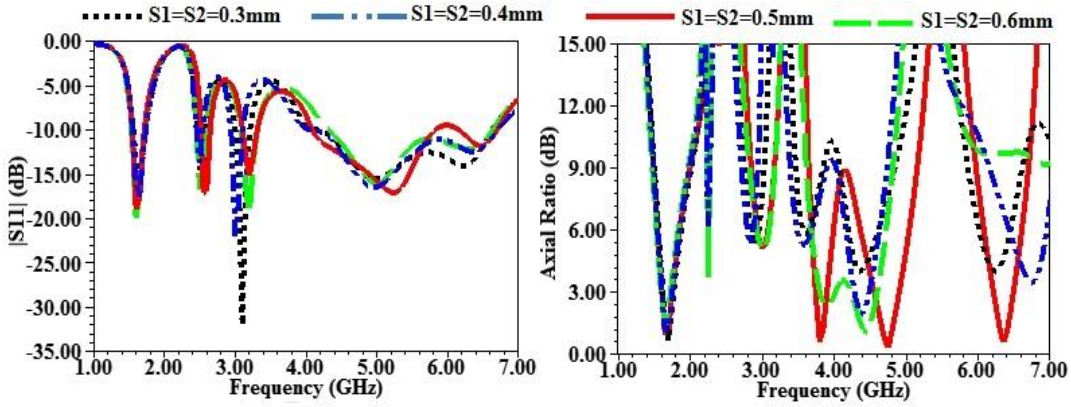

(a) (b)

Figure 76 The impact of s1and s2 on antenna behavior (a) |S11|, (b) AR

4.2.4.6 Impact of Existence of s1 and s2

Based on Figure 77, the s1 role is limited to the third band as depicted in Figure 77 (a). Also, the CP of the last band disturbance is seen in Figure 77 (b). Regarding stair slit s2, it plays a significant role in the improvement of antenna performance. When s2 does not exist, the second band is disappeared as well as the other last bands have lost the circular polarization property. So, both of them remain in order to keep the |S11| and circular polarization in all bands.

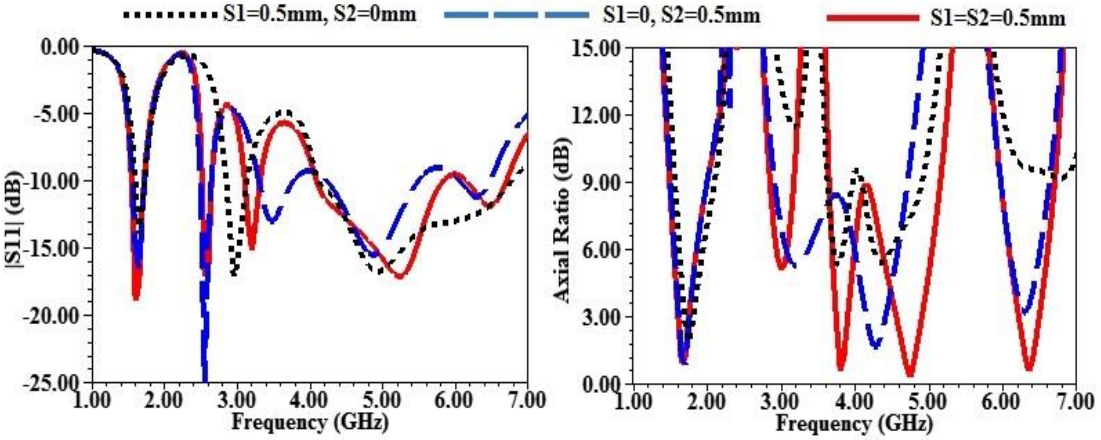

(a) (b)

Figure 77 The impact of the existence of s1 and s2, (a) |S11|, (b) AR

4.2.5 Results and Discussions

From the above study, the appropriate values of all antenna parameters are listed in the Table1

Table 1 Dimensions of open ring multiband CP antenna

Parameter	Unit (mm)	Parameter	Unit (mm)	Parameter	Unit (mm)
W	45	G3	18	L6	1.914
W1	4.071	G4	15	Lf	14.421
W2	3.071	G5	5.5	S1	0.5
W3	2	G6	4.5	S2	0.5
W4	3.343	L1	6.757	T1	4.5
Wf	3	L2	7.525	T2	10
L	65	L3	13.757	T3	4.5
G1	40	L4	12.242	T4	4.5
G2	22	L5	8		

4.2.5.1 Reflection Coefficient and Axial Ratio

As it is known, the reflection coefficient and axial ratio consider one of most important parameter parameters for test any circular polarization antenna. So, the proposed antenna has been simulated via HFSS then fabricated and measured practically by vector network analyzer (VNA) as depicted in Figure 78. The axial ratio (AR) should be within an operating band as seen in Figure 78. For instance, the first band starts at 1.55 GHz and ends at 1.72 GHz, the AR≤3dB calculated within the mentioned frequency ranges, and found that axial ratio bandwidth (ARBW) extends from 1.60 GHz to 1.75 GHz. If the AR≤3dB locate out of operation band it will be neglected such as the AR $\leq$ 3 dB from (3.74-3.90 GHz) as illustrated in Figure 79. In other words, the AR $\leq$ 3 dB condition should verified within the desired band as possible as for ensuring the high performance of the antenna.

Also, Figure 79 indicates that there is harmonization between simulated results and practically for somewhat. The practically tests concerning the reflection coefficient pointed that good matching in first and second bands. Also, they are similar with simulated first and second band s almost. Regarding the third band, the coupling under -10 dB is very poor while it observed that the realistic result moved about 500 MHz to

the high-frequency region as compared to the simulated result and began from 4.66 GHz to 6.51 GHz. Concerning the axial ratio bandwidths (ARBWs), the outcome is comparable between simulation and experiment as presented in Figure 79. The circular polarization bands visible in three regions as shown in Table 2. Regarding the middle bands (2.51-2.64 GHz) and (3.10-3.31 GHz), they are linear polarization.

Table 2 The ARBWs for first proposed antenna

No.	Simulated AR ≤ 3 dB in GHz	Measured AR ≤ 3 dB in GHz	ARBWs in MHz (Simulated, Measured)
1	1.60-1.75	1.59-1.73	15, 14
2	4.54-4.90	4.58-4.93	36, 35
3	6.21-6.49	6.25-6.50	28, 25

4.2.5.2 Gain and Radiation Patterns

Figure 80 indicates the peak gains of the first suggested antenna while Figure 81 represents the radiation patterns. The simulated and experimented outcomes are analogous for somewhat. The values of gains extract from its figure that indicates that the measured values similar to the simulated values as shown in Table 3

Table 3 The simulate and particular gains at resonance frequencies

No.	Simulated gains dBi	Measured gains dBi	Frequency GHz
1	1.87	1.75	1.65
2	3.83	3.72	2.55
3	3.2	3.2	3.2
4	5.95	5.87	4.75
5	7.67	7.61	6.35

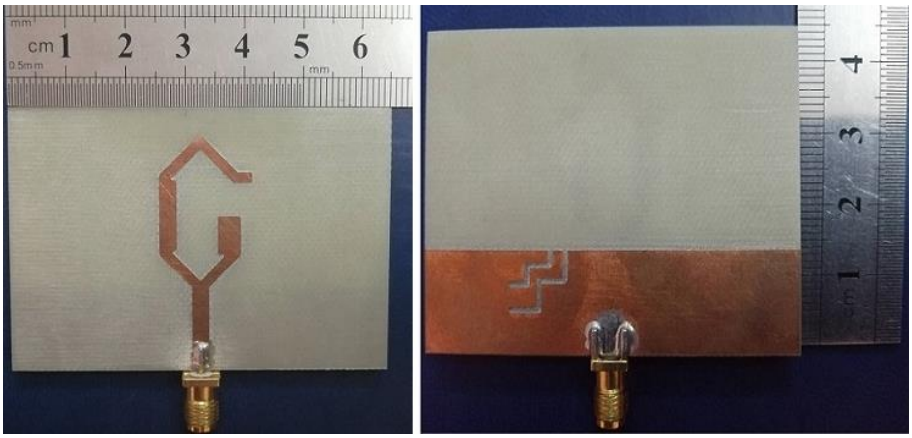

(a) (b)

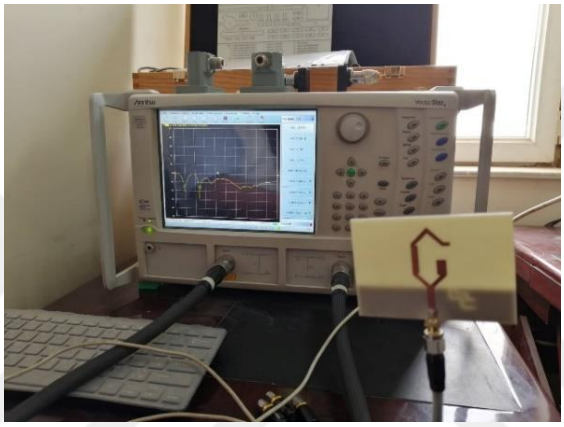

(c)

Figure 78 The fabricated antenna (a) Top view, (b) Bottom view, (c) During the testing

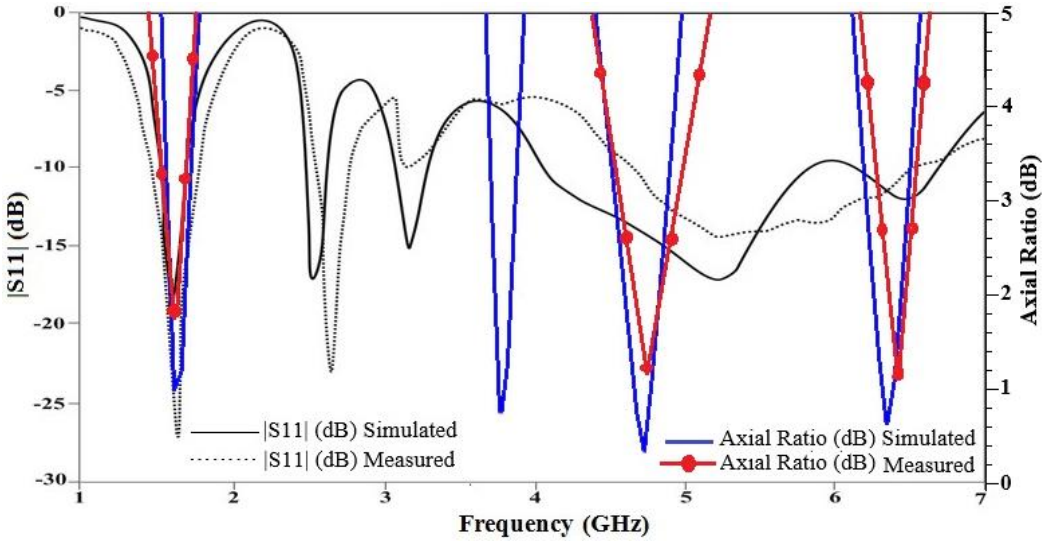

Figure 79 The simulated and measured outcomes of reflection coefficient and axial ratio of penta band CP antenna

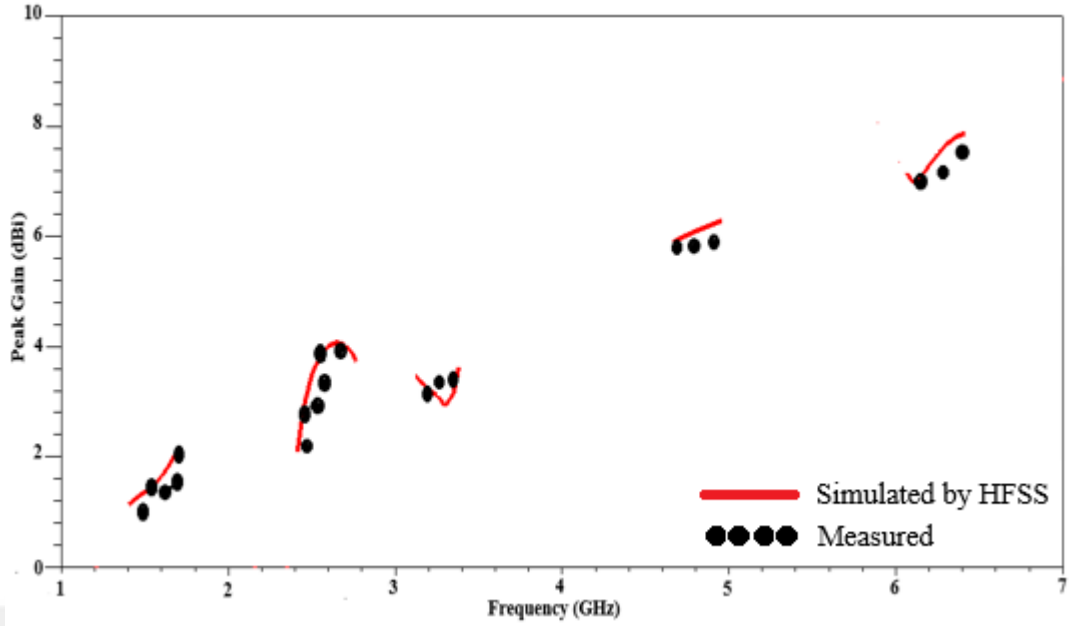

Figure 80 The peak gain against the frequency of the penta band CP antenna

Figure 81 presents the simulated and particularly radiation pattern at resonance frequencies. The proposed antenna has been simulated and tested in both planes XZ and YZ respectively. The experimental results imply that there is confirmation with simulated results. In Figure 81 (a) and (e) the antenna radiates right-handed circular polarization in +z direction whereas left-handed circular polarization in Figure 81 (d). The cross-polarization in the first band about 22 dB while in the fourth and fifth band is more than 25 dB at θ=0°. Regarding the second and third bands, they are considered linear polarization.

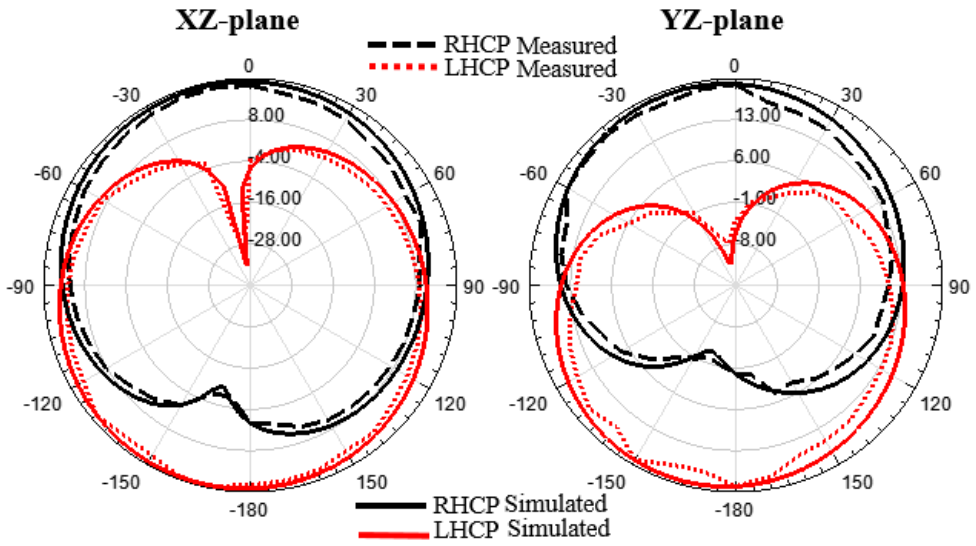
XZ-plane
YZ-plane
RHCP Measured
LHCP Measured
RHCP Simulated
LHCP Simulated
8.00
-16.00
-28.00
13.00
6.00
-1.00
-8.00

(a)

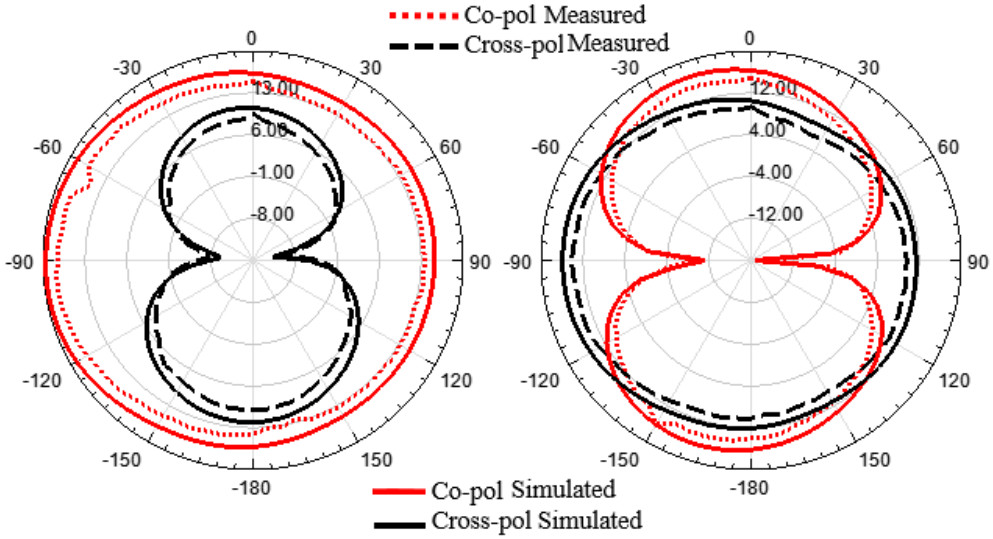
Co-pol Measured
Cross-pol Measured
Co-pol Simulated
Cross-pol Simulated
13.00
6.00
-1.00
-8.00
12.00
4.00
-4.00
-12.00

(b)

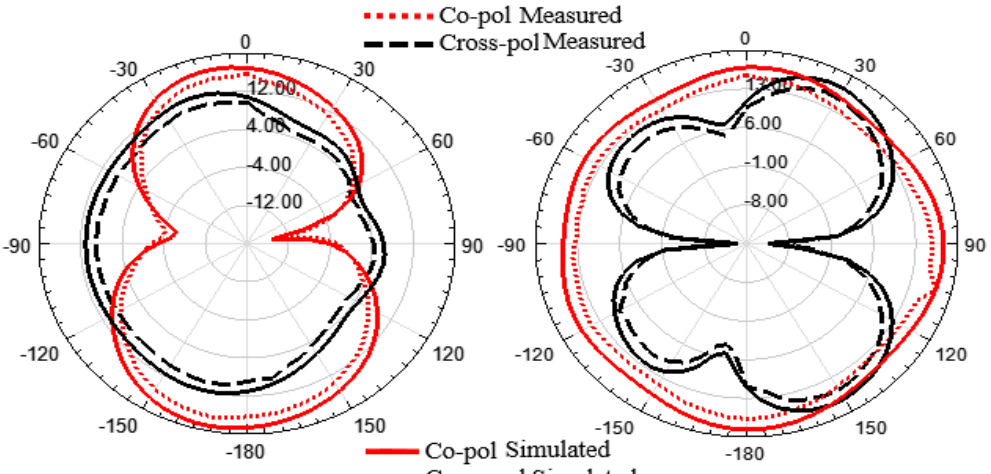
Co-pol Measured
Cross-pol Measured
Co-pol Simulated
Cross-pol Simulated
12.00
4.00
-4.00
-12.00
6.00
-1.00
-8.00

(c)

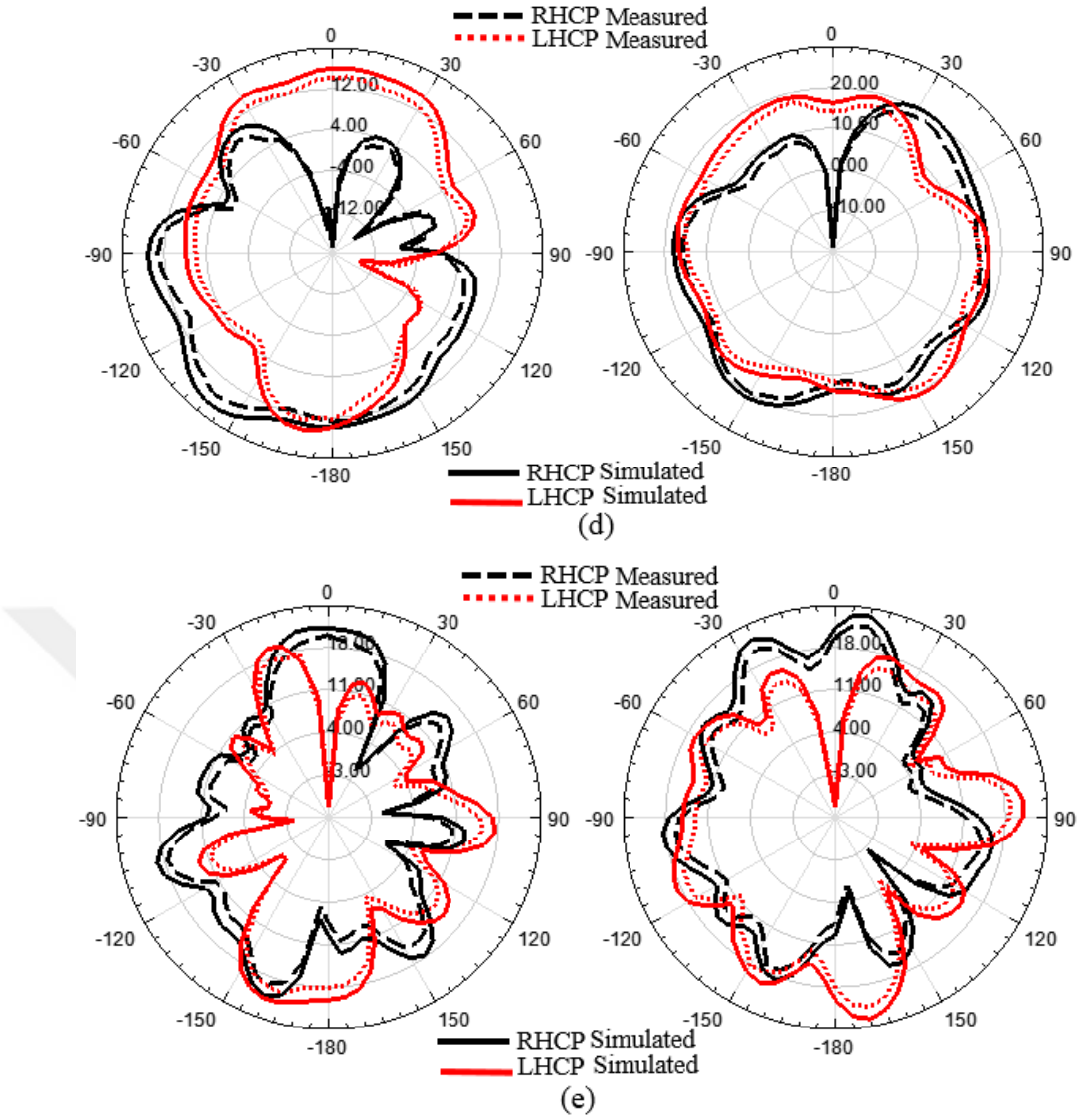

Figure 81 Radiation patterns of the open ring penta band triple sense CP antenna at (a) 1.65 GHz, (b) 2.55 GHz, (c) 3.20 GHz, (d) 4.75 GHz, (e) 6.35 GHz

4.2.5.3 Comparison of Penta Band Triple Sense CP Antenna with Previous Works

Table 4 summarizes the comparisons of the presented antenna in Figure 67 with some other previously works. During the comparison, it found that current work has many merits more than the others like compactness, low profile, number of bands as well as carry out an enhancement in ARBW.

Table 4 Comparison of penta triple sense CP antenna with previous works

Ref.	Size (mm^2)	IBW (GHz, fc, %)	|S11|<–10 dB Bands	3-dB ARBWs (GHz, fc, %)	3-dB ARBW Bands	Polarization
[20]	45×65	1.57-1.85, 1.71, 16.37 1.99-2.19, 2.09, 9.56 2.52-2.77, 2.645, 9.45	Triple	1.56-1.62, 1.57, 3.70 1.98-2.08, 2.02, 4.90 2.50-2.63, 2.55, 5.06	Triple	RHCP LHCP LHCP
[21]	55×66	1.527-1.917, 1.722, 22.7 2.598-3.248, 2.923, 22.3	Dual	1.579-1.637, 1.61, 3.6 2.67-2.822, 2.74, 5.6	Dual	LHCP RHCP
[94]	95×93	1.55-1.60, 1.57, 3.18 2.37-2.53, 2.40, 6.66 2.96-3.03, 3.00, 2.33	Triple	1.5275-1.5925, 1.56 2.3875-2.4725, 2.43 2.985-3.015, 3.00	Triple	RHCP RHCP RHCP
[102]	54×54	1.84-3.25, 1.41, 55.4	Single	1.86-3.53, 1.67, 61.96	Single	LHCP
Our Work	45×65	1.55-1.72, 1.60, 10.62 2.51-2.64, 2.55, 5.09 3.10-3.31, 3.20, 6.56 4.08-5.83, 5.20, 33.65 6.14-6.70, 6.50, 8.61	Penta	1.60-1.75, 1.65, 9.10 ------ ------ 4.54-4.90, 4.75, 7.58 6.21-6.49, 6.35, 4.41	Triple	RHCP LP LP LHCP RHCP

4.3 Design and Analysis Triple Band Antenna with Dual Sense CP

4.3.1 Antenna Structure

The physical shape of the triple band with dual sense CP is demonstrated in Figure 82. The open ring radiator print on a substrate while the reduced ground plane past on another side. Concerning the partial ground plane (tg×w), two pairs of slits have been etched in it. Also, two strips with rectangular shapes (nh×nw) are emerged from both sides (left and right) of the reduced plane. The type of substrate is FR4 type with relative permittivity 4.4 and thickness1.6 mm. Concerning the excitation of the proposed antenna, it fed via a direct feed line (hf×wf). The length of the antenna is 70 mm, whereas the width is 45 mm. All parameters that are presented in Table 5 and Table 6 have been built by the HFSS V13 simulator and verified experimentally.

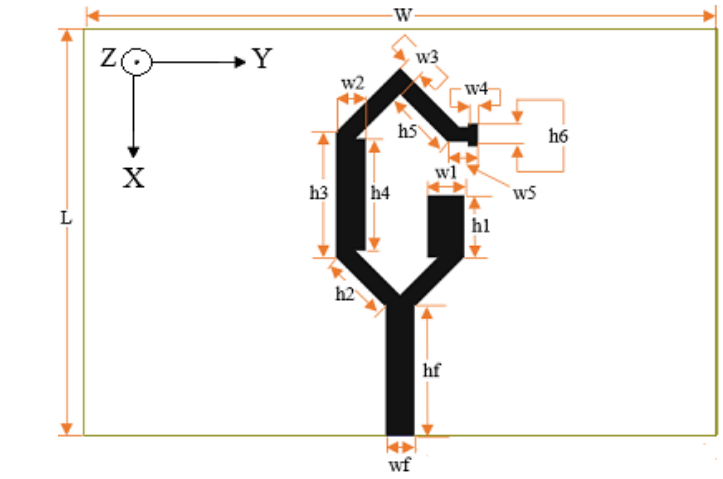

(a)

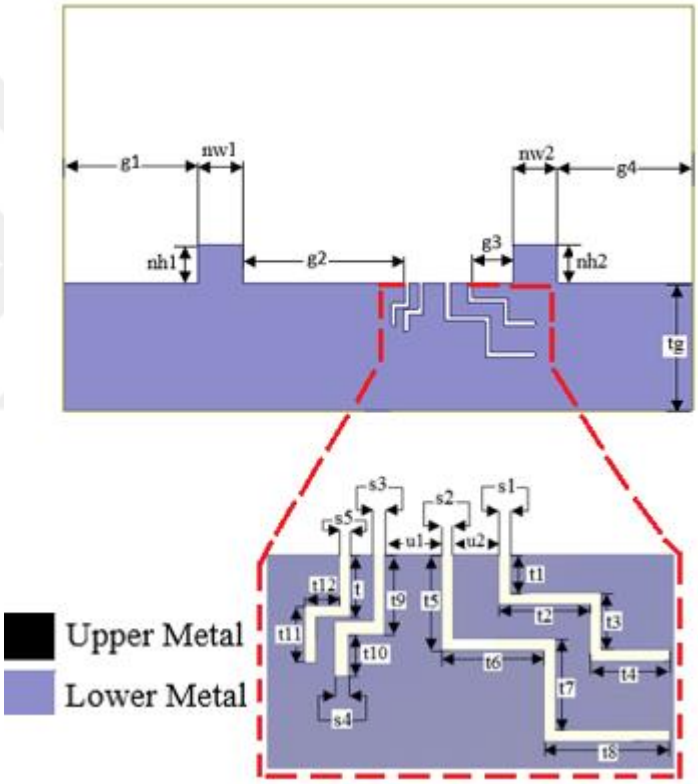

(b)

Figure 82 Structure of the open ring hexagonal triple band dual sense CP modified antenna (a) Top view, (b) Bottom view

Table 5 Dimensions of open ring triple band dual sense CP antenna

Parameter	Value (mm)	Parameter	Value (mm)
L	45	h5	7.41
W	70	h6	2.5
w1	4.07	hf	14.42
w2	3.27	g1	15
w3	2	g2	18
w4	1	g3	4.5
w5	2.25	g4	15
wf	3	tg	14.2
h1	6.75	nh1	4.3
h2	7.52	nh2	4.3
h3	13.75	nw1	5
h4	12.24	nw2	5

Table 6 Dimensions of stair slits

Parameter	Value (mm)	Parameter	Value (mm)
t1	1.7	t11	2.5
t2	4	t12	1.5
t3	2.5	t	2.7
t4	3.5	s1	0.5
t5	4.2	s2	0.5
t6	4.5	s3	0.5
t7	4	s4	0.6
t8	5.5	s5	0.5
t9	3.5	u1	2.5
t10	1.8	u2	2

4.3.2 Current Distributions on Surfaces

The allocation of current on the surface conductors is needful for explaining CP propagating manner. It implemented an open ring modified at the first band with resonance frequency of 1.575 GHz and second band at 4.5 GHz, as observed in Figure 83 sequentially. Figure 83 describes the allocation of current in two time instants first when $t=0^{\circ}$ and second at $t=90^{\circ}$ for 1.575 GHz and 4.5 GHz, sequentially. As noted in Figure 83, the circular polarization can be observed clearly at $t=0^{\circ}$ and $t=90^{\circ}$. For

instance, at 1.575 GHz, the identical amplitudes of current with phase difference 90° checked on surface conductors, particularly in $\vec{J}_4$ with $\vec{J}_6$ and $\vec{J}_1 + \vec{J}_2$ with $\vec{J}_3 + \vec{J}_5$ at t= 0° and when t= 90°, the $\vec{J}_5$ with $\vec{J}_7$ and $\vec{J}_1$ with $\vec{J}_4$. Concerning the resonance frequency of last band (4.5 GHz), when t=0°, the perpendicularity and identically fruited at the upper and lower part of open-loop hexagonal radiators such as $\vec{J}_5$ with $\vec{J}_6$ and $\vec{J}_1 + \vec{J}_2$ with $\vec{J}_3 + \vec{J}_4$ as well as the currents in stair slits region and left rectangular strip emerged from the ground plane. Also, as related to t=90°, upper and lower part of open-loop hexagonal radiators such as $\vec{J}_5$ with $\vec{J}_6$ and $\vec{J}_1 + \vec{J}_2$ with $\vec{J}_3$ as well as the currents in stair slits region and left rectangular strip emerged from the ground plane. From Figure 83 (a), it observed that the kind of propagated wave is RHCP in the direction of propagation since the summation of the current vector ($\vec{J}_{sum}$) roll around counterclockwise as time raises on the contrary at 4.5 GHz, it viewed that the $\vec{J}_{sum}$ rolls around clockwise trend as time raises. Thus, LHCP radiation is made along the direction of propagation. The current vectors intensity with reverse way are disregard, as shown in Figure 83 (b).

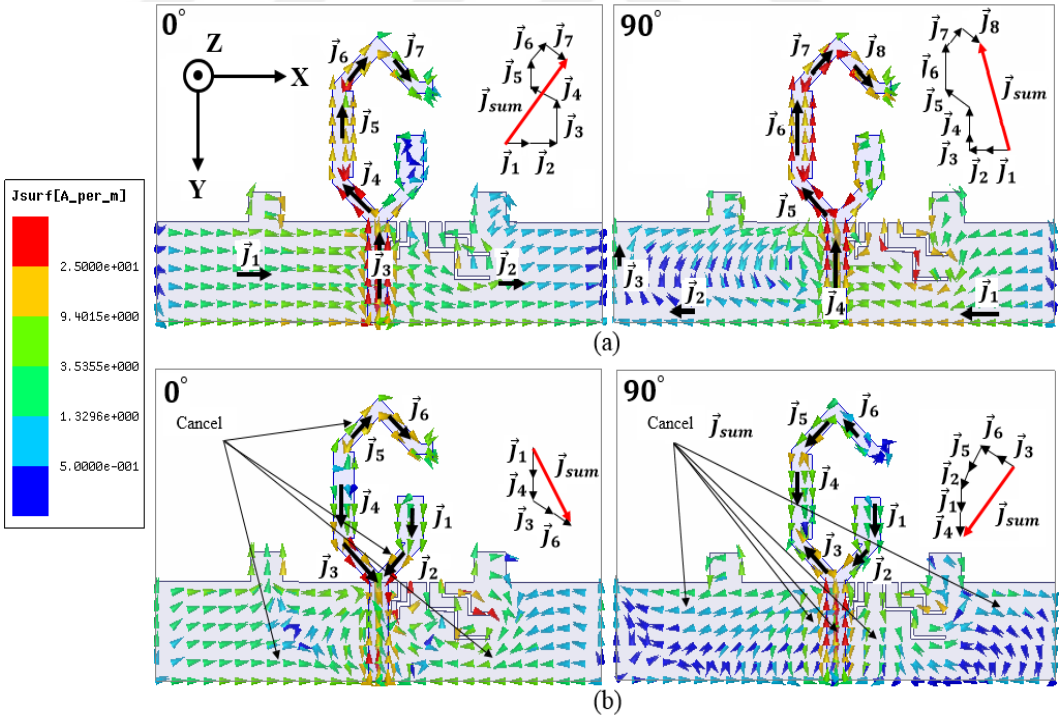

Figure 83 Allocation of currents on antenna surfaces at (a) 1.575 GHz, (b) 4.5 GHz.

4.3.3 Parametric Study

4.3.3.1 Impact of Parameter, w4

Figure 84 (a) demonstrates the effect of the parameter w4 on |S11| (reflection coefficient) while Figure 84 (b) describes the AR response. It observed that the w4 plays a major role at 2.55 GHz. The impedance matching enhanced at w4=1 mm. Regarding the AR level, the CP condition (AR≤3 dB) increased from 0,55 GHz to 1.03 GHz which implies that the perpendicularity of the electric field raised to the max.

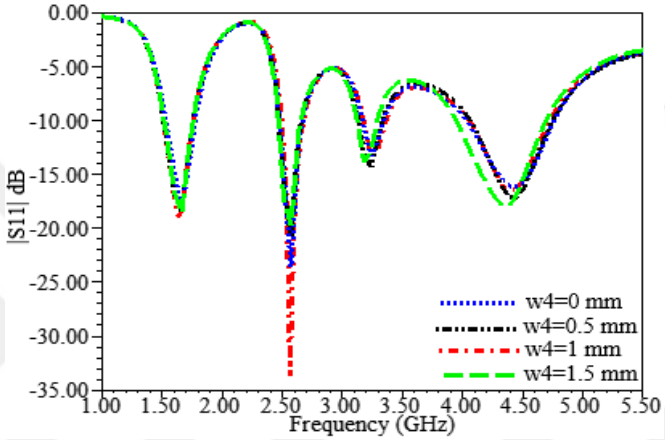

(a)

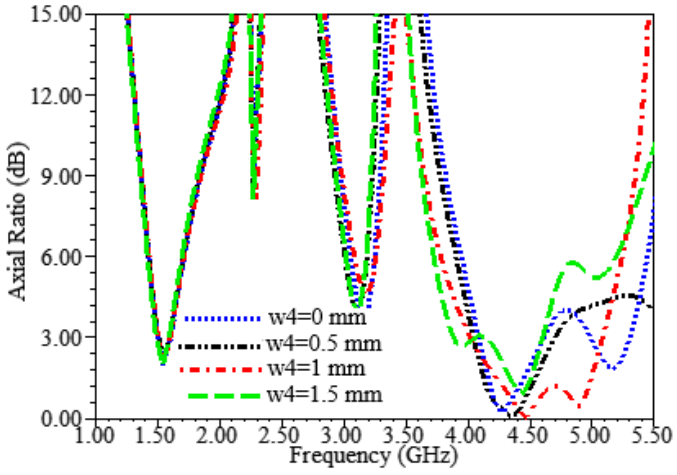

(b)

Figure 84 The impact of w4 on antenna behavior (a) |S11|, (b) AR

4.3.3.2 Impact of Parameter, s1 and s2

Figure 85 explains the influence of the parameters s1 and s2 on the reflection coefficient and axial ratio level. The mentioned figure clarifies that the stair slit s2 has a major role in impedance matching improvement regarding the first band. Also, it

observed that the second band is disappeared completely when s2 goes to zero. So, it is in charge of the mentioned band production. Concerning the s1, its role appeared at first and last bands, As related to the first band, one of them is adequate to satisfy the CP condition. However, for the last band, the axial ratio bandwidths (ARBW) become superior when s1 and s2 exist together in the ground plane.

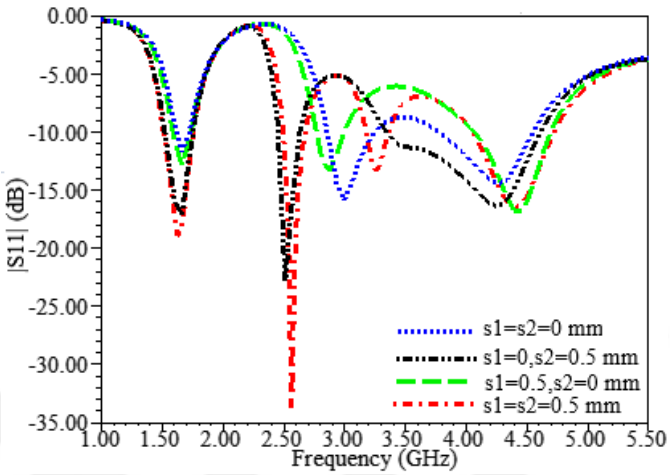

(a)

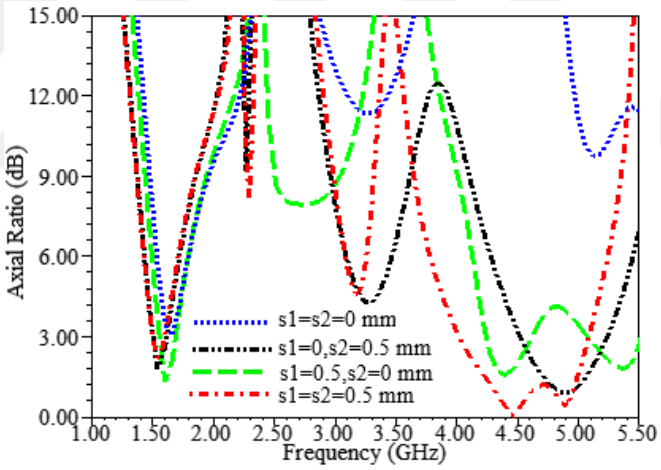

(b)

Figure 85 The impact of s1 and s2 on antenna behavior (a) |S11|, (b) AR

4.3.3.3 Impact of Parameters, s3, s4, and s5

Figure 86 presents the essential impact of parameters s3, s4, and s5 on the |S11| and AR. The significance of them appeared on the last band, whether in reflection coefficient or axial ratio. The optimum case viewed when s3=s4=0.5 mm, s5=0.6 since they offered a max axial ratio bandwidth. Moreover, they generate an appropriate matching impedance at the last band that coats it completely with an axial ratio lower than 3dB.

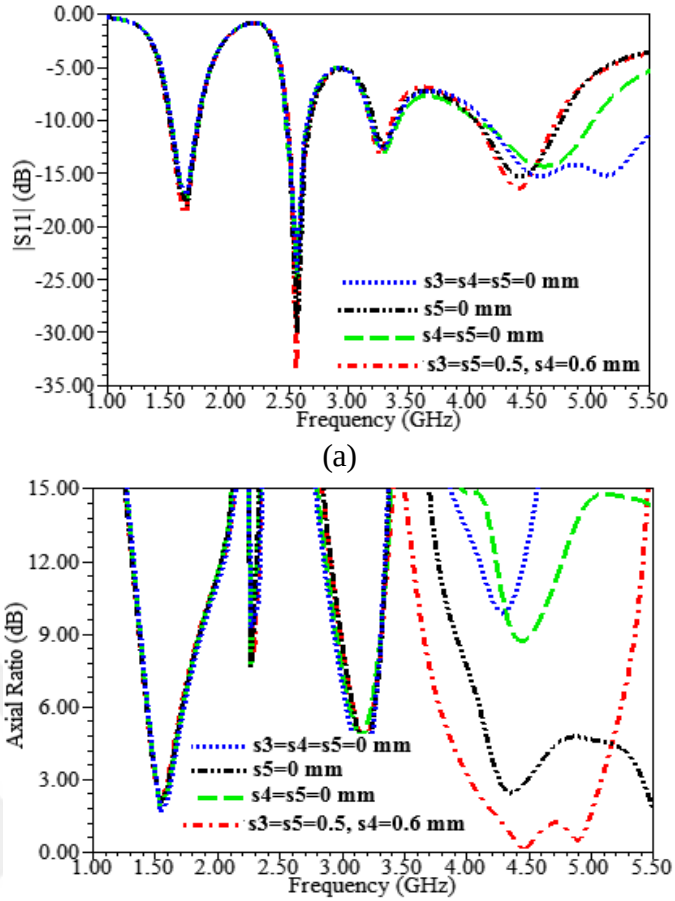

Figure 86 The impact of s3, s4, and s5 on antenna behavior (a) |S11|, (b) AR

4.3.3.4 Impact of Parameters, rectangular strips (nh×nw)

The function of rectangular strips (4.3×5) mm^2 together was clear in axial ratio bandwidth (ARBW) improvement. At the last band, the ARBW is boosted from 4.8% to 23.2%. In addition, the reflection coefficient became coupled with the axial ratio as observed in Figure 87.

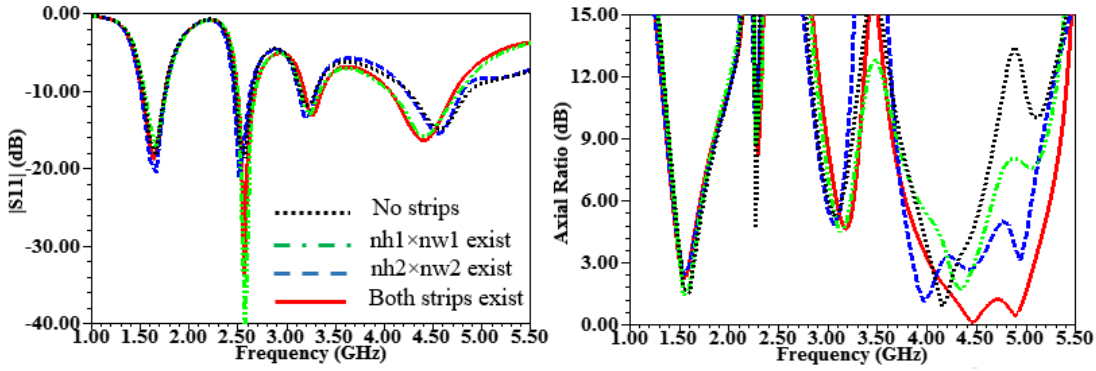

Figure 87 The impact rectangular strips on antenna behavior (a) |S11|, (b) AR

4.3.4 Results and Discussions

4.3.4.1 The |S11| and AR

For verifying the simulated outcome, the antenna should be fabricated and pass the measurement successfully. Figure 88 demonstrates the practical side of it. Figure 88 (a) and (b) present the fabricated antenna: front side and backside whereas the other two subfigures show the antenna under test. The reflection coefficient of it tested by a vector network analyzer (VNA) while the axial ratio, gains, and radiation patterns tested at the anechoic chamber.

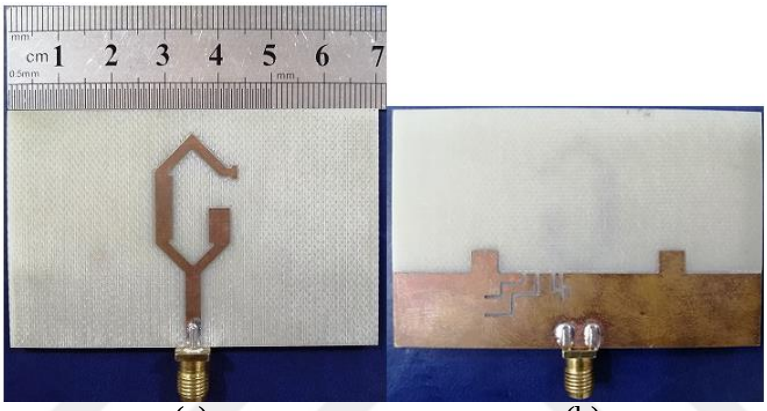

(a) (b)

(c)

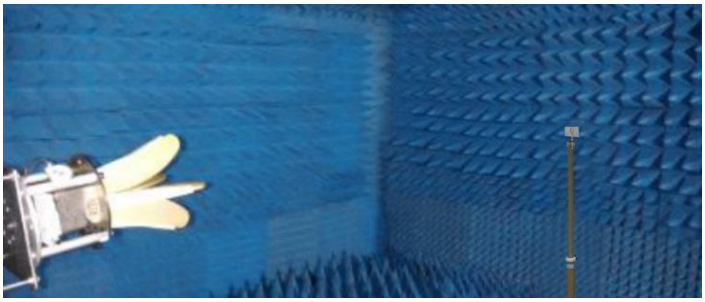

(d)

Figure 88 The fabricated of the modified antenna (a) Top view, (b) Bottom view, (c) Under VNA test (d) Measurement of radiation in the anechoic chamber

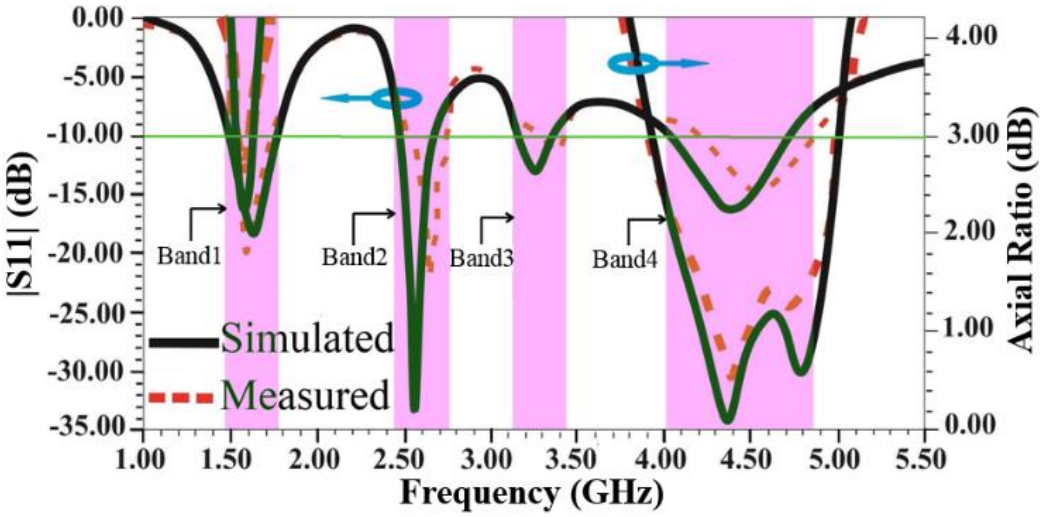

Figure 89 The |S11| and AR against frequency of the modified antenna.

The outcomes of the simulated and measured of the reflation coefficient and axial ratio collected in Figure 89. It indicates that there is unison between simulated and practical results at band1 as related to impedance matching and axial ratio level whereas the others are a little moved towards the right side (high-frequency zone) because of the dielectric material characteristic and connector sensitivity. Moreover, the AR is under 3 dB at both the band1 and band 4 zones. This matter implies that the modified antenna can be propagated or receive the signals that own a circular polarization characteristic. Concerning the second and third bands, AR>> 3 dB, so they have linear polarization (LP) merits. As related to the third band, it is omitted due to the S11> -10 dB. Table 7 presents the all simulated and measured values regarding the |S11| and ARBWs.

Table 7 The simulated and experimented outcomes of the modified antenna

Bands	**(Simulated) IBWs (GHz, f2-f1, %)**	**(Measured) IBWs (GHz, f2-f1, %)**	**(Simulated) 3-dB ARBWs (GHz, %)**	**(Measured) 3-dB ARBWs (GHz, %)**
Band1	(1.515-1.761), 246, 15	(1.478-1.714), 236, 14.7	(1.508-1.604), 6.2	(1.510-1.606), 6.2
Band2	(2.496-2.679), 183, 7.1	(2.54-2.72), 180, 6.8	None	None
Band3	(3.178-3.363), 185, 5.7	(3.32-3.42), 100, 3	None	None
Band4	(4.054-4.732), 669, 15.2	(4.29-4.89), 600, 13.1	(4.025-5.081), 23.2	(4.035-5.07), 22.7

4.3.4.2 Gain and Radiation Patterns

Figure 90 and Figure 91 demonstrate the gains and radiation patterns of the modified antenna respectively. They are obtained by HFSS simulator and practically in far field region at anechoic chamber. Concerning the gains, the simulated and experimental outcome shown in Table 8.

Table 8 The simulate and particular gains at resonance frequencies for modified antenna

No.	Simulated gains dBi	Measured gains dBi	Frequency GHz
1	2.17	2	1.575
2	3.94	3.5	2.55
3	5	4.9	4.5

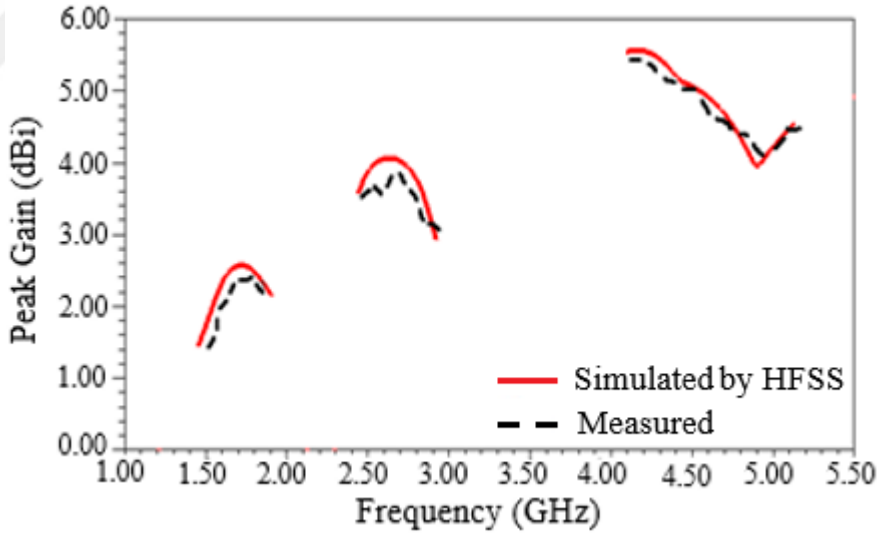

Figure 90 Simulated and experimented peak gain values of the modified antenna.

Concerning another criterion (radiation pattern), also the simulated and practical results compared and the results were convergent at XZ and YZ planes at center frequencies shown below. At first band, the right hand circular polarization (RHCP) propagated along with the +z trend while left hand circular polarization (LHCP) along the reverse side. Regarding Figure 91 (b), the co and cross polarized wave plotted in both planes. When phi=**0**$^{\circ}$, the divergence between them becomes 15 dB in the trend

of propagation. In addition, the wave shape of co polarization is omnidirectional while its bi directional in another plane. At a center frequency of the last band, the radiated shape can be seen in Figure 91 (c). It indicates that the antenna radiates left hand circular polarization (LHCP) along the direction of propagation. Furthermore, the pattern form is a little tilted from the major axis in XZ and YZ planes due to the asymmetrical structure of the radiator.

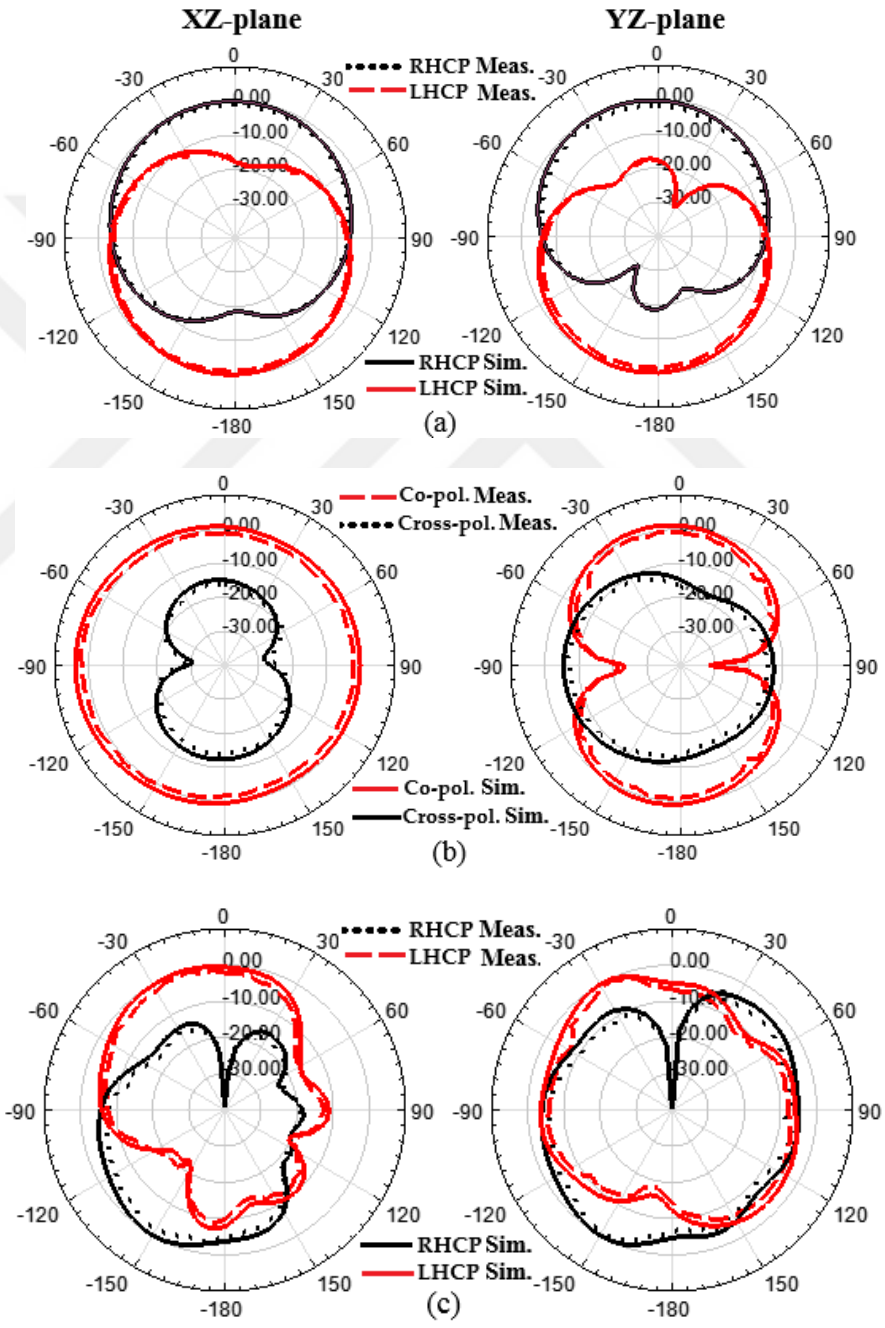

Figure 91 Normalized radiation patterns of the open loop hexagonal triple band dual sense CP antenna (a) 1.575 GHz, (b) 2.55 GHz, (c) 4.5 GHz.

4.3.4.3 Comparison of Triple Band Dual Sense CP Antenna with Previous Works

The designed antenna as demonstrated in Figure 82 is distinctive from other recently published works in one of specification at least. Table 9 describes the comparison between current work and others. It observed that it is compact as compared to others as well as ARBW has been enhanced.

Table 9 Comparison of triple band dual sense CP antenna with previous works

Ref.	Size (mm^2)	IBW (GHz, fc, %)	$\|s11\| < -10$ dB Bands	3-dB ARBWs (GHz, fc, %)	Polarization
[12]	80×80	1.26-1.654, 2.46, 26.7 2.44-2.738, 2.59, 11.3	Dual	1.474-1.566, 1.5, 6.1 2.512-2.677, 2.6, 6	RHCP LHCP
[13]	70×70	1.54-1.68, 1.6, 8.7 1.96-2.47, 2.2, 23	Dual	1.54-1.675, 1.6, 8.4 2.02-2.45, 2, 19	RHCP LHCP
[24]	63.5×55	1.57-2.04, 1.75, 26.04 2.87-3.47, 3.25, 18.93	Dual	1.6-2, 1.8, 22.2 3.15-3.5, 3.325, 10.53	RHCP LHCP
[79]	230×210	1.42-1.6, 1.51, 12 2.14-2.56, 2.35, 18	Dual	1.49-1.53, 1.51, 3 2.34-2.43, 2.38, 4	RHCP RHCP
[83]	60×60	2.4-2.5, 2.45, 9.1 4.98-6.5, 5.8, 26.2	Dual	2.42-2.47, 2.45, 1.842 5.72-5.89, 5.8, 2.97	RHCP RHCP
[84]	60×60	2.4-2.53, 2.45, 5.27 5.6-6.15, 5.8, 9.36	Dual	2.428-2.471, 2.45, 1.76 5.877-5.877, 5.8, 2.67	LHCP LHCP
[85]	100×100	2.015–2.37, 2.19, 16.2 2.64–2.95, 2.79, 11.29	Dual	2.238-2.285, 2.256, 2.1 2.645-2.69, 2.667, 2	LHCP LHCP
[86]	80×80	1.595–1.632, 1.61, 2.3 2.395–2.574, 2.45, 7.2	Dual	1.609-1.619, 1.61, 0.6 2.474–2.509, 2.49, 1.4	LHCP RHCP
This work	70×45	1.48-1.714, 1.59, 14.7 2.54-2.72, 2.63, 6.8 4.29-4.89, 4.59, 13.1	Triple	1.51-1.606, 1.558, 6.2 ---------- 4.035-5.07, 4.552, 22.7	RHCP LP LHCP

CHAPTER 5

DESIGN AND ANALYSIS OF MULTIBAND CIRCULAR POLARIZATION SQUARE SLOT ANTENNAS (CPSSAs)

5.1 Introduction

New designs of multiband circular polarization antennas have been presented in this chapter. These monopole antennas feed by coplanar waveguide (CPW). The behavior of these antennas have been inspected via HFSS simulator which gave clear information regard to each operation band. For instance, an axial ratio level considers an important parameter to know the circular polarization in each band. Furthermore, the other parameters such as radiation pattern, gain, radiation efficiency have been expressed and analyzed. The suggested technique displays a new alternative to build low cost, omnidirectional radiation pattern CP antennas suitable for a wide range of wireless communication system.

5.2 Design and Analysis Triple Band CPSSA.

5.2.1 Antenna Configuration

The physical shape of the suggested antenna is displayed in Figure 92. The radiator and ground plane are printed on one side of the substrate. The radiator consists of two hooks with opposite contacted direction. Regarding the ground, it composed of open loop square ring with loaded by two rectangular strips (a1×b1, a2×b2). These strips are located at opposite corner of inner square ring to produce CP waves. The thickness of substrate, relative permittivity (ε_r), and loss tangent $tan\ \delta$ is 1 mm, 4.4 and 0.02 respectively. The overall dimension of the antenna is as consolidated as 40×40×1 mm^3. Regarding the radiating part, it seems to be two hooks with the opposite connected direction which fed by CPW (coplanar waveguide) 50 Ω. The optimized parameters of the proposed antenna after numerically studied on HFSS are listed in Table 10.

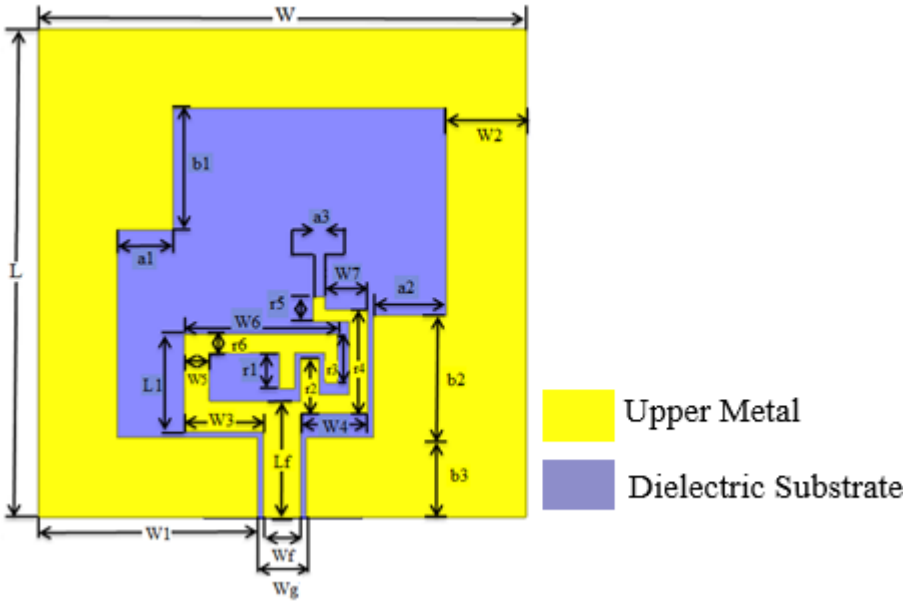

Figure 92 The structure of the triple band CPSSA.

Table 10 Dimensions of the triple band CPSSA

Parameter	L	L1	Lf	W	W1	W2	W3
Unit (mm)	40	8	9.5	40	18	6.5	6.5
Parameter	W4	W5	W6	W7	Wg	Wf	a1
Unit (mm)	5.5	2	12.5	3.5	4	3	3.5
Parameter	a2	b1	b2	b3	r1	r2	r3
Unit (mm)	6	10	10	6.5	3	4.5	4
Parameter	r4	r5	r6	a3			
Unit (mm)	8.5	2	1.5	1			

5.2.2 Design Procedure

The proposed antenna passed through four scientific steps as shown in Figure 93. The results of Ant.1 were negative. The results came logically because there is no clear radiator part. In Ant.2, the radiator started to appear as a hook. The responses were positive comparatively. The first band configured with impedance bandwidth (IBW) from (4.2 to 6 GHz) whereas second band appeared from (10.8 to 11.3 GHz) and axial ratio (AR) near to 3-dB as seen in Figure 94 (a) and (b) respectively.

In Ant.3, the radiator modified and became to be as two inverted hooks which changed the antenna characteristics by improving the reflection coefficient |S11| value at 11 GHz region. In the last stage, so as to reach or satisfy the circular polarization target, the axial ratio must be less than 3-dB in operating frequencies. One of method is that adding two patches in opposite direction of corners [22,91]. The method is activated in this design. when unequal rectangular patches added, the CP waves started to appear clearly in two operating bands. Furthermore, a new band appeared at (7.60 to 8.40 GHz) with ARBW 5%.

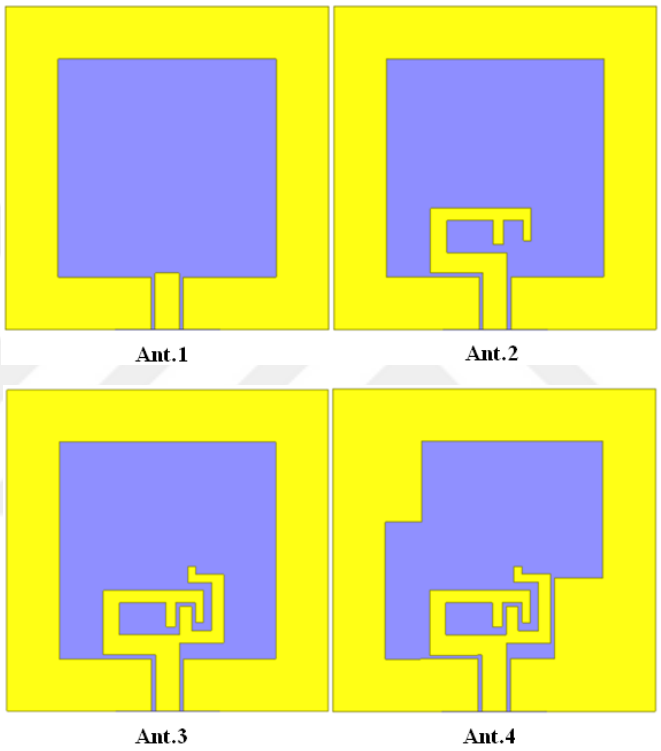

Figure 93 The steps to perceive the triple band CPSSA

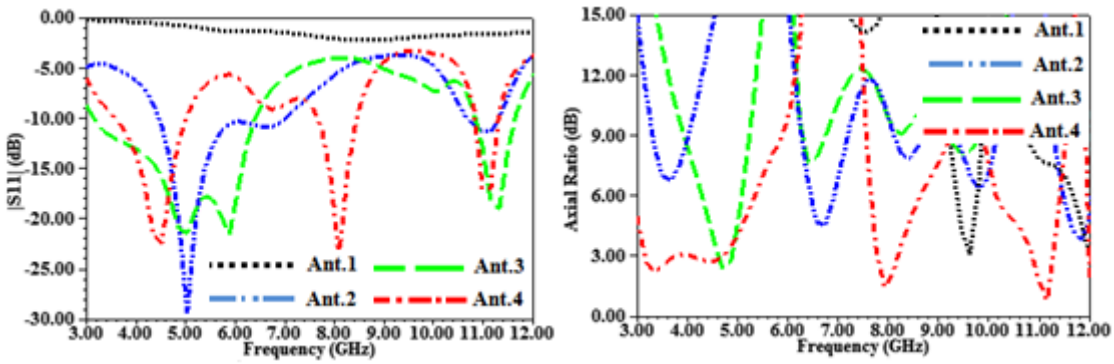

(a) (b)

Figure 94 The response of each step of the proposed CPSSA (a) |S11|, (b) AR

5.2.3 Current Surface Distributions

The radiated wave from circularly polarized antenna may be right or left hand circularly polarized. To investigate this property from proposed antenna, the current distribution on the surface conductor must be known. As shown in Figure 95, the current allocation is inquired at all operating bands 3.2 GHz, 8 GHz and 11 GHz respectively.

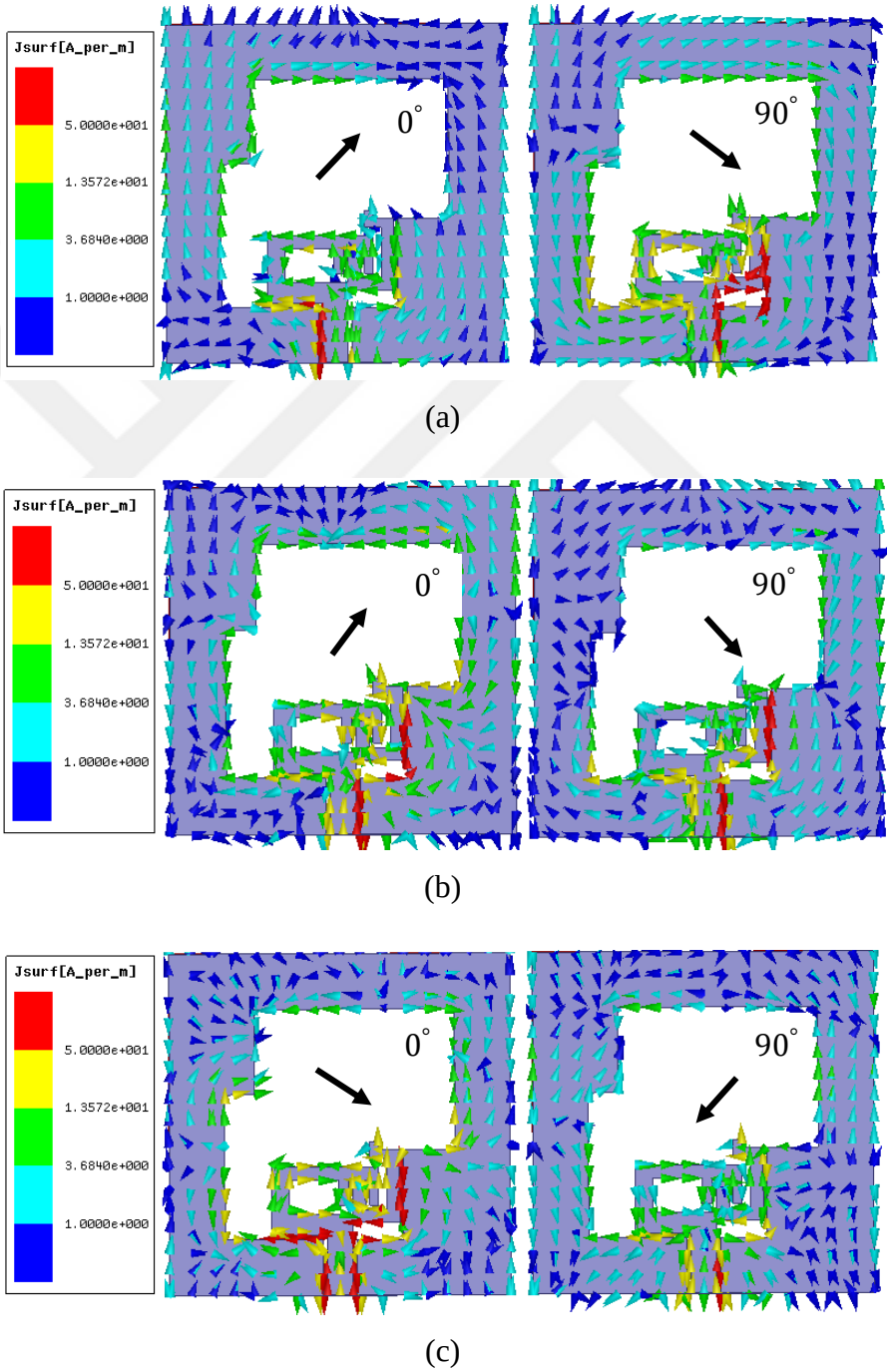

Figure 95 The surface current distribution of the triple band CPSSA at (a) 4 GHz, (b) 8 GHz, (c) 11GHz in $0^{\circ}$and 90° phase

The current distribution at 3.2 GHz, 8 GHz and 11 GHz presented in Figure 95 (a), (b), and (c) respectively with different time instants 0°, 90°. They viewed that the resultant current vector rotates clockwise direction leads to contribute left-handed circular polarization (LHCP) radiation.

5.2.4 Parametric Study of Triple Band CPSSA.

The parameters a1, b1, w7, r2, and r3 contributed to be the proposed antenna a multiband CP. In order to know the weight of each one, the study has been carried on by a superposition way. Then the effect these parameters on each band became obvious.

5.2.4.1 Effect of Parameter, a1

The a1 represents the width rectangular strip located on the ground plane (far from the radiator) as noted in Figure 96. The impact of it observed on AR, especially in the second and third bands. By taking values from (9-12) mm, the |S11| and AR responses gave appropriate response at a1=10 mm as shown in Figure 96 (a) and (b).

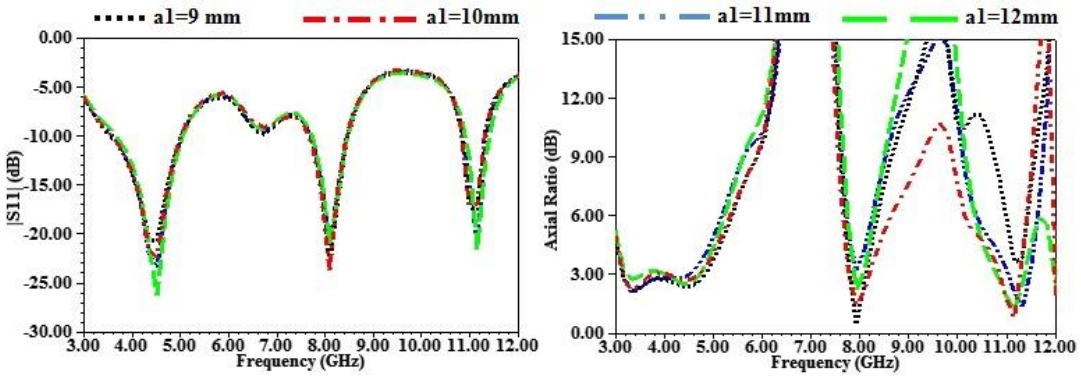

(a) (b)

Figure 96 The effect of a1 on antenna performance (a) |S11|, (b) AR

5.2.4.2 Effect of Parameter, b1

The b1 acted the length of the rectangular strip located on the ground plane as shown in Figure 92. Indeed, it plays an important role in |S11| and AR responses. As seen in Figure 97 (a), when the value of b1 raised, the |S11| is decreased in the first band while the middle band affected negatively at b1=4.5. Regarding AR, the b1 influences

significantly on the last band. As per Figure 97 (b), the AR became less than 3-dB in the last band when the b1 =3.5 mm so the mentioned value nominated.

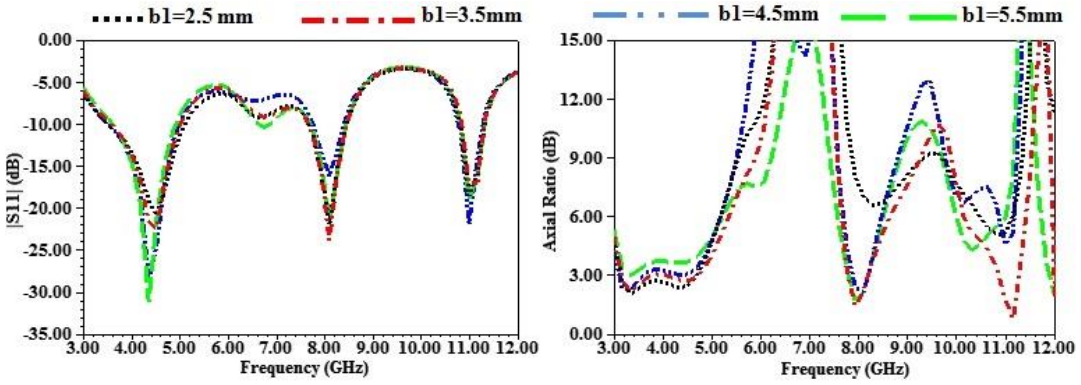

(a) (b)

Figure 97 The effect of b1 on antenna performance (a) |S11|, (b) AR

5.2.4.3 Effect of Parameter, w7

The w7 strip is a part of radiator. When the w7=3.5 mm, it contributes effectively for decreasing the AR level under 3-dB as noted in Figure 98 (b) as well as the AR for second and third band shifted to right for raising the matching between |S11| and AR as illustrated in Figure 98 (a) and (b).

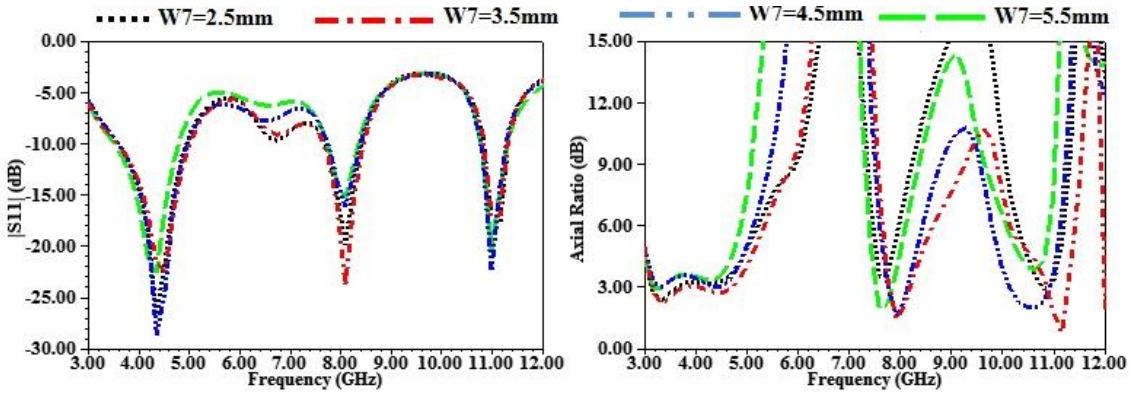

(a) (b)

Figure 98 The effect of W7 on antenna performance (a) |S11|, (b) AR

5.2.4.4 Effect of Parameter, r1

The effectiveness of r1 appears in the AR graph as illustrated in Figure 99 (b) specifically from 3 GHz - 5 GHz. The AR in the mention region exceeds the threshold of CP condition when it's equal to 3 mm. The second role is that it plays to increase

the axial ratio bandwidth (ARBW) for the middle band. Regarding |S11| response, it does not respond to major variation when the value of r1 changed from 1mm to 3 mm. when r1=4 mm, means it conducts to feed directly all of the responses will be changed except the last band, it keeps the CP characteristic as shown in Figure 99 (a) and (b).

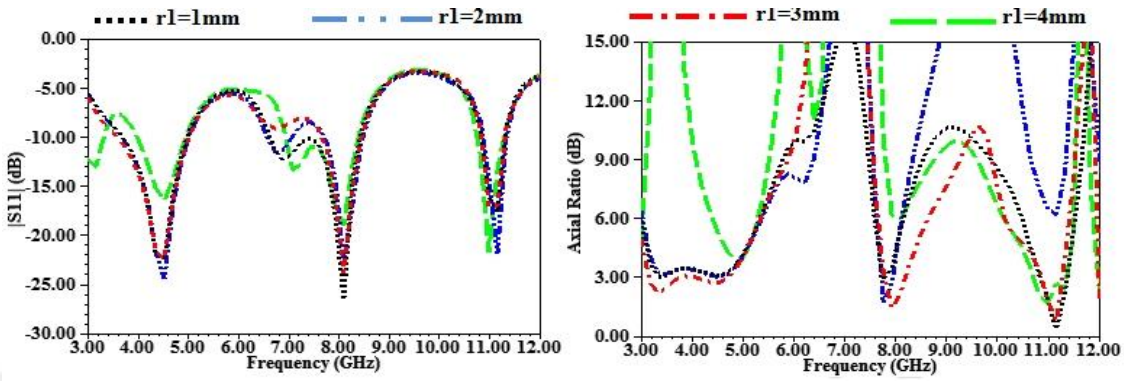

(a) (b)

Figure 99 The effect of r1 on antenna performance (a) |S11|, (b) AR

5.2.4.5 Effect of Parameter, r2

The r2 strip considers a part of the inverted hook. The influences of it do not appear significantly on |S11| response as seen in Figure 100 (a) except when r2=5 mm which means the strip contacts with another hook. The impact of it becomes clear at the AR response. From Figure 100 (b), the AR varied with r2 values. When r2= 4.5 mm, the AR response in all bands is settled under 3-dB especially in the second and third band.

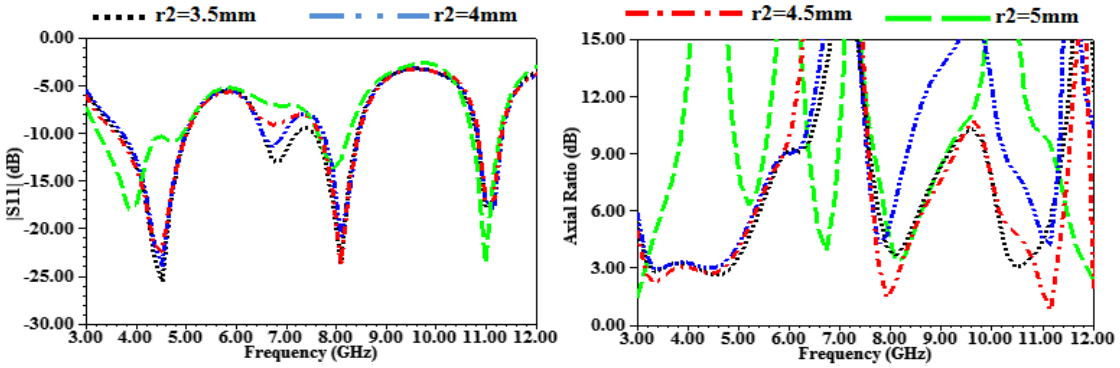

(a) (b)

Figure 100 The effect of r2 on antenna performance (a) |S11|, (b) AR

5.2.4.6 Effect of Parameter, r3

The r3 strip resembles r2 relatively. The roles of it can be note in the upper band. When r3= 4.5 mm, the axial ratio level decreased and reached to satisfy the CP condition.

Furthermore, it contributes to matching between AR<3 dB and |S11| responses as noted in Figure 101 (a) and (b).

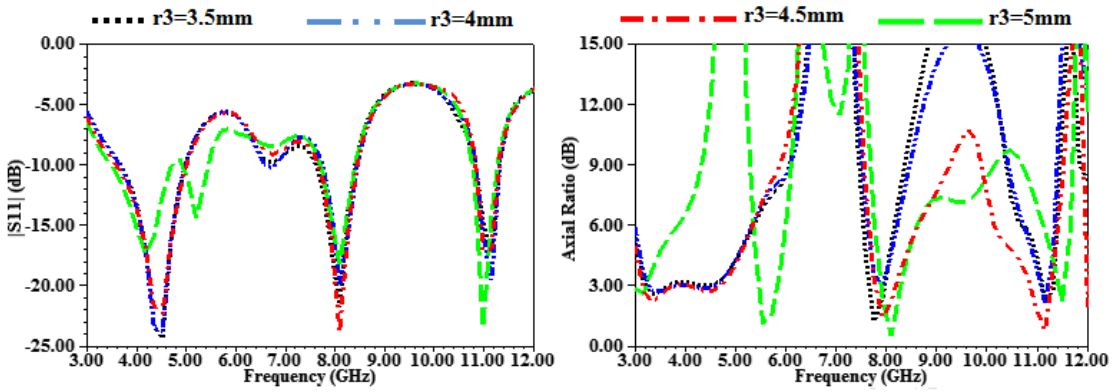

(a) (b)

Figure 101 The effect of r3 on antenna performance (a) |S11|, (b) AR

5.2.5 Results and Discussions

5.2.5.1 The |S11| and AR

In this subsection, the simulated results of the reflection coefficient and the axial ratio are presented in Figure 102 (a) and Figure 102 (b) respectively. The first band operates at (3.59-5.01 GHz) whereas the axial ratio under or equal to 3-dB appeared at (3.15-4.69 GHz). In the second band, the reflection coefficient extends from (7.64 to 8.43 GHz) while the AR≤ 3-dB located at (7.77-8.17 GHz). The last band appeared at (10.81-11.28 GHz), while the AR≤ 3-dB for that band observed at (10.84-11.25 GHz). Finally, the AR≤ 3-dB was evident in all operation bands which means that the CP exists in all operation bands.

5.2.5.2 Gain and Radiation Patterns

The simulated peak gain against frequency is illustrated in Figure 103. It noted that the proposed antenna appears variation in first band from (1-4 dBi). In second band, the peak gain is about (3.1-3.2 dBi) while in last band about (4.7-4.9 dBi). As per of the results, it obvious that all CP bands have good gains.

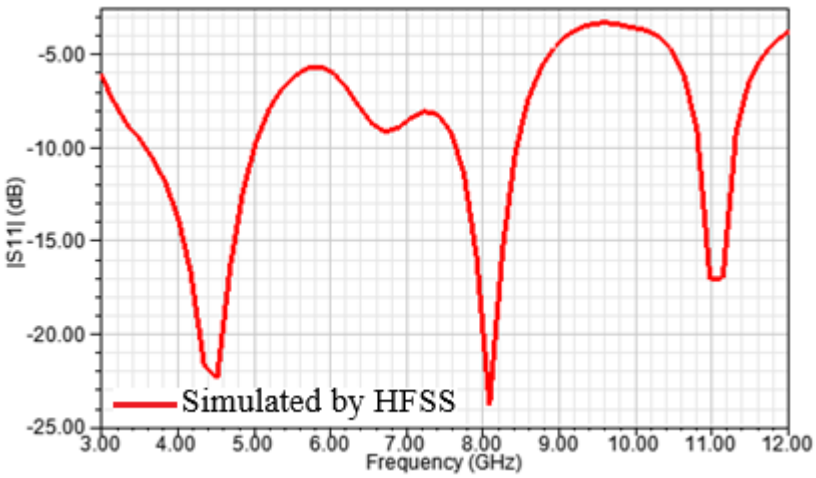

(a)

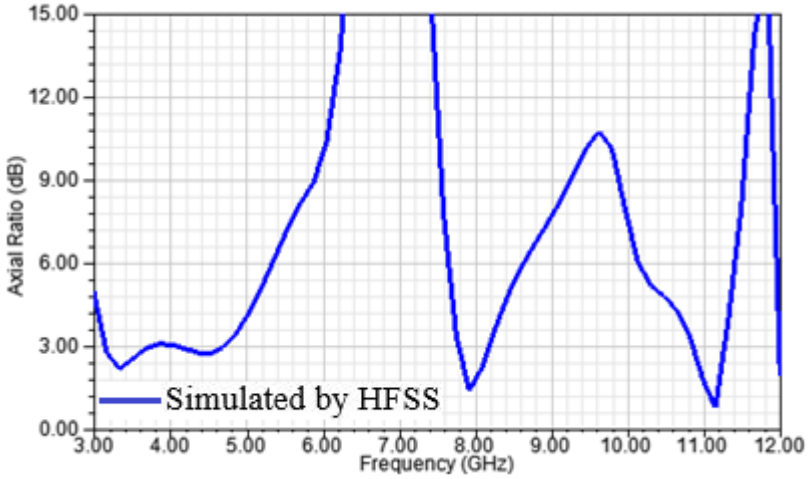

(b)

Figure 102 The |S11| and AR versus frequency of the triple band CPSSA (a) |S11|, (b) AR

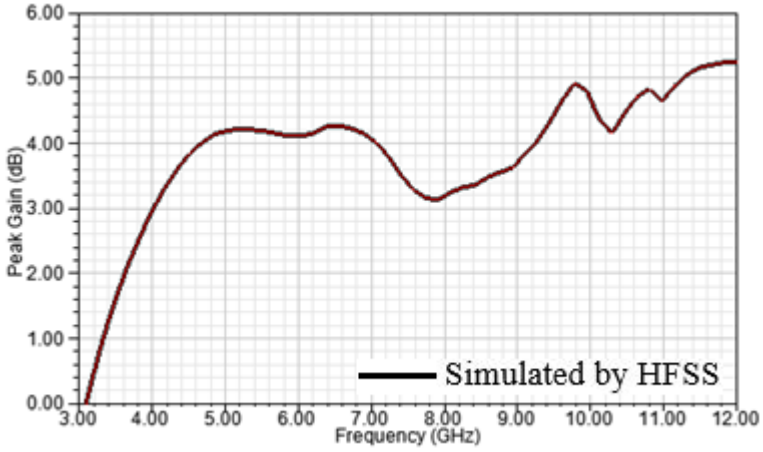

Figure 103 The peak gain of the triple band CPSSA

Figure 104 presents the simulated radiation patterns at frequencies 4.5 GHz, 8 GHz, and 11 GHz in E-plane and H-plane respectively. CPSSA radiates LHCP wave in +z direction while in opposite direction, it radiates RHCP in all selected frequencies. The cross polarization level at $\theta = 0^{\circ}$ is 16 dB, 15 dB and 26 dB in first, second, and third resonance frequency respectively.

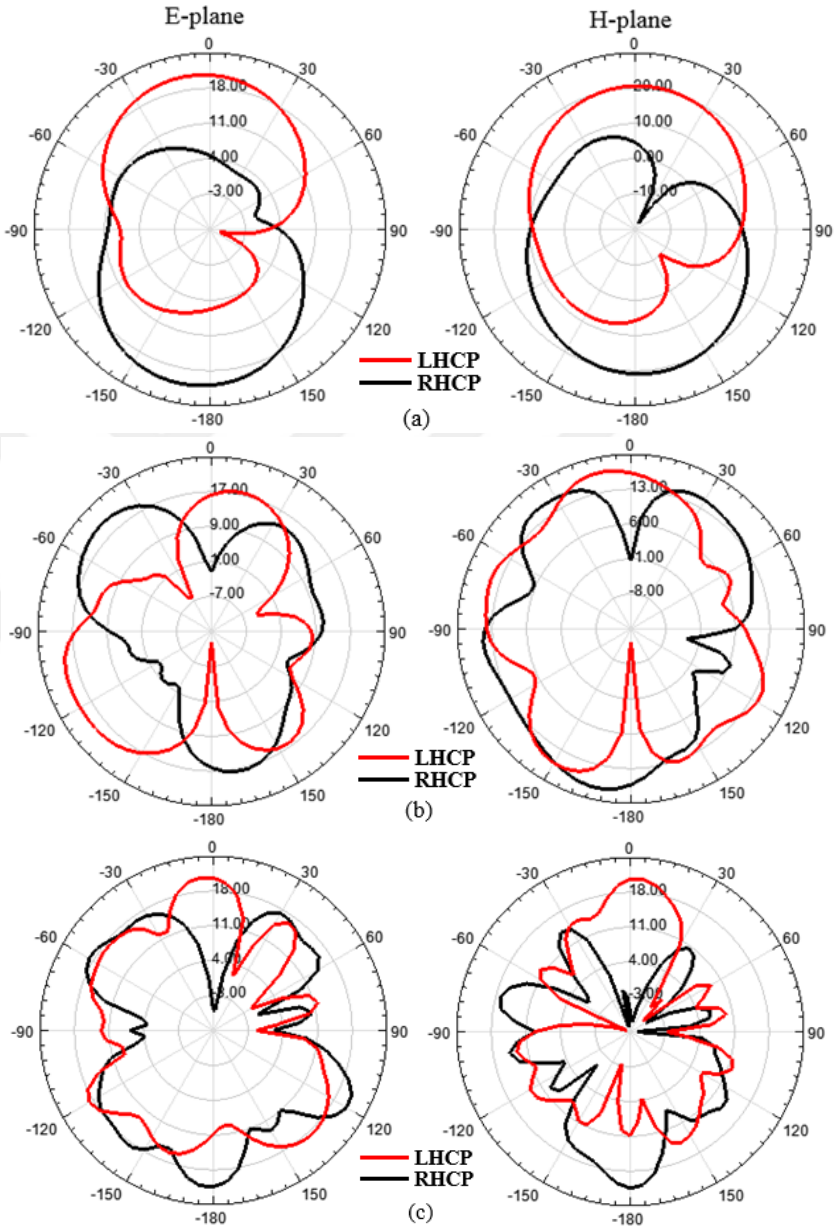

Figure 104 Radiation patterns of the triple band CPSSA at bands (a) 4.5 GHz, (b) 8 GHz, (c) 11 GHz.

5.2.5.3 Comparison of Triple Band CPSSA with Previous Works

Table 11 exhibits the comparison of the proposed antenna, which is triple-band CPSSA with previous works that have been presented recently. During the comparison, it observed that the proposed antenna features several properties. First, the number of CP bands. Second, the ARBW is enhanced obviously on all operation band as compared to others.

Table 11 Comparison of triple band CPSSA with previous works

Ref	size mm^3	S11≤ −10 dB	3-dB ARBWs (GHz, fc, %)	Number of CP bands
[14]	40×40	1871-3321 3731–7012 7887–11196	4.6-6.1, 5.35, 28	1
[99]	50×50	2.56-3.8 10.01-12.53	2.77-3.2, 2.98, 14 10.25-11.25, 10.75, 9	2
[100]	40×40	1.5-3.15	2.1-2.67, 2.38, 24	1
[110]	33×34	3.40–3.77 5.15–8.00	3.64–3.77, 3.7, 3 5.51–6.40, 5.9, 15	2
[116]	60×60	2.67-13	4.9-6.9, 5.9, 33	1
Our work	40×40	3.59-5.01 7.64 to 8.43 10.81-11.28	3.15-4.69, 3.92, 39 7.77-8.17, 7.97, 5 10.84-11.25, 11, 4	3

5.3 Design and Analysis Triple Band with Dual Band CPSSA

This antenna derivative from the first model antenna that considers a basic model for the others. The reason or justification for this update is to increase the purity of the circular polarization characteristic at the first band. As seen in Figure 105 (b), the axial ratio (AR) (Red line) for the first band of the previous model is near to 3-dB boundary means that the circular polarization was unstable for somewhat. To decrease the axial ratio, some parts of the basic model need to be changed or added. Depending on the approach employed in Refs. [115, 116], the basic model updated by adding an inverted

L-strip to the ground plane on the far corner of the radiator as shown in Figure 105. Actually, the adding of the mentioned strip directly to the ground plane leads to an impact in the first band positively. On the other hand, the second and third bands influenced negatively as illustrated in Figures 105 (a) and (b). Also, as per Figure 105 (b), the AR response at the last two bands is shifted while the impedance resonances of them remain in the same frequency as compared to | S11 | of the basic model as noted in the Figure 105 (a). This means that there is mismatching occurred between axial ratio under 3-dB and reflection coefficient responses at these bands. Moreover, the reflection coefficient increased at last bands in another meaning, the reflected power increased which affects negatively the antenna behavior. To solve this issue, the parametric study was implemented for getting more suitable results.

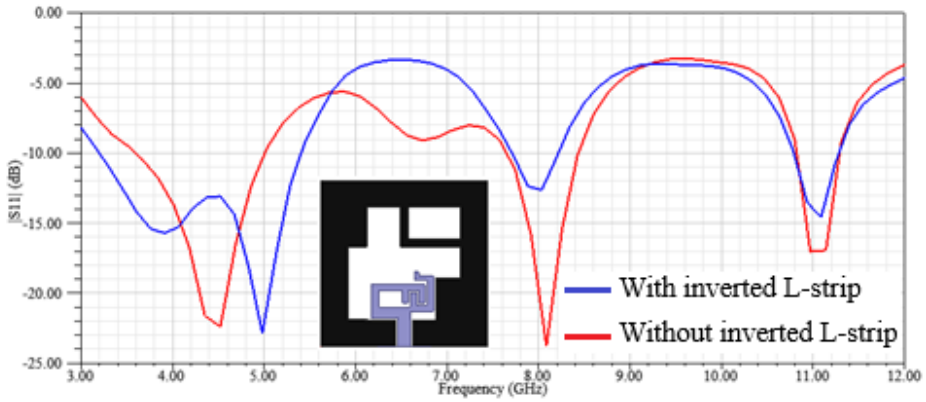

(a)

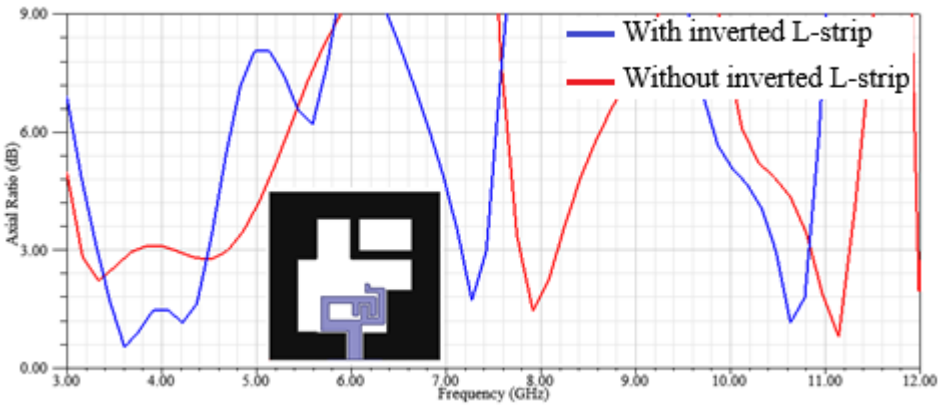

(b)

Figure 105 The responses after adding inverted L-strip and before (a) |S11|, (b) AR

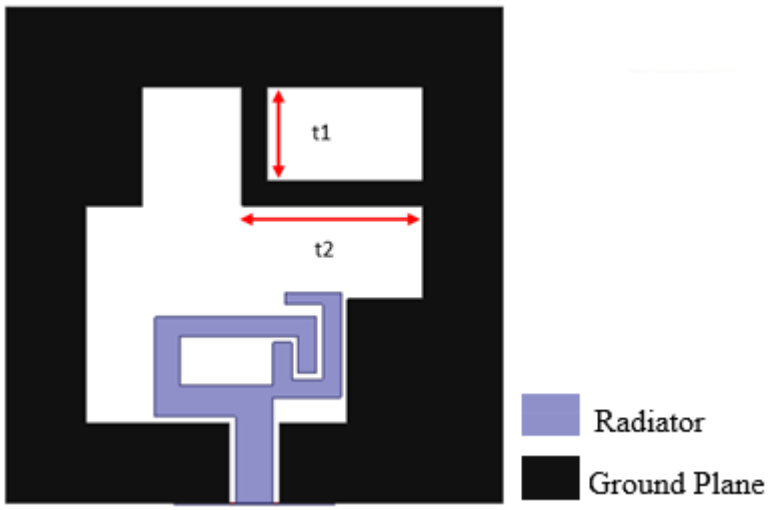

Figure 106 The structure of the first updated CPSSA

5.3.1 Parametric Study of First Updated CPSSA.

By testing all of the parameters, it found that r1 and r5 strips were behind the mentioned disorder on new model performance as observed in Figure 107 and Figure 108, so the structure updated depending on this study as shown in Figure 106.

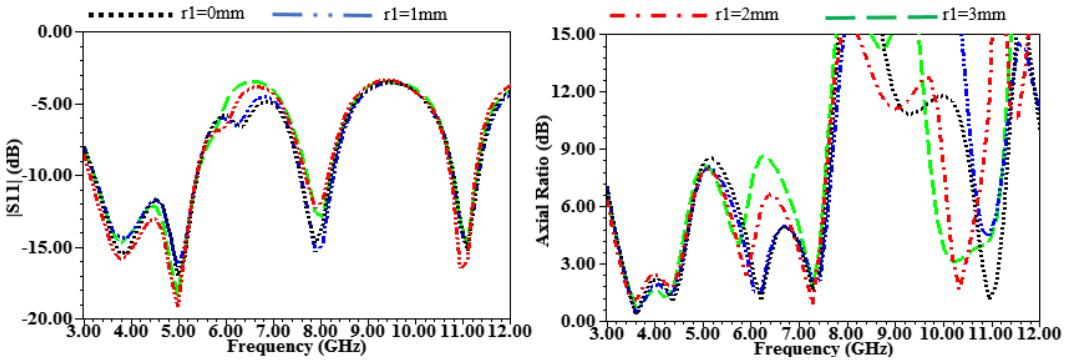

(a) (b)

Figure 107 The effect of r1 on first updated antenna performance (a) |S11|, (b) AR

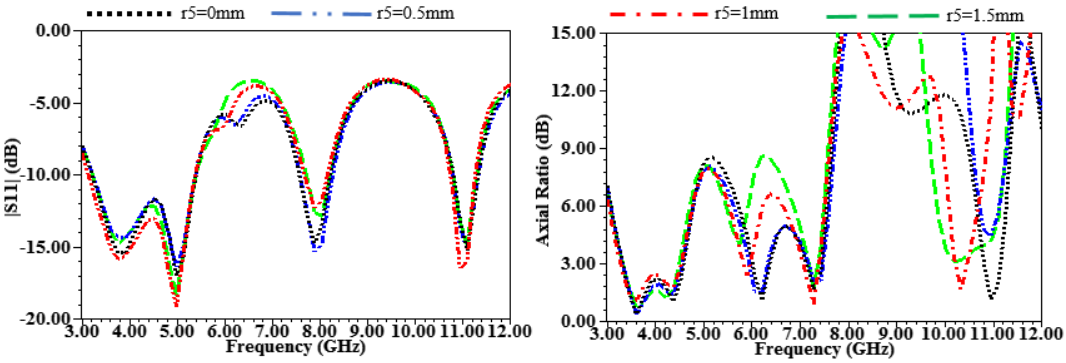

(a) (b)

Figure 108 The effect of r5 on first updated antenna performance (a) |S11|, (b) AR

5.3.1.1 Inverted L-strip

The parameters t1 and t2 compose the inverted L-strip, which considers a cornerstone regarding the stability of AR under the 3-dB level at the first band. Moreover, the value of t1 and t2 play a distinct role in satisfying the CP condition at the last band as illustrated in Figure 109 and Figure 110. By testing in the HFSS simulator, the t1 and t2 values were taken 9.5 mm and 12.5 mm respectively.

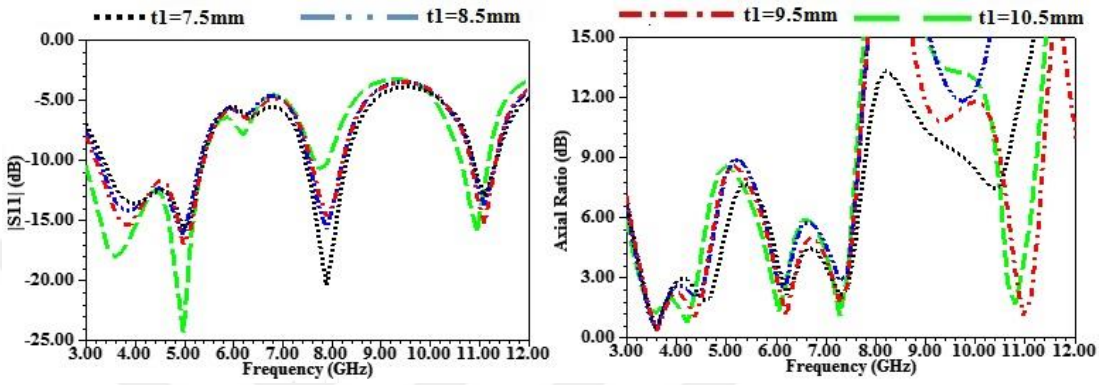

(a) (b)

Figure 109 The effect of t1 on first updated antenna performance (a) |S11|, (b) AR

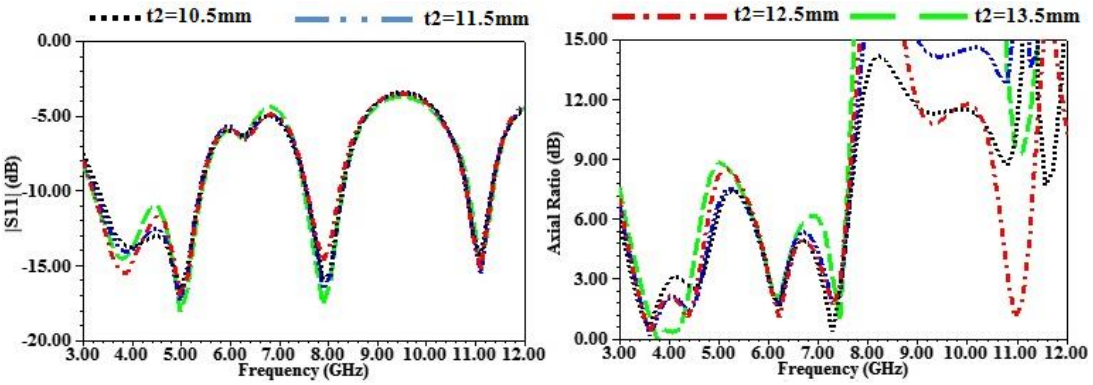

(a) (b)

Figure 110 The effect of t2 on first updated antenna performance (a) |S11|, (b) AR

5.3.2 The Results and Discussions of First Updated Antenna

In this part, the simulated results of the first updated antenna have been demonstrated in Figure 111. Based on Figure 111 (a), there are three bands have been appeared. The impedance bandwidth of the first band extends from 3.2 GHz to 5.39 GHz. The IBW of the second band started from 7.55 GHz to 8.21 GHz while the last band extends

from 10.79 GHz to 11.31 GHz. Concerning the polarization of each band, it can be found by knowing the axial ratio (AR) level. The AR at the first band region is less than 3-dB it extends from 3.32 GHz to 4.58 GHz which covers 57% of the band. Concerning the second band, the axial ratio of its more than 3-dB, so, can be considered or classified as a linear polarization band. Regarding the last band, the axial ratio level at its region satisfies the circular polarization condition that extends from 10.79 GHz to 11.13 GHz that covers 65% of the band.

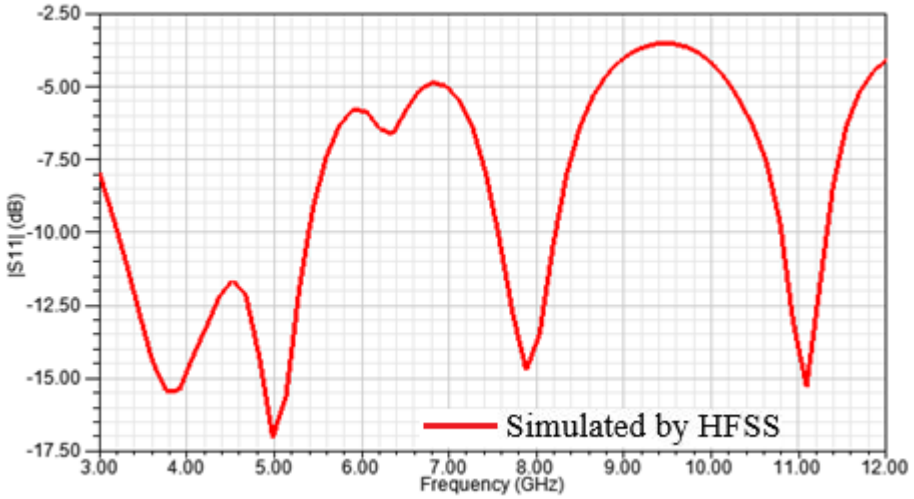

(a)

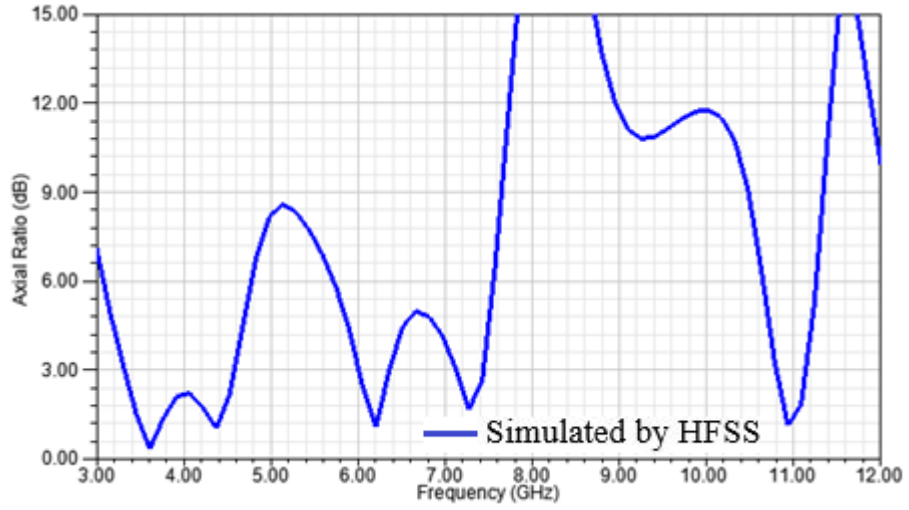

(b)

Figure 111 The |S11| and AR versus frequency of the first updated antenna (a) |S11|, (b) AR

5.3.2.1 Gain and Raddiation Pattrens

The peak gain against frequency is presented in the Figure 112. It obtained that the proposed antenna appears variation in the first band from 1.7 dBi to 4.9 dBi. In the

second band, the peak gain is about 3.2 dBi while in last band about 5.1 dBi. As per the results, it obvious that both first and last CP bands enhanced as compared to the peak gain of the basic model.

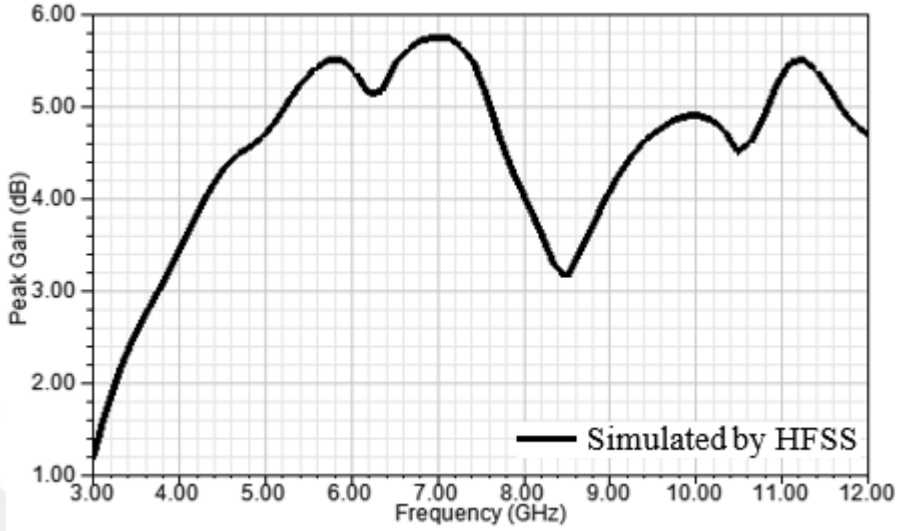

Figure 112 The peak gain of first updated CPSSA

The radiation patterns for the first updated antenna is simulated and obtained at $\text{phi} = 0^{\circ}$ and $\text{phi} = 90^{\circ}$ at 3.6 GHz, 8 GHz, and 11 GHz respectively as noted in Figure 113. For the first band, the radiated wave is LHCP in the +z direction whereas radiates RHCP in the opposite direction as shown in Figure 113 (a). Regarding the middle band as shown in Figure 113 (b), the difference between co and cross polarization about 5 dB because the axial ratio (AR=15 dB) is not high value sufficiently. For last band, it similar to first band it radiates LHCP in +z direction. The cross-polarization level in broadside is 33.6 dB and 19.3 dB at 3.6 GHz and 11 GHz respectively.

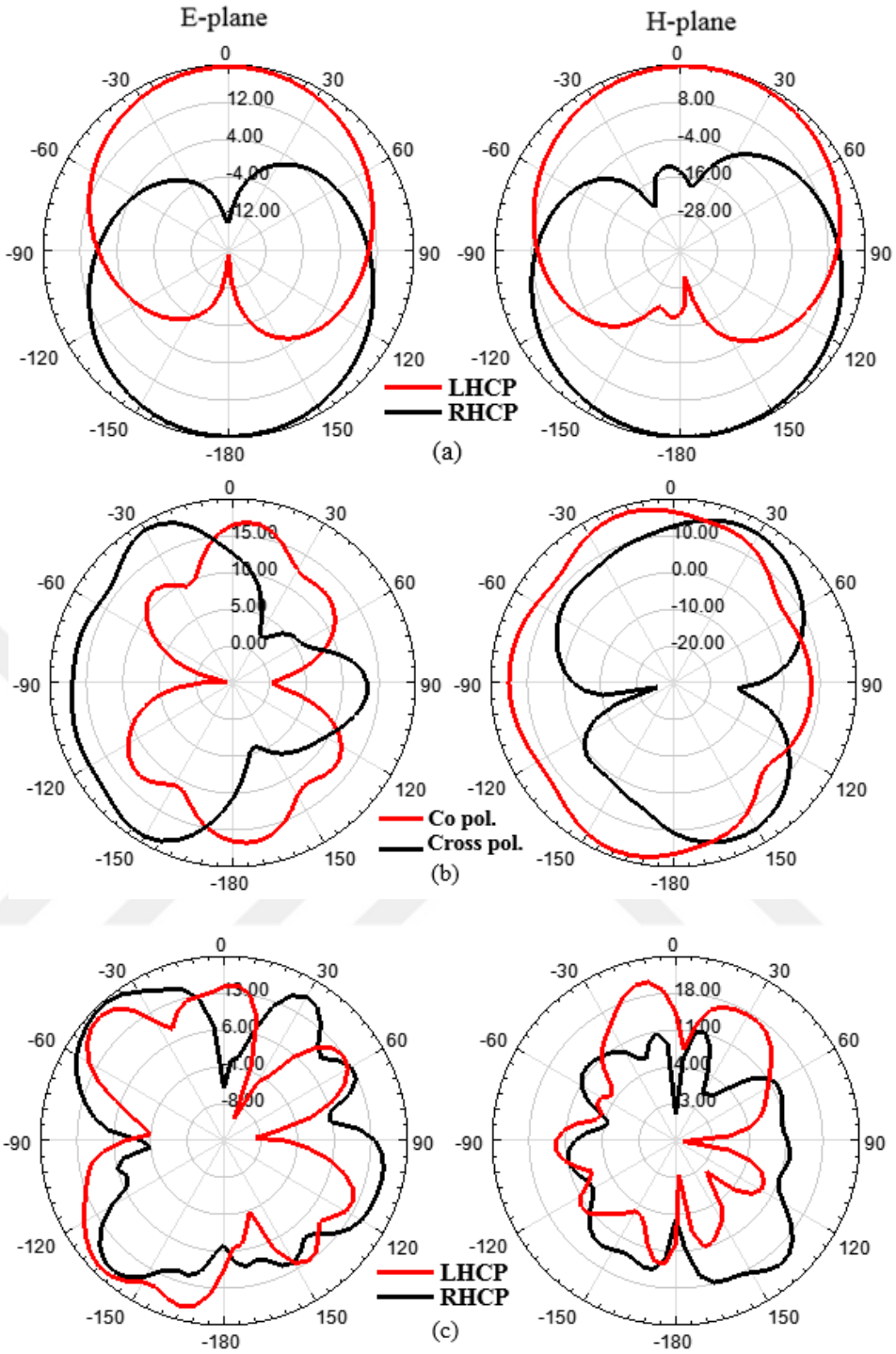

Figure 113 Radiation patterns of the first updated CPSSA at (a) 3.6 GHz, (b) 8 GHz, (c) 11 GHz

5.4 Design and Analysis Quate Band with Triple Band CPSSA

The second update of the basic model came to generate a new CP band by varying the impedance of the feedline part. This addition makes the second updated antenna to be more applicable for wide applications. Actually, the second updated antenna is based

on basic model and first update with some manipulations fulfilled to give new beneficial results. In the previous models the enhancement carried on the ground plane while the current model is used a different technique. As known, the feedline plays an essential role for antenna operation. Second update focused on feedline part as well as other previous techniques in first update and second update. The feedline in this model was etched gradually until arrived to wanted response (new band) in the final stage.

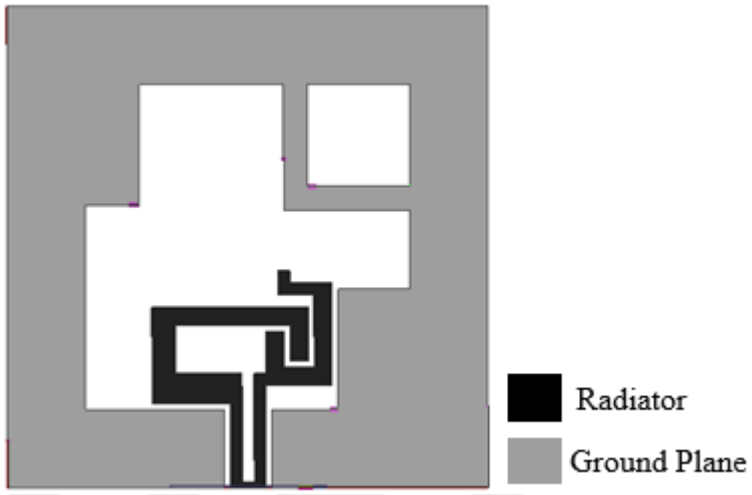

Figure 114 The structure of second update CPSSA

As presented in Figure 114, the feedline was etched. The width of the slit is 1 mm while the length is 9 mm. The last part of the feedline (near to SMA connector) is common with a length of 0.5 mm.

5.4.1 Surface Current Distributions at 5.8 GHz

The surface current distributions already did in the first section of this chapter at 3.6 GHz, 8 GHz, and 11 GHz. Now, it has been done for the new band at resonant frequency 5.8 GHz. Figure 115 presents the surface current distributions on time instants at $t=0^{\circ}$ and $t=90^{\circ}$ at 5.8 GHz. Also, Figure 115 indicates that the resultant current vector rotates clockwise direction leads to contribute left-handed circular polarization (LHCP) radiation.

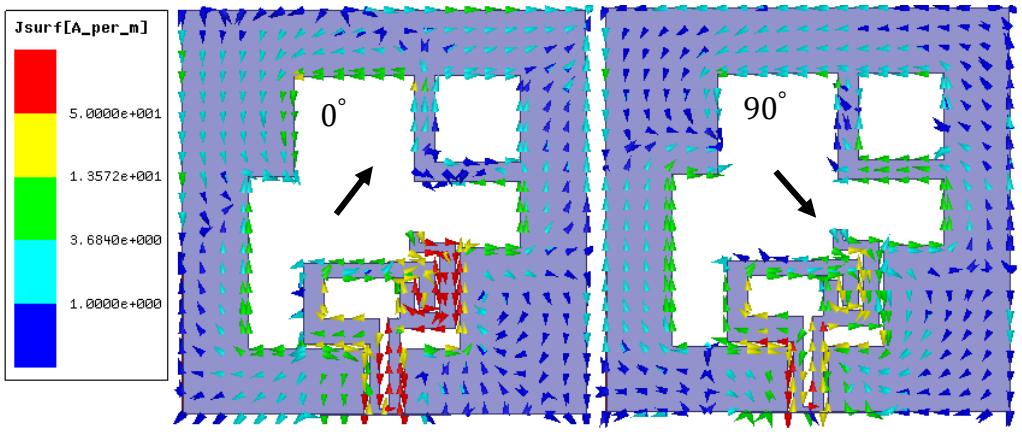

Figure 115 The surface current distribution of the second update CPSSA at 5.8 GHz

5.4.2 The Parametric Study for Second Updated Antenna

5.4.2.1 Effect of Parameters, s1

In Figure 116, the etching stage is clarified. Actually, the etching stage take several stages. When s1=0 means that there is no etching it observed that the band at 5.8 GHz is absent. Even in s1=3 mm there is no response at the mentioned band as shown in Figure 116 (a). The first thread of response appeared when s1=6 mm. when s1=9 mm, the band became manifest with a good response. The occurrence belongs to resonance happened then the power radiated not absorbed. Regarding the axial ratio (AR), it's under the 3-dB shows in three regions obviously at s1=9 mm. Actually, these regions are matched with S11 response well as noted in Figure 116 (b), then the second update model can be operated at four different useful bands the three of them are CP bands whereas another band is LP.

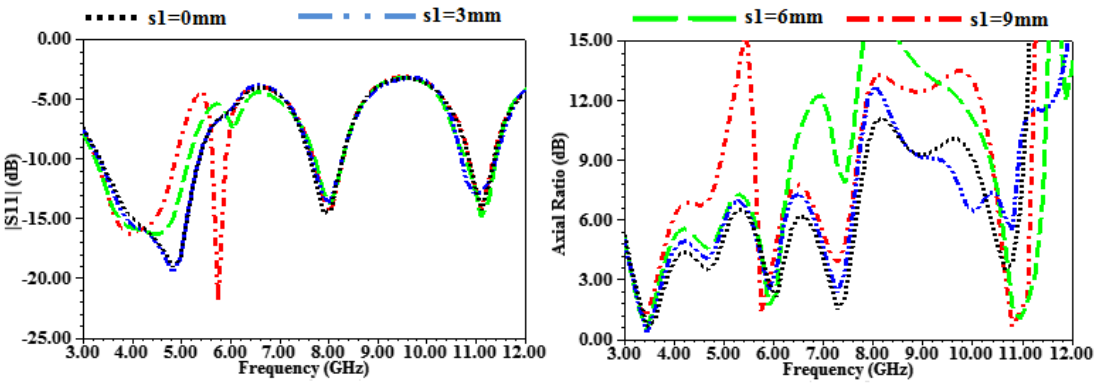

Figure 116 The effect of s1 on second updated antenna performance (a) |S11|, (b) AR

The parametric study performed to know the impaction of each parameter to the response of antenna. Basically, the two responses are tested in each parameter |S11| and axial ratio (AR).

5.4.2.2 Effect of Parameter, r5

Regarding the r5 strip, it considers a part of the radiator, it noted that connected directly with W7. The mentioned parameter tested in three different values 1 mm, 2 mm, and 3 mm. When r5= 1 mm, the |S11| response kept common bands while the axial ratio at the last band was effected significantly as seen in Figure117 (a) and (b). At r5=2 mm, the reflection coefficient increased at 5.8 GHz. Also, the axial ratio at last band lost the CP condition as shown in Figure117 (b).

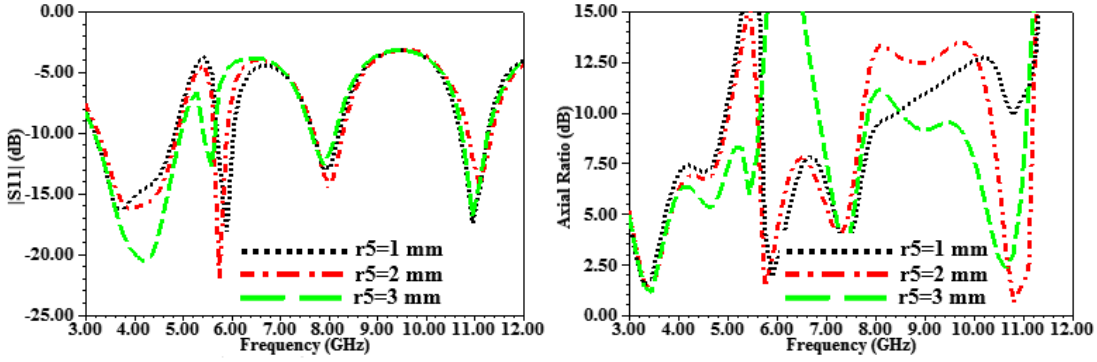

(a) (b)

Figure 117 The effect of r5 on second updated antenna performance (a) |S11|, (b) AR

5.4.2.3 Effect of Parameters, t1 and t2

The t1 and t2 parameters compose the inverted L-strip on the ground plane in first update model. The same strip exists in the second update model, but with different length values. After testing each element separately (t1 and t2). It observed that the impaction of them on |S11| with different lengths is poor as illustrated in Figures 118 (a) and 119 (a) while the effectiveness appears on axial ratio especially in the last band. When t1=10.5 mm and t2= 8.5 mm, the CP condition (AR≤3 dB) is satisfied as shown in Figures 117 (b) and 118 (b).

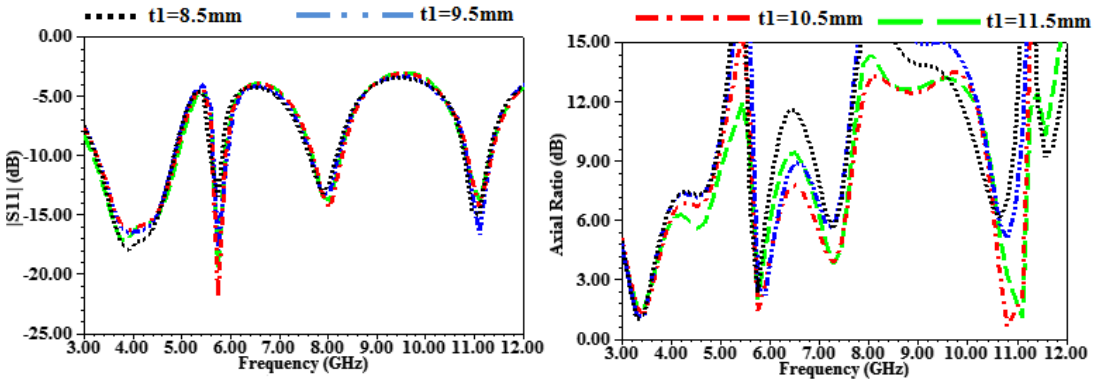

(c) (b)

Figure 118 The effect of t1 on second updated antenna performance (a) |S11|, (b) AR

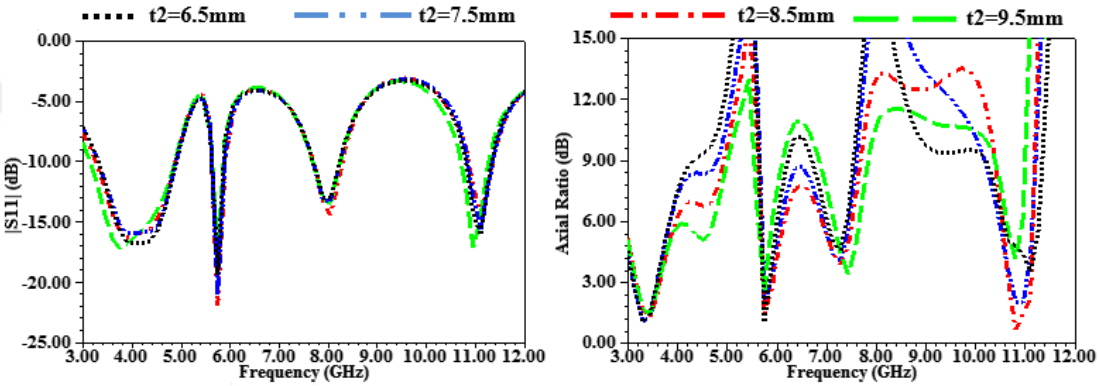

(a) (b)

Figure 119 The effect of t2 on second updated antenna performance (a) |S11|, (b) AR

5.4.3 Results and Discussions

5.4.3.1 The |S11| and AR

The reflection coefficient (|S11|) and the axial ratio (AR) of the second updated antenna have been demonstrated in Figure 120 (a) and (b) respectively. There are four bands with good impedance bandwidth as illustrated in Figure 120 (a). The first band operates at (3.27-4.88 GHz), while the second, third, and fourth band operate at the regions (5.62-5.89), (7.68-8.27 GHz), and (10.83-11.33 GHz) respectively. To know the status of each band in terms of polarity, the axial ratio against the frequency has been plotted. Based on Figure 120 (b), the condition of CP (AR≤3 dB) exists in all bands except the third band with center frequency 8 GHz. The CP exists in the first band from (3.17-3.64 GHz) whereas for second and last band exist from (5.72-5.91 GHz) and (10.64-11.1 GHz) respectively.

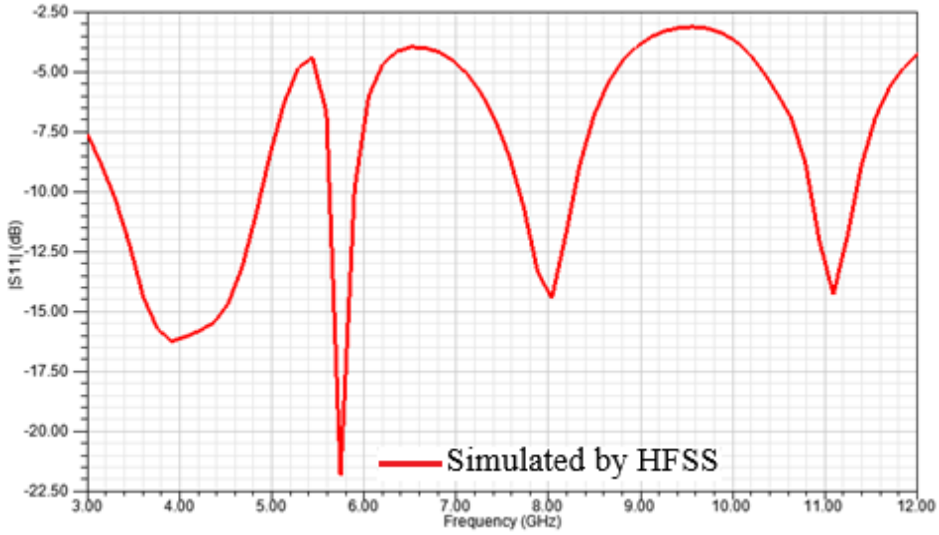

(a)

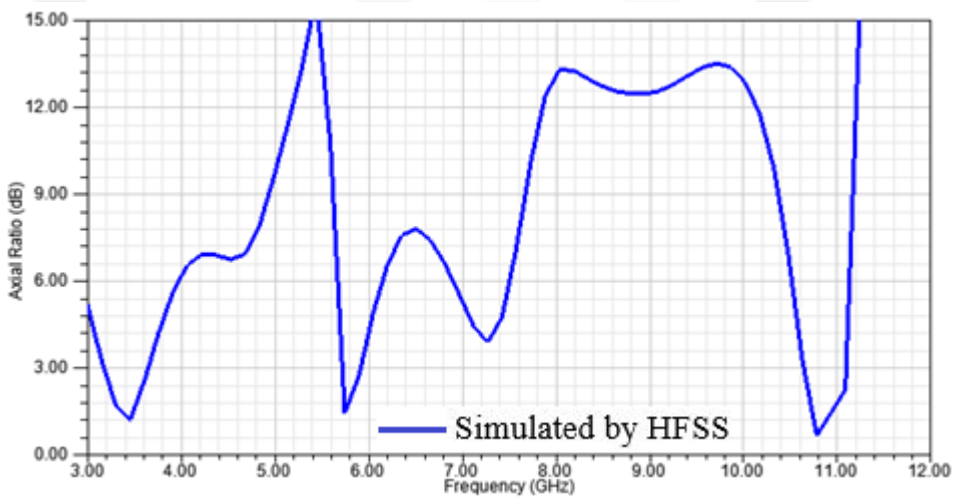

(b)

Figure 120 The |S11| and AR versus frequency of the second updated antenna (a) |S11|, (b) AR

5.4.3.2 Gain and Radiation Patterns

The simulated peak gain against frequency is illustrated in Figure 121. It noted that the proposed antenna appears variation in first band (3.27-4.88 GHz) is from 2 dBi to 4.2 dBi. In second band (5.62-5.89 GHz), the peak gain is about 2.3 dBi while at LP band (7.68-8.27 GHz) is from 3.6 dBi to 3.7 dBi. In last band (10.83-11.33 GHz) the gain about 3.9 dBi to 4.4 dBi.

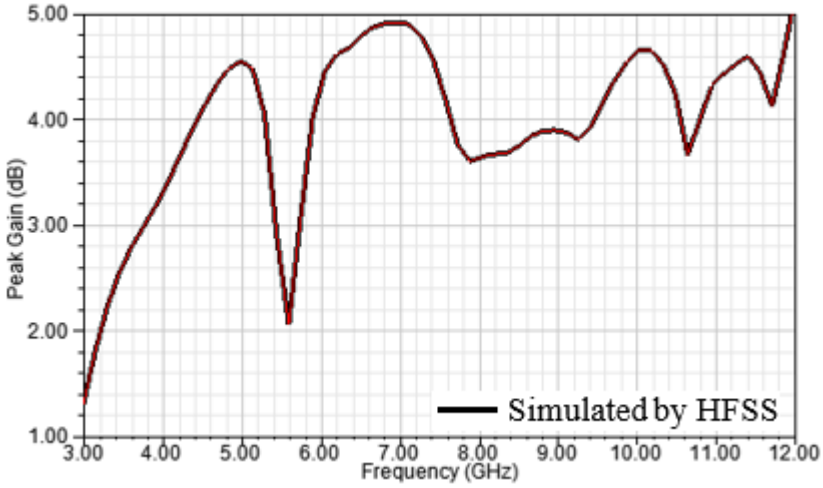

Figure 121 The peak gain of the second update CPSSA

The radiation patterns for the second updated antenna has been plotted in XZ-plane and YZ-plane at frequencies 3.5 GHz, 5.8 GHz, 8 GHz, and 11 GHz as presented in Figure 122 (a), (b), (c), and (d) respectively. It is observed that the radiation pattern differ in each band. The reason for this is that the current distribution is different in each frequency in other meaning, the current distribution is changing if the wavelength changed and this leads to appear different shapes when the frequency is changed.

It's noted from Figure 122 (a) and (b) that the antenna radiates LHCP wave in +z-direction whereas RHCP wave in the –z-direction. When $\theta = 0^{\circ}$, the simulated cross-polarization level at 3.5 GHz about 23 dB, whereas 25 dB at 5.8 GHz. Also, in both planes, the co-polarization pattern is a bi-directional shape. At 8 GHz, the radiation pattern has been presented in Figure 122 (c), which describes the radiation shape in both planes. It noted that the cross-polarization level low for somewhat. It is about 7dB. Concerning the radiation pattern at 11 GHz, it can be observed in Figure 122 (d). the antenna at this band radiates semi-omnidirectional also, the CP type is LHCP wave in the +z-direction and RHCP wave in the opposite direction. Regarding the cross-polarization level, it is about 20 dB.

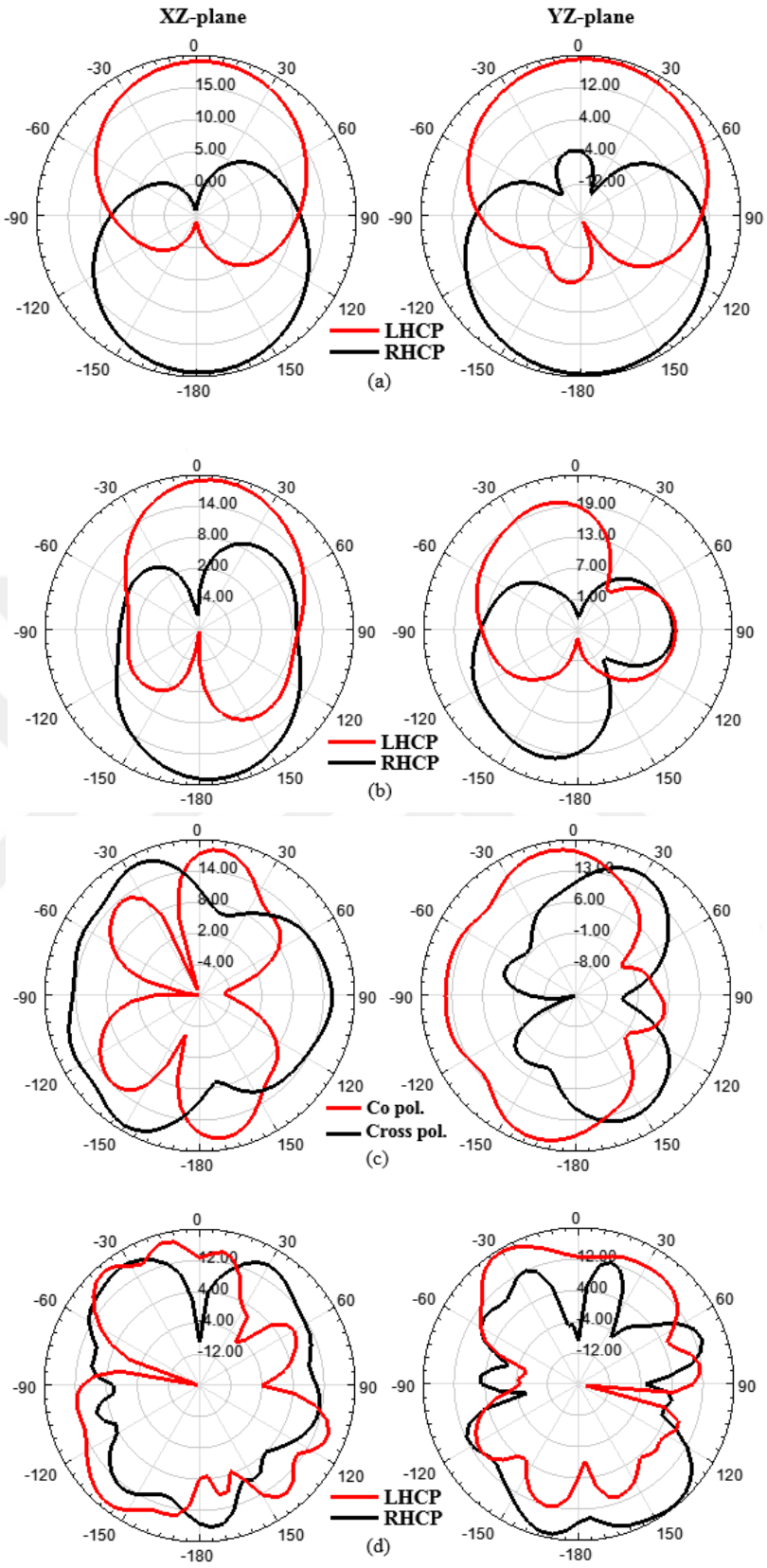

Figure 122 Radiation patterns of the second update CPSSA at (a) 3.5 GHz, (b) 5.8 GHz, (c) 8 GHz, (d) 11 GHz

CHAPTER 6

CONCLUSIONS AND SUGGESTIONS FOR FUTURE WORKS

6.1 Conclusions

In this dissertation, new multiband circular polarization antennas are proposed for modern wireless applications. In the first part of this dissertation, a new open loop hexagonal monopole antenna loaded with two stair-shaped slits in the partial ground plane is proposed in this paper. Penta operating bands with two different polarizations are obtained due to the resonances of the monopole and the slits. Three bands out of five are circularly polarized (CP) generated due to the interaction between the currents of the radiator and the loop current on the partial ground plane, which acts as a magnetic monopole. There are two linear polarization (LP) bands generated besides the CP bands, the frequency band (2.51-2.64) GHz is produced due to the existence of a slot on the ground plane whereas another frequency band (3.10-3.31) GHz is obtained from open loop hexagonal radiator. Then it is modified by etching and adding another pair of stair slits and rectangular strips with dimensions of nh1×nw1 and nh2×nw2 on the partial ground plane. The aim of the first design in part one is to create a different polarization and triple sense in one antenna structure while the second design was come to increase the ARBW, especially in the last band. Regarding the second part, new designs of multiband circular polarization antennas have been built. These antennas are feeding by CPW. Depending on current distribution, the antennas are uniting sense. The proposed technique indicates a new alternative to build low cost, omnidirectional radiation pattern CP antennas suitable for a wide range of wireless communication systems. The research highlights can be summarized as follows:

1. The radiator shape plays an important role to find the multiband and also gives an essential indication if it can radiate a circular polarization wave or not.
2. Exist a loaded part on the radiator may contribute to enhance the orthogonal electric field or to equalize the amplitude of two vectors and therefore the circular polarization has displayed.

3. Exist slits in stair shape contribute to enhance ARBW as well as decrease the AR which leads to transfer elliptical wave to circular.
4. The pair of rectangular strips in the ground plane have a significant role in increasing the ARBW of band4.
5. The method of adding two patches in the opposite direction of corners in the open square ring in the second design contribute to appear positive results regarding the CP. When unequal rectangular patches added, the CP waves started to appear clearly in three operating bands.

6.2 Suggestions of Future Work

Recommendations for future works are following listed:

1. Regarding the demonstrated work in section 4.2 (Penta band antenna with triple sense CP), additional research work can be performed by changing the polarization of the middle bands from linear to circular. This operation can be implemented by etching suitable slits in the ground plane.
2. The gain of the proposed antenna in section 4.3 (Triple Band Antenna with Dual Sense CP) can be enhanced by employing metamaterial technique with keeping the compact size.
3. The proposed antennas can be employed in a 4×4 MIMO wireless system for the fifth generation (5G) applications.
4. Concerning the triple band CPSSA in section 5.2, it can be invested to be a reconfigurable antenna to radiate RHCP and LHCP by adding suitable diodes based on the parametric study and surface current distribution.

REFERENCES

1. **Gao S. S., Luo Q., and Zhu F., (2014),** *"Circularly Polarized Antennas"*, Wiley IEEE Press, pp. 1-7.
2. **Smith B.L., Carpentier M. H., (1994),** *"The Microwave Engineering Handbook"*, Microwave Technology Series, vol. 3. pp. 21-40.
3. **Davis W. A., Agarwal K., (2001),** *"Radio Frequency Circuit Design"*, John Wiley & Sons, Inc, New York, pp. 166 –173.
4. **Pozar D. M., (2005),** *"Microwave Engineering"*, John Wiley & Sons, New York, pp. 130 –235.
5. **Parkinson B.W., Spilker J. J., (1996),** *"Global Positioning System: Theory and Applications"*, American Institute of Aeronautics and Astronautics, pp. 547–568.
6. **Counselman C. C., (1999),** *"Multipath rejecting GPS antennas"*, Proceedings of IEEE, vol. 87, no. 1, pp. 86–91.
7. **Davies K., (1965),** *"Ionospheric Radio Propagation"*, NBS Monograph 80, 181, US Government Printing Office, Washington, DC, pp.105-130.
8. **Brookner E., Hall W. M., Westlake R. H., (1985),** *"Faraday Loss for L-Band Radar and Communications Systems"*, IEEE Transactions on Aerospace and Electronic Systems, vol.21, no.4, p.p 459–469.
9. **Öhgren M., Bonnedal M., Ingvarson P., (2010),** *"Small and Lightweight GNSS Antenna for Previse Orbit Determination"*, Proc. of 2010 ESA Space Antennas Workshop, Noordwijk, Netherlands, Section 16, pp. 1–5.
10. **Chen C.C., Gao S., Maqsood M., (2012),** *"Space Antenna Handbook"*, John Wiley & Sons, Ltd, pp.549-570.
11. **Chen, X., Parini C., Collins B., Yao Y., Rehman M., (2012),** *"Antennas for Global Navigation Satellite Systems"*, John Wiley & Sons, Inc., pp. 103-117.

12. **Bao X., Ammann M. J., (2008),** *"Dual-Frequency Dual-Sense Circularly-Polarized Slot Antenna Fed by Microstrip Line"*, IEEE Transactions on Antennas and Propagation, vol. 56, no. 3, pp. 645-649.
13. **Chen C., Yung E. K. N., (2009),** *"Dual-Band Dual-Sense Circularly-Polarized CPW-Fed Slot Antenna with Two Spiral Slots Loaded"*, IEEE Transactions on Antennas and Propagation, vol. 57, no. 6, pp. 1829-1833.
14. **Rezaeieh S. A., Kartal M., (2011).** *"A New Triple Band Circularly Polarized Square Slot Antenna Design with Crooked T and F-shape Strips for Wireless Applications"*, Progress In Electromagnetics Research, vol. 121, pp. 1–18.
15. **Wang L., Guo Y.-X., Sheng W.X., (2012),** *"A Single-Feed Capacitively Circularly Polarized Dual-Annular Slot Antenna for Wireless Applications*", Journal of Electromagnetic Waves and Applications, vol. 26, no. 11-12, pp.1389-1396.
16. **Shao Y., Chen Z., (2012),** *"A Design of Dual-Frequency Dual-Sense Circularly-Polarized Slot Antenna"*, IEEE Transactions on Antennas and Propagation, vol. 60, no. 11, pp. 4992-4997.
17. **Noghabaei S. M., Sharul A., Soh P. J., Abedian M., Guy V., (2013),** *"A Dual-Band Circularly-Polarized Patch Antenna with a Novel Asymmetric Slot for WiMAX Application"*, Radioengineering, vol. 22, no. 1, pp. 291-295.
18. **Bod M., Hassani H.R., (2014),** *"Multi-Band Circularly Polarized Slot Antenna for GPS, Bluetooth and WiMAX bands"*, Progress In Electromagnetics Research C, vol. 49, pp. 171-178.
19. **Hoang T. V., Le T. T., Li Q. Y., Park H. C., (2015),** *"Quad-Band Circularly Polarized Antenna for 2.4/5.3/5.8 GHz WLAN and 3.5-GHz WiMAX Applications"*, IEEE Antennas and Wireless Propagation Letters, vol. 15, pp. 1032-1035.
20. **Brar R. S., Saurav, K., Sarkar D., Srivastava K. V., (2017),** *"A Triple Band Circular Polarized Monopole Antenna for GNSS/UMTS/LTE"*. Microw. Opt. Technol. Lett., vol. 59, pp. 298-304.
21. **Wang C., Li J., Zhang A., Joines W. T., Liu Q. H., (2017),** "Dual-Band Capacitively Loaded Annular-Ring Slot Antenna for Dual-Sense Circular Polarization", Journal of Electromagnetic Waves and Applications, vol. 31, no. 9, pp. 867-878.

22. **Patil S., Singh A., Kanaujia B., Lal R., (2017),** *"Design of Dual Band Dual Sense Circularly Polarized Wide Slot Antenna with C-shaped Radiator for Wireless Applications"*, Frequenz, vol. 72, no. 7-8, pp. 1-9.
23. **Altaf A., Seo M., (2018),** *"A Tilted-D-Shaped Monopole Antenna with Wide Dual-Band Dual-Sense Circular Polarization"*, IEEE Antennas and Wireless Propagation Letters, vol. 17, no. 12, pp. 2464-2468.
24. **Saini, R., Bakariya P., (2018),** *"Dual-Band Dual-Sense Circularly Polarized Asymmetric Slot Antenna with F-Shaped Feed Line and Parasitic Elements"*, Progress In Electromagnetics Research M. vol. 69, pp. 185-195.
25. **Tharehalli Rajanna P. K., Rudramuni K., Kandasamy K., (2019),** *"Compact Tri-Band Circularly Polarized Planar Slot Antenna Loaded with Split Ring Resonators"*, Int J RF Microw Comput Aided Eng., pp. 1-9.
26. **Misra D. K., (2004),** "Radio-Frequency and Microwave Communication Circuits", John Wily & Sons, 2nd Edition, pp. 215-225.
27. http://www.antenna-theory.com/definitions/vswr.php
28. **Balanis C.A., (2005),** *"Antenna Theory: Analysis and Design"*, Hoboken, NJ: John Wiley & Sons, Inc., pp. 123-154.
29. **Stutzman W. L., Thiele G.A., (1997),** *"Antenna Theory and Design"*, 2nd edn, NewYork: John Wiley & Sons, Inc., pp. 55-69.
30. http://hyperphysics.phy-astr.gsu.edu/hbase/phyopt/polclas.html
31. **Kraus J. D., Fleisch D. A., (1999),** *"Electromagnetics with Applications"*, Fifth ed.: The McGraw Hill Companies, Inc., pp. 34-67.
32. **Gothard G. K., German F. J., (1999),** "Time Domain Electromagnetics", Academic Press, Pages, pp. 237-277.
33. **Garg R., Bhartia P., Bahl I., (2001),** *"Microstrip Antenna Design Handbook"*, 1st ed. MA Artech House, pp. 25-43.
34. **K. R. Carver, Mink J. M., (1981),** *"Microstrip Antenna Technology"*, IEEE Antennas and Propagation, vol.29, no.1, pp.3-9.
35. **Munson R. E., (1974),** *"Conformal Microstrip Antennas and Phased Arrays"*, IEEE Trans. Antennas & Propagation, vol. 22, no. 1, pp. 74-78.

36. **Lo Y. T., Solomon D., Richards W. F., (1979),** *"Theory and Experiments on Microstrip Antennas"*, IEEE Transactions on Antennas and propagation, vol. 27, no. 2, pp. 137-145.

37. **Benella A., Gupta K. C., (1988),** *"Multiport Network Model and Transmission Characteristics of Two-Port Rectangular Microstrip Patch Antennas"*, IEEE Transactions on Antennas and Propagation, vol. 36, no.10, pp. 1337–1342.

38. **Itoh T., Menzel W., (1981),** *"A Full-Wave Analysis Method for Open Microstrip Structure"*, IEEE Trans. Antennas Propagation, vol. 29, no. 1, pp. 63-68.

39. **Harrington R. F., (1967),** *"Matrix Method for Field Problems"*, Proceeding of IEEE, vol. 55, no. 2, pp. 136-149.

40. **Bansal R., (2004),** *"Handbook of Engineering Electromagnetics"*, New York: Marcel Dekker, Inc., pp. 37-55.

41. https://www.feko.info.

42. http://www.nec2.org/.

43. **Kunz K.S., Luebbers R.J., (1993),** *"The Finite Difference Time domain Method for Electromagnetics"*, Springer, Boston, MA., pp. 5-34

44. **Taflove A., (1995),** *"Computational Electrodynamics: The Finite-Difference Time-Domain Method"*, Norwood, MA: Artech House, pp.1-24.

45. **Sadiku N. O., (2007),** *"Elements of Electromagnetics"*, Fourth ed, Oxford University Press, pp.106-120.

46. http://apsimtech.com/.

47. http://www.remcom.com/xf7.

48. **Alett P. L., Baharaniand A. K., Zienkiewicz O.C., (1968),** *"Application of Finite Elements to The Solution of Helmholtz's equation"*, IEE Proceedings, vol. 115, pp. 1762–1766.

49. http://www.ansys.com.

50. **Weiland T., (1977),** *"A Discretization Method for The Solution of Maxwell's Equations for Six-Component Fields"*, Electronics and Communications AEU, vol. 31, no. 3, pp. 116–120.

51. **Marklein R., (2002),** *"The Finite Integration Technique as a General Tool to Compute Acoustic, Electromagnetic, Elastodynamic and Coupled Wave Fields"*, IEEE Press, pp.23-27.

52. www.cst.com.

53. **Kumar G., Ray K. P., (2003),** *"Broadband Microstrip Antennas"*, Artech House, pp. 66-70.

54. **Mehta A., (2015),** *"Microstrip Antenna"*, International Jornul of Scintefic & Technology Research, vol. 4, no.3, pp. 54-57.

55. **Wei K., Li J.-Y., Wang L., Xing Z., Xu R., (2015),** *"Study of Multi-Band Circularly Polarized Microstrip Antenna with Compact Size"*, Progress In Electromagnetics Research C, vol. 58, pp. 11-19.

56. **James J.R., Hall P.S., (1989),** *"Handbook of Microstrip Antennas"*, Peter Peregrinus Ltd., U.K, pp. 45-55.

57. **Al-Lawati H. M., (2014),** *"Design and Analysis of Low Profile Circularly Polarized Antennas"*, pp. 23-33.

58. **Huang J., (1984),** *"Circularly Polarised Conical Patterns from Circular Microstrip Antennas"*, IEEE Transaction on Antennas and Propagation, vol. 32, no. 9, pp. 991-994,.

59. **Huang J., (1986),** *"A Technique for an Array to Generate Circular Polarizations with Linealry Polarized Elements"*, IEEE Transaction on Antennas and Propagation, vol. 34, no. 9, pp. 1113-1124.

60. **Nakano H., (1987),** *"Helical and Spiral Antennas: A Numerical Approach"*, Research Studies Press Ltd,.

61. **Kraus J. D., Marhefka R. J., (2002),** *"Antennas for all Applications"*, New York, McGraw-Hill, pp.30-38.

62. **Imbraile W., Gao S., Boccia L., (2012),** *"Space Antenna Handbook"*, Chichester, John Wiley & Sons, Ltd, pp.1-31.

63. **Pozar, D. M., Schaubert D., (1995),** *"Microstrip Antennas: The Analysis and Design of Microstrip Antennas and Arrays"*, New York. John Wiley & Sons, Inc., pp. 43-60.

64. **Hirota T., Minakawa A., Muraguchi M., (1990),** *"Reduced-Size Branch-Line and Rat-Race Hybrids for Uniplanar MMICs"*, IEEE Trans. Microw. Theory Tech., vol. 38, no. 3, pp. 270–275.

65. **Okabe H., Caloz C., Itoh T., (2004),** *"A Compact Enhanced-Bandwidth Hybrid Ring Using an Artificial Lumped Element Left-Handed Transmission-Line Section"*, IEEE Trans. Microw. Theory Tech., vol. 52, no.3, pp. 798–804.

66. http://www.thornett.net/Rosliston_Archive_200911/html/cross_dipole_antenna.html

67. https://commons.wikimedia.org/wiki/File:Dipole_antenna_standing_waves_animation_461x217x150ms.gif

68. http://homepage.tudelft.nl/v0e47/demos/codes/AHelix/helix.html.

69. **Toh B. Y., Cahill R., Fusco V. F., (2003),** *"Understanding and Measuring Circular Polarisation"*, IEEE Trans. Education, vol. 46, no. 3, pp. 313–318.

70. **King H. E., Wongand J. L., Newman E. H., (2007),** *"Antenna Engineering Handbook"*, McGraw-Hill, pp. 86-98.

71. **Amin M., Cahill R., (2005),** *"Compact Quadrifilar Helix Antenna"*, Electronics Letters, vol. 41, no. 12, pp. 672-674.

72. **Best, S. R., (2004),** *"A 7-Turn Multi-Step Quadrifilar Helix Antenna Providing High Phase Center Stability and Low Angle Multipath Rejection for GPS Applications"*, IEEE Antennas and Propagation Society International Symposium, vol. 3, pp. 2899-2902.

73. **Tranquilla J. M., Best S. R., (1990),** *"A Study of The Quadrifilar Helix Antenna for Global Positioning System (GPS) Applications"*, IEEE Transactions on Antennas and Propagation, vol. 38, no. 10, pp. 1545–1550.

74. https://www.maxtena.com/company/white-papers/innovations-quadrifilar-helix-printed-antennas/

75. **Kumar R., Chaudhary R. K., (2017),** *" Wideband Circularly polarized dielectric resonator antenna coupled with meandered-line inductor for ISM/WLAN applications"*. Int J RF Microw Comput Aided Eng., pp. 1-7.

76. **Olver A. D., Clarricoats P. J. B., Kishk A. A., Shafai L., (1994),** *"Microwave Horns and Feeds"*, London, IEEE Press, pp. 45-78.

77. **Hazdra P., Galuscak R., Mazanek M., (2006),** *"Optimization of Prime-Focus Circular Waveguide Feed with Septum Polarization Transformer for 1.296 GHz EME Station"*, Proceedings of the First European Conference on Antennas and Propagation (EuCAP), Nice, France, pp. 1-5.

78. **Franco M. J., (2011),** *"A High-Performance Dual-Mode Feed Horn for Parabolic Reflectors with a Stepped Septum Polarizer in a Circular Waveguide"*, IEEE Antennas and Propagation Magazine, 53(3): 142–146.

79. **Chen C.-H., Yung E. K. N., (2011),** "A Novel Unidirectional Dual-Band Circularly-Polarized Patch Antenna", IEEE Trans. Antennas Propag., vol. 59, no. 8, pp. 3052–3057 .

80. **Jan J. Y., Wong K. L., (2000),** *"A Dual-Band Circularly Polarized Stacked Elliptic Microstrip Antenna"*, Microwave and Optical Technology Letters, vol. 24, no. 5, pp. 354–357.

81. **Su C. M., Wong K.L., (2002),** *"A Dual-Dand GPS Microstrip Antenna"*, Microwave and Optical Technology Letters, vol. 33, no. 4, pp. 238–240.

82. **Falade O. P., Rehman M. U., Gao Y., Chen X., Parini C. G., (2012),** *"Single Feed Stacked Patch Circular Polarized Antenna for Triple Band GPS Receivers"*, IEEE Transactions on Antennas and Propagation, vol. 60, no. 10, pp. 4479-4484.

83. **Ooi T. S., Rahim S. K. A., Abdulrahman A. Y., Koh B. P., Lee S. K., (2011),** *"Compact dual-band circularly polarized patch antenna with bandwidth enhancement"*, J. Optoelectron. Adv. Mater., vol. 13, no. 10, pp. 1279–1284.

84. **Zakaria N., Rahim S. K. A., Ooi T. S., Tan K. G., Reza A. W., Rani M. S. A., (2012),** *"Design of Stacked Microstrip Dual-Band Circular Polarized Antenna"*, Radioengineering, vol. 21, no. 3, pp. 875–880.

85. **Deng C., Li Y., Zhang Z., Pan G., Feng Z., (2013),** *"Dual-Band Circularly Polarized Rotated Patch Antenna with a Parasitic Circular Patch Loading"*, IEEE Antennas Wireless Propag. Lett., vol. 12, pp. 492–495.

86. **Chen K., Yuan J., Luo X., (2017),** *"Compact Dual-Band Dual Circularly Polarised Annular-Ring Patch Antenna for BeiDou Navigation Satellite System Application"*, IET Microw., Antennas Propag., vol. 11, no. 8, pp. 1079–1085.

87. **Maci S., Gentili G.B., Piazzesi P., Salvador C., (1995),** *"Dual-Band Slot-Loaded Patch Antenna"*, IEE Proc., Microw. Antennas Propag., vol. 142, no. 3, pp. 225–232.

88. **Hsieh G. B., Chen M. H., Wong K. L., (1998),** *"Single-Feeddual-Band Circularly Polarized Microstrip Antenna"*, Electronics Letters, vol. 34, no. 12, pp. 1170 –1171.

89. **Sun X. B., (2010),** *"Circular-Slotted Microstrip Antenna for GPS"*, Microwave and Optical Technology Letters, vol. 52, no. 5, pp.999–1000.

90. **Kim S. M., Yoon K. S., Yang W. G., (2007),** *"Dual-Band Circular Polarization Square Patch Antenna for GPS and DMB"*, Microwave and Optical Technology Letters, vol. 49, no. 12, pp. 2925–2926.

91. **Yang K. P., Wong K. L., (2001),** *"Dual-Band Circularly-Polarized Square Microstrip Antenna"*, IEEE Trans. Antennas Propagat., vol. 49, no. 3, pp. 377–382.

92. **Gaffar M., Zaman M. A., Choudhury S. M., Matin M. A., (2011),** *"Design and Optimisation of an Ovel Dual-Band Circularly Polarised Microstrip Antenna"*, IET Microwave, Antennas & Propagation, vol. 5, no.14, pp. 1670-1674.

93. **Nasimuddin, Chen Z. N., Qing X., (2010),** *"Dual-Band Circularly Polarized S-Shaped Slotted Patch Antenna with a Small Frequency-Ratio"*, IEEE Trans. Antennas Propagat., vol. 58, no. 6, pp. 2112–2115.

94. **Wang L., Guo Y.-X., Sheng W. X., (2012),** "Tri-Band Circularly Polarized Annular Slot Antenna for GPS and CNSS Applications", J. Electromagn. Waves Appl., vol. 26, no. 14, pp. 1820-1827

95. **Bao X. L., Ammann M. J., (2007),** *"Dual-Frequency Circularly-Polarized Patch Antenna with Compact Size and Small Frequency Ratio"*, IEEE Trans. Antennas Propagat., vol. 55, no. 7, pp. 2104-2107.

96. **Gonzalez I., Gómez J., Tayebi A., Cátedra F., (2012),** *"Optimization of a Dual-Band Helical Antenna for TTC Applications at S Band"*, IEEE Antennas and Propagation Magazine, vol. 54, no. 4, pp. 63-77.

97. **Sharaiha, A., Letestu T., (2010),** *"Quadrifilar Helical Antennas: Wideband and Multiband Behaviour for GPS Applications"*, 2010 International Conference on Electromagnetics in Advanced Applications, pp. 620-623.

98. **Xu R., Li J., Qi Y., Guangwei Y., Yang J., (2017),** *"A Design of Triple-Wideband Triple-Sense Circularly Polarized Square Slot Antenna"*, IEEE Antennas and Wireless Propagation Letters, vol. 16, pp. 1763-1766.

99. **Chen Q., Zhang H., Yang L., Li H., Zhong T., Min X., Tan, S., (2017),** *"Novel Dual-Band Asymmetric U-Shaped Slot Antenna for Dual-Circular Polarization"*, Int. J. RF Microw. Comput. Aided Eng., pp. 1-3.

100. **Rezaeieh S. A., Abbosh A., (2012),** *"Broadband CPW-Fed Slot Antenna with Circular Polarization for On-Body Applications at ISM Band"*, 2012 Asia Pacific Microwave Conference Proceedings, Kaohsiung, pp. 1184-1186.

101. **Chen C. H., Yung E. K. N., (2011),** *"Dual-Band Circularly-Polarized CPW-Fed Slot Antenna with a Small Frequency Ratio and Wide Bandwidths"*, IEEE Trans. Antennas Propagat., vol. 59, no. 4, pp. 1379-1384, 2011.

102. **Samsuzzaman M., Islam M. T., (2014),** *"Wideband Hook-Shaped Circularly Polarised Antenna"*, Electron. Letters, vol. 50, no. 15, pp. 1043-1045

103. **Samsuzzaman M., Islam M. T., (2018),** *"Circularly Polarized Broadband Printed Antenna for Wireless Applications"*, Sensors, vol. 18, no. 12, pp. 1-14.

104. **Pratap L. B., Mohan A., (2017),** *"Microstrip-Fed Broadband Circularly Polarized Antenna for Lower UWB"*, Wireless Pers. Commun., vol. 96, no. 3, pp. 4167-4175.

105. **Chen Q., Zhang H., Yang L. -C., Min X. -L., (2017),** *"Wideband Asymmetric Microstrip-Fed Circularly Polarized Antenna with Monofilar Spiral Stub for WLAN Application"*, Int. J. RF Microw. Comput. Aided Eng., vol. 27, no. 8, pp. 1096-4290.

106. **Tang H., Wang K., Wu R., Yu C., Zhang J., Wang X., (2017),** *"A Novel Broadband Circularly Polarized Monopole Antenna Based on C-Shaped Radiator"*, IEEE Antennas and Wireless Propagation Letters, vol. 16, pp. 964-967.

107. **Zhang L., Jiao Y. -C., Ni T., (2015),** *"A Planar Monopole Antenna with Wideband Circularly Polarized Characteristic"*, Electromagnetics, vol. 35, no. 4, pp. 227-239.

108. **Wu J., Jou C. F., Wang C., (2009),** *"Dual-Band Circularly Polarized Monopole Antenna"*, 2009 IEEE International Workshop on Antenna Technology, Santa Monica, CA, pp. 1-4

109. **Kumar A., Sankhla V., Deegwal J. K., Kumar A., (2018),** *"An Offset CPW-Fed Triple-Band Circularly Polarized Printed Antenna for Multiband Wireless Applications"*, AEU - International Journal of Electronics and Communications, vol. 86, pp. 133-141.

110. **Sankhla V., Kumar A., (2020),** *"An Offset CPW-Fed Dual-Band Circularly Polarized Printed Antenna for Multiband Wireless Applications"*, Optical and Wireless Technologies, Lecture Notes in Electrical Engineering, vol. 546, pp. 411–418.

111. **Jou C. F., Wu J. W., Wang C. J., (2009),** *"Novel Broadband Monopole Antennas with Dual-Band Circular Polarization"*, IEEE Transactions on Antennas and Propagation, vol. 57, no. 4, pp. 1027–1034.

112. **Wang X., Sun L., Lu X., Liang S., Lu W., (2017),** *"Single-Feed Dual-Band Circularly Polarized Dielectric Resonator Antenna for CNSS Applications"*, IEEE Transactions on Antennas and Propagation, vol. 65, no. 8, pp. 4283-4287.

113. **Zhang B., Zhang J., Liu C., Wu Z., (2017),** *"Investigation of Microstrip-Fed Low-Profile Broadband Circularly Polarized Rectangular Dielectric Resonator Antennas"*, Microw. Opt. Technol. Lett., vol. 59, pp. 2767-2772.

114. **Rezaeieh S.A., Şimşek S., Pourahmadazar J., (2013),** *"Design of a Compact Broadband Circularly-Polarized Slot Antenna for Wireless Applications"*, Microw. Opt. Technol. Lett., vol. 55, pp. 413-418.

115. **Shokri M., Ghobadi C., Nourinia J., Shirzad H., Asiaban S., Amiri Z., (2012),** *"Tiny Circularly Polarized Printed Slot Antenna for UWB Usage"*, Life Science Journal, vol. 9, no. 3, pp. 2238-2241.

116. **Pourahmadazar J., Ghobadi C., Nourinia J., Felegari N., Shirzad H., (2011),** *"Broadband CPW-Fed Circularly Polarized Square Slot Antenna with Inverted-L Strips for UWB Applications"*, IEEE Antennas and Wireless Propagation Letters, vol. 10, pp. 369-372.

APPENDIX

PUBLICATIONS RELATED TO Ph.D. THESIS

The following papers have been published in SCI indexed journals during the course of Ph.D. research:

1. M. AL-MIHRAB, A. SALIM, J. ALI, "A compact multiband printed monopole antenna with hybrid polarization radiation for GPS, LTE, and satellite applications," in IEEE Access, vol. 8, pp. 110371-110380, 2020, doi: 10.1109/ACCESS.2020.3000436.

2. M. AL-MIHRAB, A. SALIM, H. AL-SAEDI, J. ALI, “A compact size multiband printed monopole antenna with triple sense circular polarization for wireless applications,” Journal of Optoelectronics and Advanced Materials, vol. 22, iss. 9-10, pp. 483-494, 2020.